

CHAPTER 35

The Condensed Matter Physics of QCD

K. Rajagopal

F. Wilczek

THE CONDENSED MATTER PHYSICS OF QCD

KRISHNA RAJAGOPAL AND FRANK WILCZEK

*Center for Theoretical Physics, Massachusetts Institute of Technology
Cambridge, MA USA 02139*

Important progress in understanding the behavior of hadronic matter at high density has been achieved recently, by adapting the techniques of condensed matter theory. At asymptotic densities, the combination of asymptotic freedom and BCS theory make a rigorous analysis possible. New phases of matter with remarkable properties are predicted. They provide a theoretical laboratory within which chiral symmetry breaking and confinement can be studied at weak coupling. They may also play a role in the description of neutron star interiors. We discuss the phase diagram of QCD as a function of temperature and density, and close with a look at possible astrophysical signatures.

Contents

1	Introduction and Summary	4
2	Color-Flavor Locking	6
2.1	Form of the Condensate	7
2.2	Symmetry Breaking	9
2.3	Elementary Excitations	13
2.4	The Modification of Electromagnetism	16
2.5	Quark-Hadron Continuity	19
3	2SC and Other Variants	22
3.1	Two Flavors	22
3.2	Two+One Flavors	23
3.3	One Flavor	24
3.4	Four or More Flavors	24
3.5	Two Colors	25
3.6	Many Colors	25
3.7	QCD at Large Isospin Density	26
4	Calculational Methods	26
4.1	Renormalization Toward the Fermi Surface	28
4.2	Model Hamiltonian by Variational Methods	37
4.3	Model Hamiltonian by Diagrammatic Methods	47

<i>The Condensed Matter Physics of QCD</i>	3
4.4 Asymptotic Analysis	50
4.5 Challenges for the Future	62
5 The Phase Diagram	63
6 Color Superconductivity in Compact Stars	73
6.1 Equation of State	74
6.2 Cooling by Neutrino Emission	75
6.3 Supernova Neutrinos	76
6.4 R-mode Instabilities	77
6.5 Magnetic Field Evolution	77
6.6 Crystalline Color Superconductivity and Glitches in Quark Matter	78

1 Introduction and Summary

In this article we shall discuss the behavior of QCD at high density. We shall mainly be concerned, more precisely, with the regime of very large baryon number density and relatively low temperature. The appeal of the subject should be obvious. It provides the answer to a child-like question: What happens to matter, as you squeeze it harder and harder? Moreover, this regime may be realized in neutron star interiors and in the violent events associated with collapse of massive stars or collisions of neutron stars, so it is important for astrophysics. Finally, we may hope to gain insight into QCD at moderate or low density — the realm of ordinary matter and of terrestrial experiments — by extrapolating from above.

What is less obvious, but turns out (with certain qualifications) to be true, is that the high density regime of QCD is tractable theoretically. Heuristic arguments to this effect, invoking asymptotic freedom,¹ go back to the earliest days of the subject.² High density brings in a large energy scale, the chemical potential μ , and one might hope that the relevant coupling to describe the dynamics is $g(\mu)$. This becomes small as $\mu \rightarrow \infty$, and suggests the possibility of a perturbative treatment. This naive expectation, however, does not stand up to critical scrutiny. As we shall discuss at length below, perturbation theory around the naive ground state (free quark Fermi spheres) encounters infrared divergences. Furthermore, the naive perturbative ground state is unstable. Therefore, straightforward perturbative treatment of QCD at high density fails.

Fortunately, related difficulties have been met and overcome previously, in the theory of superconductivity. There we learn that arbitrarily weak attractive interactions can change the ground state qualitatively. In the true ground state there is an effective mass for photons — the Meissner effect — and energy gaps for charged excitations. These phenomena remove potential infrared divergences, and render the perturbation theory around the true ground state regular (nondegenerate).

We can readily adapt the methods of superconductivity theory to QCD. It is also instructive to consider, in this connection, variants of QCD with different numbers of colors and flavors, and different spectra of quark masses. A rich and highly structured theory emerges, displaying calculable, highly non-trivial dependence on all these variables.

The central result of the analysis is the identification of condensates in diquark channels, analogous to the Cooper pairs of electrons in ordinary superconductors. This is the phenomenon of color superconductivity.^{3,4,5,6}

Compared to ordinary superconductivity, color superconductivity, though it appears superficially to be more complex mathematically, is in a profound sense simpler and more directly related to fundamentals. Ordinary superconductivity takes place in solids and the accurate effective interactions are

determined by band structure and other complicated effects. Furthermore, ordinary superconductivity in a metal involves electron pairing, and the fundamental interaction between electrons (the screened Coulomb interaction) is repulsive. The effective attraction near the Fermi surface that leads to superconductivity arises in classic superconductors only as a subtle consequence of retarded phonon interactions, and in the cuprate superconductors through some mechanism yet unknown. In color superconductivity, by contrast, the attractive interaction can arise already from the primary, strong, interactions. This has two consequences. First, the accurate form of these interactions can be calculated from first principles, using asymptotic freedom. This makes calculations at high enough density robust. Second, at accessible densities, where the strong interactions are much stronger than the electromagnetic interactions, we expect the color superconductors themselves to be robust in the sense that the ratio of their gaps and critical temperatures to the Fermi energy should be quite large.

In QCD with three colors and three flavors, we find an improved ground state at high density, based on color superconductivity, around which weak-coupling perturbation theory is valid. In particular, all the colored degrees of freedom acquire gaps. Thus, the improved ground state differs qualitatively from the naive one.

The resulting predictions regarding the low-energy spectrum and dynamics are striking. Color symmetry and chiral symmetry are spontaneously broken. The spectrum of elementary excitations is quite different from that found in naive perturbation theory. Nominally massless quarks and gluons become massive, new massless collective modes appear, and various quantum numbers get modified. All the elementary excitations carry integral electric charges.⁷ Altogether, one finds an uncanny resemblance between the properties one computes at asymptotic densities, directly from the microscopic Lagrangian, and the properties one expects to hold at low density, based on the known phenomenology of hadrons. In particular, the traditional “mysteries” of confinement and chiral symmetry breaking are fully embodied in a controlled, fully microscopic, weak-coupling (but nonperturbative!) calculation, that accurately describes a directly physical, intrinsically interesting regime.^{7,8}

Though some of the ideas go back a decade or more,^{3,4} the full power of color superconductivity to provide a rigorous foundation for the investigation of high density QCD has only become apparent relatively recently, and the subject is developing rapidly. In this survey we shall emphasize what we see as the most fundamental ideas that have appeared in the field to date, and attempt to identify some significant challenges for the future. Although we shall supply extensive references we will not attempt to catalogue all the very latest results, nor snapshot the developing state of the art in its technical and quantitative aspects.

In Section 2, we shall discuss in detail the high-density behavior of a slightly idealized version of real-world QCD, in which we imagine there are three flavors of massless quarks. This is the case for which the clearest and most beautiful results emerge, based on the phenomenon of color-flavor locking. In Section 3, we shall discuss what changes must be made, in order to take into account the realistic quark spectrum. We shall also briefly discuss QCD variants with unrealistic numbers of colors and flavors, which shed additional light on the theory. In Section 4, we shall discuss in greater depth the theoretical analysis which underlies the preceding sections, and the techniques it relies upon. In Section 5, we shall synthesize the preceding discussion, to produce a tentative sketch of the phase diagram for high-density QCD. Finally in Section 6 we shall discuss possible applications to astrophysics, including both existing results and some avenues that we believe might reward further investigation.

2 Color-Flavor Locking

In this Section we shall analyze the high-density, zero-temperature behavior of a slight idealization of QCD, in which the masses of the u , d and s quarks are set to zero, and those of the c , b and t quarks to infinity. This idealization gives rise to an especially clear and beautiful form of the theory. Also, as we shall discuss in Sections 3 and 5, the analysis applies with only very minor modifications to an important phase of real-world QCD.

In this Section our discussion will be broadly conceptual. The formal and algorithmic underpinnings are spelled out in more detail in Section 4, and of course in the primary literature. In particular, we focus in this section on a presentation of the physical properties of dense quark matter in the idealized three-flavor world, deferring discussion of quantitative calculations of the magnitude of the gap at the Fermi surface as much as possible to Section 4.

Let us briefly describe the foundational argument justifying the weak-coupling approximation at high density, leaving a more detailed and precise discussion to Section 4. The relevant degrees of freedom in cold, dense quark matter are those which involve quarks with momenta near the Fermi surface. At high density, when the Fermi momentum is large, the QCD gauge coupling $g(\mu)$ is small. When a pair of quasi-particles scatter, the typical momentum transfer is of order μ and the interaction is therefore weak. The exception, of course, is the case of scattering by a small angle. In QCD at asymptotically high densities, the long-range magnetic gauge interactions are unscreened in the absence of superconductivity, which raises the possibility of infrared problems in small angle scattering. The Meissner effect induced by the superconducting condensate itself can provide the requisite screening, however, regulating the putative collinear divergence and guaranteeing that the calcula-

tion is truly a weak-coupling calculation, at least at truly asymptotic density. Quantitative calculations support this qualitative conclusion, although it turns out that dynamical screening is more important than the Meissner effect in the regulation of small angle scattering.

2.1 Form of the Condensate

Because of the infinite degeneracy among pairs of quarks with equal and opposite momenta at the Fermi surface, an attractive interaction between quarks, even if arbitrarily weak, renders the Fermi surface unstable to the formation of a condensate of quark Cooper pairs. Creating a pair costs no free energy at the Fermi surface, while the attractive interaction results in a free energy benefit. The consequence of an attractive interaction between opposite-momentum modes near the Fermi surface is therefore the formation of a condensate in the zero temperature ground state. We expect those quark quasiparticles which interact with the condensate to acquire an energy gap, and we expect a Meissner effect to occur for all gauge bosons except those which see the condensate as neutral.

Single gluon exchange, the QCD analogue of the Coulomb interaction between two quarks, is attractive if the quarks are antisymmetric in color and the pair is therefore in the color $\bar{\mathbf{3}}$ channel. At weak-coupling, this interaction dominates and this argument suffices to guarantee condensation in the color $\bar{\mathbf{3}}$ channel. The instanton interaction is also attractive in the $\bar{\mathbf{3}}$ channel, which may be relevant at stronger coupling. At any coupling, attraction in the $\bar{\mathbf{3}}$ channel is quite reasonable intuitively, for in this channel the total color flux is reduced as one brings the quarks together.

Thus, according to the preceding discussion, we should expect the formation of a condensate in a color $\bar{\mathbf{3}}$ channel. The form of the condensate can be anticipated by analyzing the renormalization of couplings toward the Fermi surface starting from realistic microscopic couplings, as we describe in Section 4. This indicates the most likely flavor and spin channels for condensate formation. Ultimately, one must compare the energies of different candidate ground states, constructed along the lines indicated by BCS, and choose the most favorable.

An analysis of this sort indicates that the true ground state contains nonzero condensates approximately of the form⁷

$$\langle \psi_{iL}^{a\alpha}(\vec{p}) \psi_{jL}^{b\beta}(-\vec{p}) \epsilon_{ab} \rangle = - \langle \psi_{iR}^{a\alpha}(\vec{p}) \psi_{jR}^{b\beta}(-\vec{p}) \epsilon_{ab} \rangle = \Delta(p^2) \epsilon^{\alpha\beta A} \epsilon_{ijA} . \quad (1)$$

We have explicitly displayed color (α, β) , flavor (i, j) , and spinor (a, b) indices. The A -index is summed and therefore links color and flavor. We have used a two-component spinor notation; note that properly the right-helicity fields should involve dotted spinors. The important information conveyed by the

spinors is that the condensation does not violate rotational invariance. The relative minus sign between left-helicity and right-helicity condensates signifies that the ground state is a scalar, rather than a pseudoscalar, so that parity is unbroken. The magnitude of the condensate depends on the magnitude of the 3-momentum \vec{p} . In weak coupling, it is largest for $|\vec{p}|$ near the nominal (free-particle) Fermi surface.

Many different treatments have shown that a condensate of the form (1) is the dominant condensate in three-flavor QCD.^{7,9,10,11,12} The essential physical argument that favors this pattern is that, by leaving the maximal unbroken symmetry group, this pattern allows quarks of all three colors and all three flavors to pair.⁷ Less symmetric condensates in which not all quarks pair do not lower the free energy as much as the “maximal” choice (1).^{10,12}

In reality, condensation in the color $\bar{\mathbf{3}}$ channel (1) induces a small but nonzero condensate in the color $\mathbf{6}$ channel even if the interaction is repulsive in this channel,⁷ because this additional condensation breaks no further symmetries.¹³ This means that the right hand side of (1) is slightly more complicated and should, in fact, be written in terms of two gap parameters κ_1 and κ_2 , as $\kappa_1(p^2)\delta_a^\alpha\delta_b^\beta + \kappa_2(p^2)\delta_b^\alpha\delta_a^\beta$. The pure color $\bar{\mathbf{3}}$ condensate displayed in (1) has $\kappa_2 = -\kappa_1$. Using (1) is a good approximation because the induced color $\mathbf{6}$ condensate is much smaller than the dominant color $\bar{\mathbf{3}}$ condensate mandated by the attraction in this channel.^{7,10,11}

We can now explain the term “color-flavor locking”. Writing $\epsilon^{\alpha\beta A}\epsilon_{abA} = \delta_a^\alpha\delta_b^\beta - \delta_b^\alpha\delta_a^\beta$, we see that the condensates (1) involve Kronecker delta functions that link color and flavor indices. These condensates transform nontrivially under separate color and flavor transformations. Neither color transformations nor flavor transformations, separately, are valid symmetries of the ground state. However, the delta functions *do* remain invariant if we simultaneously rotate both color and flavor. Thus these symmetries are locked together.

Pairing which locks two previously unrelated symmetries is not a new phenomenon. The condensate for the color-flavor locked state of QCD perhaps most directly resembles that found in the B phase of superfluid helium 3. In an ordinary nonrelativistic system, orbital and spin rotations are separate symmetries. In the B phase, however, a condensate of pairs of atoms formed at the Fermi surface transforms nontrivially under spin and orbital rotations but is invariant under simultaneous rotations of both: it locks spin and orbital rotations. Another analogy is to the physics of chiral symmetry breaking in the QCD vacuum. There, the formation of a condensate of left-handed quarks and right-handed antiquarks locks the $SU(3)_L$ and $SU(3)_R$ flavor symmetries.

All the main qualitative properties of the color-flavor locked state are direct consequences of (1), properly interpreted. Elucidation of these consequences will occupy us for the remainder of the Section.

2.2 Symmetry Breaking

An aspect of (1) that might appear troubling at first sight is its lack of gauge invariance. This actually turns out to be a profound advantage.

There are powerful general arguments that local gauge invariance cannot be broken.¹⁴ Indeed, local gauge invariance is really a tautology, stating the redundancy of variables. Yet its “breaking” is central to two of the most successful theories in physics, namely BCS superconductivity theory and the standard model of electroweak interactions. In BCS theory we postulate a nonzero vacuum expectation value for the Cooper pair field, which is electrically charged. In the electroweak standard model we postulate a nonzero value for the Higgs field, which violates both the weak isospin $SU(2)$ and the hypercharge $U(1)$ gauge symmetries.

In each case, we should interpret the condensate as follows. We are working in a gauge theory at weak coupling. It is then very convenient to fix a gauge, because after we have done so — but not before! — the gauge potentials in which we perturb will make only small fluctuations around zero. Of course at the end of any calculation we must restore the gauge symmetry, by averaging over the gauge fixing parameters. Only gauge-invariant results will survive this averaging. However, in the intermediate steps, within a fixed gauge, one can capture important correlations that characterize the ground state by specifying the existence of nonzero condensates relative to the ambient gauge. In superconductivity, the essence of the physics is the correlation in the fermionic wave function which describes the Cooper pairs, and the resulting modification of the dispersion relations which describe the excitation spectrum. In particular, the gap in the spectrum of fermionic excitations at the Fermi surface is a gauge invariant quantity. Describing this physics within a fixed gauge as a condensate which “breaks” the gauge symmetry is a convenient fiction.

In the standard electroweak model one employs a nonzero vacuum expectation value for a Higgs doublet field $\langle \phi^a \rangle = v \delta_1^a$, which is not gauge invariant. One might be tempted to use the magnitude of its absolute square, which is gauge invariant, as an order parameter to characterize the symmetry breaking. However, $\langle \phi^\dagger \phi \rangle$ never vanishes, whether or not any symmetry is broken. In fact there can be no gauge invariant order parameter for the electroweak phase transition, since it has long been known that one can, by allowing the $SU(2)$ gauge couplings to become large, go over into a “confined” regime, encountering no sharp phase transition along the way.¹⁵ The absence of massless gauge bosons and of long-range forces is the essence of the Meissner-Anderson-Higgs effect — and it is also the essence of confinement!

So evidently, when used with care, the notion of spontaneous gauge symmetry breaking can be an *extremely* convenient fiction. In particular, by forging a connection with superconductivity and condensate formation, it brings

the universality class of confinement down to earth, and makes it accessible to weak coupling methods. These condensates need not break any true (i.e. global) symmetries. If a global symmetry *is* broken, some combination of the condensates themselves is a gauge invariant physical observable, and not just a convenient fiction.

With this discussion in mind, let us consider the consequences of (1) for symmetries.⁷ (See also Ref. 16 in which this ordering was considered at zero density.)

The exact microscopic symmetries of QCD with three massless flavors are

$$G_{\text{microscopic}} = SU(3)_{\text{color}} \times SU(3)_L \times SU(3)_R \times U(1)_B, \quad (2)$$

where the first factor is the (local) vector color gauge symmetry, the second and third factors are global chiral flavor symmetries, and the fourth factor is baryon number. (For the present, we set the electromagnetic coupling constant to zero, and therefore neglect the fact that the $U(1)$ subgroup of $SU(3)_L \times SU(3)_R$ which describes electromagnetism is in fact a local symmetry.)

The color-flavor locked phase (1) features two condensates, one involving left-handed quarks alone and one involving right-handed quarks alone. The former locks $SU(3)_L$ flavor rotations to $SU(3)_{\text{color}}$: the condensate is not symmetric under either alone, but is symmetric under simultaneous $SU(3)_{L+\text{color}}$ rotations. Similarly, the condensate involving right-handed quarks alone locks $SU(3)_R$ flavor rotations to $SU(3)_{\text{color}}$. As a consequence, of all the symmetries in $G_{\text{microscopic}}$, only the subgroup

$$G_{\text{CFL}} = SU(3)_{\text{color}+L+R} \times Z_2 \quad (3)$$

leaves the correlated ground state (1) invariant. The color and chiral flavor symmetries are broken, by color-flavor locking, down to the (global) vector “diagonal” symmetry, that makes equal transformations in all three sectors – color, left-handed flavor, and right-handed flavor. Baryon number symmetry is broken down to a discrete Z_2 symmetry under which all quark fields are multiplied by -1 . Even though the condensates in (1) do not *appear* to lock $SU(3)_L$ to $SU(3)_R$, they manage to do so by locking both to $SU(3)_{\text{color}}$. Color-flavor locking, therefore, provides a mechanism by which chiral symmetry can be broken.

The spontaneous breaking of chiral symmetry is a familiar phenomenon in zero-density QCD. Here, at high density, it occurs by a rather different mechanism. In zero-density QCD chiral symmetry breaking is due to condensation of left-handed quarks with right-handed antiquarks. The pairing of opposite helicities, of course, breaks chiral symmetry. Here we have only pairing of left-handed quarks with left-handed quarks, and right-handed quarks with right-handed quarks. Nevertheless chiral symmetry is broken indirectly, as we have described.

Now we must mention explicitly a general formal consequence of symmetry breaking, that we glided over earlier. That is, the form of the condensate in (1) is not unique. There are states with equally good energy where the correlated ground state is subjected to the action of any transformation in $G_{\text{microscopic}}$. This action will in general (except for elements of G_{CFL}) alter the form of the condensate. So there is a manifold of distinct vacua associated with the broken symmetries. By interpolating among these vacua, with small space-time gradients, one produces low-energy excitations around a fixed, reference ground state such as the one specified by (1).

The significance of such states is familiar from other contexts. When the broken symmetry is a global symmetry, they lead to Nambu-Goldstone particles. When the broken symmetry is a local gauge symmetry, the Meissner-Anderson-Higgs mechanism is triggered, and the would-be Nambu-Goldstone particles become the longitudinal parts of massive gauge fields.

Here the local color symmetry has been broken completely. Thus all the gluons acquire mass. This result has a major positive consequence for the logical status of our analysis. It removes the possibility of infrared divergences associated with gluon exchange. Similarly, the existence of an energy gap for all the quarks removes the other potential source of infrared divergences, from integration over low-energy excitations around the Fermi surface. Altogether, then, weak coupling perturbation theory *around the correct, condensed ground state* is free of the difficulties that appeared around the naive ground state.

The spontaneous violation of baryon number is perhaps less familiar to a particle physicist. On first hearing, one might think this is a dramatic or even catastrophic prediction, since we know that baryonic matter in the Universe is stable over very long periods of time. That is obviously too naive an interpretation, however, since in the theory of ordinary superconductors we deal with electron pairing without worrying over the violation of lepton number, and in the theory of helium superfluids we deal with condensates of atoms or diatoms, which formally violate both baryon and lepton number. Finally, and (as we shall see below) most directly to the point, ordinary nuclear matter is a superfluid in which nucleon-nucleon pairing violates baryon number symmetry.

In all these cases, if we are dealing with a finite sample of the superconductor or superfluid, there is no true violation of the conservation laws. Indeed, we may draw a surface surrounding the sample, and apply Gauss' law to the equation of current conservation (modified, within the sample, to include the condensate) in the usual way to see that changes in the bulk quantum numbers are accompanied by appropriate compensating fluxes. The correct interpretation of the formal "violation" of these symmetries is that there can be large fluctuations and easy transport of the corresponding quantum numbers within the sample. These are precisely the phenomena of superconductivity and superfluidity. The mathematical connection between broken symmetry

and super-transport is quite direct: As we have discussed, the symmetry breaking order parameter can point in any one of a manifold of “directions”; the supercurrents are carried by spatial variation in the “direction” of the condensate; that is, the phenomenon of superfluidity is a direct manifestation of the Nambu-Goldstone mode associated with the spontaneous breaking of a global symmetry; similarly, superconductivity is a direct manifestation of the mode which becomes the longitudinal component of a massive gauge boson and is thus a direct manifestation of the breaking of a gauge symmetry.

As already mentioned, the standard Higgs mechanism in the electroweak sector of the standard model has no gauge-invariant order parameter. With color-flavor locking the situation is more fortunate, because global as well as gauge symmetries are broken. Physically, this implies that there are sharp differences between the color-flavor locked phase and the quark-gluon plasma phase (in which all symmetries of the QCD lagrangian are unbroken), so that any passage between them must be marked by one or more phase transitions. In fact, it is a simple matter to abstract gauge invariant order parameters, which have a strict meaning valid at any coupling, from our primary, gauge variant condensate at weak coupling. For instance, to form a gauge invariant order parameter capturing chiral symmetry breaking we may take the product of the left-handed version of (1) with the right-handed version and saturate the color indices, to obtain

$$\langle \psi_{Li}^\alpha \psi_{Lj}^\beta \bar{\psi}_{R\alpha}^k \bar{\psi}_{R\beta}^l \rangle \sim \langle \psi_{Li}^\alpha \psi_{Lj}^\beta \rangle \langle \bar{\psi}_{R\alpha}^k \bar{\psi}_{R\beta}^l \rangle \sim \Delta^2 \epsilon_{ijm} \epsilon^{klm} . \quad (4)$$

Likewise we can take a product of three copies of the condensate and saturate the color indices, to obtain a gauge invariant order parameter for the baryon-number violating superfluid order parameter. These secondary order parameters will survive gauge unfixing unscathed. Unlike the primary condensate, from which they were derived, they are more than convenient fictions.

If we turn on a common mass for all the quarks, the chiral $SU(3)_L \times SU(3)_R$ flavor symmetry of $G_{\text{microscopic}}$ will be reduced to the diagonal $SU(3)_{L+R}$. If we turn on unequal masses, the symmetry will be even less. In any case, however, the $U(1)$ of baryon number a good microscopic symmetry, and the corresponding six-quark order parameter remains a strict signature of the color-flavor locked phase, distinguishing it both from the quark-gluon plasma phase, and from some other states of quark matter we shall encounter in Section 3.

As it stands the order parameter (4) is not quite the usual one, but roughly speaking its square. It leaves invariant an additional Z_2 , under which only the left-handed quark fields change sign. Actually this Z_2 is not a legitimate symmetry of the full theory, but suffers from an anomaly. So we might expect that the usual chiral order parameter is induced by the anomalous interactions that violate the axial baryon number symmetry of the classical Lagrangian. To put this another way, because axial baryon number is not a symmetry of QCD,

once chiral symmetry is broken by color-flavor locking there is no symmetry argument precluding the existence of an ordinary chiral condensate. Indeed, instanton effects do induce a nonzero $\langle \bar{\psi}_R \psi_L \rangle$ because the instanton-induced interaction is a six-fermion operator which can be written as a product of $\bar{\psi}_R \psi_L$ and the operator in (4) which already has a nonzero expectation value,⁷ but this turns out to be a small effect.^{9,10}

At weak coupling, we can be more specific about these matters. The most important interactions near the Fermi surface, quantitatively, arise from gluon exchange. These are responsible for the primary condensation. The instanton interaction is much less important asymptotically because the gauge fields which make up the instantons themselves are screened, the effects of instantons are intrinsically smaller for more energetic quarks, and because the instanton-induced interaction involves six fermion fields, and hence (one can show) becomes irrelevant upon renormalization toward the Fermi surface. The instanton interaction is qualitatively important, however, because it represents the leading contribution to axial baryon number violation. It is only such $U(1)_A$ violating interactions that remove the degeneracy among states with different relative phases between the left- and right-handed condensates in (1). In the absence of intrinsic $U(1)_A$ breaking, the spontaneous violation of this symmetry in the color-flavor locked phase would be accompanied by the existence of a pseudoscalar $SU(3)_{\text{color}+L+R}$ singlet Nambu-Goldstone bosons. Since the intrinsic violation of this symmetry is parametrically small, the corresponding boson will not be strictly massless, but only very light. Quantum fluctuations in this light η' -field, among other things, will keep the conventional chiral symmetry breaking order parameter small compared to (4) at high density.

2.3 Elementary Excitations

The physics of the excitations in the CFL phase has been the focus of much recent work.^{7,8,13,17,9,18,19,20,10,11,12,21,22,23,24,25,26,27,28,29,30,31,32,33,34,35} There are three sorts of elementary excitations. They are the modes produced directly by the fundamental quark and gluon fields, and the collective modes associated with spontaneous symmetry breaking. These modes can be classified under the unbroken $SU(3) \times Z_2$ symmetry, and the unbroken rotation and parity symmetries.

The quark fields of course produce spin 1/2 fermions. Some of these are true long-lived quasiparticles, since there are no lighter states of half-integer spin that they might decay into. With the conventions we have been using, as expressed in (1), the quark fields are triplets and antitriplets under color and flavor, respectively. Thus they decompose into an octet and a singlet under the diagonal $SU(3)_{\text{color}+L+R}$. There is an energy gap for production of pairs

above the ground state. More precisely, there are two gaps: a smaller one for the octet, and a larger one for the singlet.⁷ The dispersion relations describing these fermionic quasiparticle excitations in the CFL phase have been described in some detail.^{13,20,34}

The gluon fields produce an $SU(3)_{\text{color}+L+R}$ octet of spin 1 bosons. As previously mentioned, they acquire a common mass by the Meissner-Anderson-Higgs mechanism. The quantitative expressions for the masses of these vector mesons which have been computed at weak coupling^{21,36,28,34} and in an instanton-liquid model.³⁷

The fermionic excitations have a gap; the vector mesons have mass; but, the Nambu-Goldstone bosons are massless. These bosons form a pseudoscalar octet associated with chiral symmetry breaking, and a scalar singlet associated with baryon number superfluidity. The octet, but not the singlet, will be lifted from zero mass if the quarks are massive. Finally there is the parametrically light, but never strictly massless, pseudoscalar singlet associated with $U(1)_A$ breaking.

The Nambu-Goldstone bosons arising from chiral symmetry breaking in the CFL phase are Fermi surface excitations in which the orientation of the left-handed and right-handed diquark condensates oscillate out of phase in flavor space. The effective field theory describing these oscillations has been constructed.^{19,21,26} Up to two derivatives, it is given by

$$\mathcal{L}_{\text{eff}} = \frac{f_\pi^2}{4} \text{Tr} \left(\partial_0 \Sigma \partial_0 \Sigma^\dagger + v_\pi^2 \partial_i \Sigma \partial^i \Sigma^\dagger \right) - c \left(\det M \text{Tr} (M^{-1} \Sigma) + \text{h.c.} \right) . \quad (5)$$

The Nambu-Goldstone boson field matrix Σ is a color singlet and transforms under $SU(3)_L \times SU(3)_R$ as $\Sigma \rightarrow U_L \Sigma U_R^\dagger$ as usual. $M = \text{diag}(m_u, m_d, m_s)$ is the quark mass matrix. The construction of Σ from rotations of the CFL condensates can be found in Refs. 19,21: one first finds the 19 putative Nambu-Goldstone bosons expected when $G_{\text{microscopic}}$ is broken to G_{CFL} ; one then identifies 8 of these which become the longitudinal parts of massive vector bosons; the remaining ten are the octet described by (5), the singlet η' and the superfluid mode. See Refs. 19,21 for the singlet terms in the effective Lagrangian. The higher derivative terms in the effective Lagrangian have also been analyzed.²⁶ It has also been suggested that once higher derivative interactions are introduced, the effective theory may support Skyrmions, in which the Nambu-Goldstone boson field configuration has nonzero winding number.¹⁸ These solitons have energies comparable to the gap,³⁵ and are an alternative description of the gapped fermionic excitations in the CFL phase, in the same sense that baryons can alternatively be described as Skyrmions of the vacuum pion field.

The masses of the pseudoscalar mesons which are the pseudo-Nambu-Goldstone bosons associated with chiral symmetry breaking can be obtained

from \mathcal{L}_{eff} of (5).²¹ For example,

$$m_{\pi^\pm}^2 = \frac{2c}{f_\pi^2} m_s (m_u + m_d) , \quad m_{K^\pm}^2 = \frac{2c}{f_\pi^2} m_d (m_u + m_s) . \quad (6)$$

Thus, the kaon is lighter than the pion, by a factor of $m_d/(m_u + m_d)$.²¹ Note that the effective Lagrangian is quadratic in M . This arises because L_{eff} respects the Z_2 symmetry under which only the left-handed quarks change sign.⁷ As we discussed in the previous section, this is almost a symmetry of the CFL phase: it would be a symmetry if instanton effects could be neglected.⁷ However, instanton effects generate a nonzero, but small, ordinary $\langle \bar{\psi}_R \psi_L \rangle$ condensate, which breaks the Z_2 ,^{7,9,10} and results in a contribution to the meson m^2 which is linear in M and which may be numerically significant.²⁴ The induced $\langle \bar{\psi}_R \psi_L \rangle$ was significantly overestimated in Refs. ^{9,10}, however:³⁰ Making the already small $\langle \bar{\psi}_R \psi_L \rangle$ even smaller will significantly reduce the Z_2 -violating contributions to the meson masses.

If we were describing pions in vacuum, or pions in nuclear matter, the only way to obtain the coefficients in the effective theory would be to measure them in an experiment or, if possible, to calculate them on the lattice. Indeed in any theory with strong interactions, the purpose of writing an effective theory for the low energy degrees of freedom is to express the predictions for many low energy processes in terms of a few parameters, which must be obtained from experiment. In the color-flavor locked phase, however, the full theory is weakly coupled at asymptotically high densities. In this regime, therefore, the coefficients f_π^2 , v_π^2 and c are calculable from first principles using weak coupling methods! Up to possible logarithmic corrections, the result is^{21,22,23,24,25,27,33,34}

$$f_\pi^2 = \frac{21 - 8 \log 2}{36\pi^2} \mu^2 , \quad v_\pi^2 = \frac{1}{3} , \quad c = \frac{3\Delta^2}{2\pi^2} . \quad (7)$$

The electromagnetic^{29,33} and nonzero temperature³³ corrections to these quantities have also been calculated.

Quantitatively, (see Section 4 for a discussion of estimates of Δ) we estimate that the lightest pseudoscalar meson, the kaon, has a mass in the range of 5 to 20 MeV at $\mu = 400$ MeV, and becomes lighter still at higher densities. There are two reasons why the Nambu-Goldstone bosons are so much lighter in the CFL phase than in the vacuum. First, their mass² is proportional to m_{quark}^2 rather than to m_{quark} , as at zero density. In addition, there is a further suppression by a factor of Δ/μ , which arises because the Nambu-Goldstone bosons are collective excitations of the condensates formed from particle-particle and hole-hole pairs near the Fermi surface, whereas the quark mass term connects particles with antiparticles, far from the Fermi surface.²³

In QCD with unequal quark masses, at very high densities the CFL phase is much as we have described it, except that the gaps associated with $\langle us \rangle$, $\langle ds \rangle$ and $\langle ud \rangle$ pairing will differ slightly, the Fermi momenta for the different quark flavors may differ slightly,³⁸ and there may therefore be a small electron chemical potential μ_e . (We discuss lower densities, where the differences between Fermi momenta become comparable to Δ , in Section 3.) Because the strange quarks are less numerous due to their greater mass, it would seem that the requirement of overall charge neutrality can only be satisfied if $\mu_e > m_e$ and there is a nonzero density of electrons. Schäfer has recently noted, however, that if $\mu_e > m_{K^-}$, charge neutrality will be achieved by the formation of a condensate of K^- bosons, rather than by the formation of a small Fermi sphere of electrons.³⁰ The CFL condensate rotates in the K^- direction, relative to the direction favored by the quark mass term in the effective Lagrangian. This costs energy, but because it introduces a negative electric charge it is free-energetically favored, if $\mu_e > m_{K^-}$.

The formation of a kaon condensate in the CFL phase changes none of its symmetries. In this sense, it is a less dramatic effect than the formation of a kaon condensate in nuclear matter made of neutrons and protons only:³⁹ there, kaon condensation breaks $U(1)_S$. This symmetry is already broken in the CFL phase. Kaon condensation in the CFL phase is more akin to kaon condensation in hypernuclear matter made up of equal measures of all the octet baryons, in which $U(1)_S$ is already broken by hyperon-hyperon pairing. We shall elaborate much further on this connection in Section 2.5.

2.4 The Modification of Electromagnetism

It is physically significant, and proves extremely instructive, to consider the effect of color-flavor locking on the electromagnetic properties of high-density hadronic matter.

To do this, we consider coupling in the appropriate additional $U(1)_{\text{EM}}$ gauge field A_μ , representing the photon. This couples to u, d, s quarks with strength $\frac{2}{3}e, -\frac{1}{3}e, -\frac{1}{3}e$, respectively. Evidently this $U(1)_{\text{EM}}$ symmetry is broken by the condensate (1), through the terms pairing differently-charged quarks. Were this the complete story, the color-flavor locked phase would be an electromagnetic superconductor. The truth is far different, however.

The situation is analogous to what occurs in the electroweak sector of the standard model. There, the Higgs field condensate breaks both the original weak $SU(2)$ and the hypercharge $U(1)$. However, one linear combination of these symmetries leaves the condensate invariant, and remains a valid gauge symmetry of the ground state. Indeed, this is how we identify electromagnetism within the standard model.

Here we must similarly consider the possibility of mixing broken color

$SU(3)$ and (original) electromagnetic $U(1)_{\text{EM}}$ generators to find a valid residual symmetry. Indeed, we should expect this to occur, by the following argument. In QCD with three flavors, $U(1)_{\text{EM}}$ is a subgroup of $SU(3)_{L+R}$. When we neglected electromagnetism, we found that in the color-flavor locked phase $SU(3)_{L+R}$ is broken but $SU(3)_{\text{color}+L+R}$ is an unbroken global symmetry. We therefore expect that gauging a $U(1)$ subgroup of $SU(3)_{L+R}$ must correspond, in the CFL phase, to gauging a $U(1)$ subgroup of the unbroken $SU(3)_{\text{color}+L+R}$.

Once we are alerted to this possibility, it is not difficult to identify the appropriate combination of the photon and gluons which remains unbroken.^{7,40} The unbroken $U(1)$ is generated by

$$\tilde{Q} = Q + \eta T_8 \quad (8)$$

with $\eta = 1/\sqrt{3}$. Q is the conventional electromagnetic charge generator and T_8 is associated with one of the gluons. In the representation of the quarks,

$$\begin{aligned} Q &= \text{diag}\left(\frac{2}{3}, -\frac{1}{3}, -\frac{1}{3}\right) \quad \text{in flavor } u, d, s \text{ space,} \\ T_8 &= \frac{1}{\sqrt{3}} \text{diag}(-2, 1, 1) \quad \text{in color } r, g, b \text{ space.} \end{aligned} \quad (9)$$

As is conventional, we have taken $\text{tr}(T_8 T_8) = 2$. By construction, the \tilde{Q} -charges of all the Cooper pairs in the condensate (1) are zero. (For example, with these conventions, red up quarks pair only with green down or blue strange quarks, and both these pairs have $\tilde{Q} = 0$ in sum.) The condensate is \tilde{Q} -neutral, the $U(1)$ symmetry generated by \tilde{Q} is unbroken, and the associated \tilde{Q} -photon will remain massless. To see exactly which gauge field remains unbroken, look at the covariant derivative of the condensate,

$$D_\mu \langle q_a^\alpha q_b^\beta \rangle = \left(\partial_\mu + e A_\mu Q + g G_\mu^8 T_8 \right) \langle q_a^\alpha q_b^\beta \rangle. \quad (10)$$

The kinetic term $|D \langle q_a^\alpha q_b^\beta \rangle|^2$ will give a mass to one gauge field

$$A_\mu^X = \frac{-\eta e A_\mu + g G_\mu^8}{\sqrt{\eta^2 e^2 + g^2}} = -\sin \alpha_0 A_\mu + \cos \alpha_0 G_\mu^8, \quad (11)$$

while the orthogonal linear combination

$$A_\mu^{\tilde{Q}} = \frac{g A_\mu + \eta e G_\mu^8}{\sqrt{\eta^2 e^2 + g^2}} = \cos \alpha_0 A_\mu + \sin \alpha_0 G_\mu^8 \quad (12)$$

is the \tilde{Q} -photon which remains massless. That is, $B^{\tilde{Q}}$ satisfies the ordinary Maxwell equations while B^X experiences a Meissner effect. The denominators

arise from keeping the gauge field kinetic terms correctly normalized, and we have defined the angle α_0 which specifies the unbroken $U(1)$ via

$$\cos \alpha_0 = \frac{g}{\sqrt{\eta^2 e^2 + g^2}}. \quad (13)$$

The mixing angle α_0 is the analogue of the Weinberg angle in electroweak theory, in which the presence of the Higgs condensate causes the A_μ^Y and the third $SU(2)_W$ gauge boson to mix to form the photon, A_μ , and the massive Z boson. At accessible densities the gluons are strongly coupled ($g^2/(4\pi) \sim 1$), and of course the photons are weakly coupled ($e^2/(4\pi) \approx 1/137$), so $\alpha_0 \simeq \eta e/g$ is small. The “rotated photon” consists mostly of the usual photon, with only a small admixture of the T_8 gluon.

Let us now consider the charges of all the elementary excitations which we enumerated in Section 2.3. For reference, the electron couples to $A_\mu^{\tilde{Q}}$ with charge

$$\tilde{e} = \frac{eg}{\sqrt{\eta^2 e^2 + g^2}}. \quad (14)$$

which is less than e because the electron couples only to the A_μ component of $A_\mu^{\tilde{Q}}$. Now in computing the \tilde{Q} -charge of the quark with color and flavor indices α, a we must take the appropriate combination from

$$\frac{e(-\frac{2}{3}g, \frac{1}{3}g, \frac{1}{3}g) + g(\frac{2}{3}e, -\frac{1}{3}e, -\frac{1}{3}e)}{\sqrt{\eta^2 e^2 + g^2}}.$$

One readily perceives that the possible values are $0, \pm\tilde{e}$. Thus, in units of the electron charge, the quarks carry integer \tilde{Q} -charge! Quite remarkably, high-density QCD realizes a mathematically consistent gauge theory version of the old vision of Han and Nambu: the physical quark excitations have integer electric charges that depend on an internal color quantum number!

Similarly, the gluons all have \tilde{Q} -charges $0, \pm\tilde{e}$. Indeed, they have the \tilde{Q} -charges one would expect for an octet of massive vector bosons. The Nambu-Goldstone bosons arising from the breaking of chiral symmetry, of course, have the same charge assignments as the familiar π, K and η octet of pseudoscalars. The baryon superfluid mode is \tilde{Q} -neutral. In the color-flavor locked phase, we conclude, all the elementary excitations are integrally charged.^a This is a classic aspect of confinement, here embodied in a controlled, weak-coupling framework.

^aWe shall see in Section 3 that in two-flavor QCD, in which color-flavor locking does not occur, the color superconducting condensate which forms also leaves a \tilde{Q} -photon massless. The only difference relative to the CFL phase is that $\eta = -1/2\sqrt{3}$. (However, the \tilde{Q} -charges of the excitations are not all integral in this theory.)

It is fun to consider how a chunk of our color-flavor locked material would look. If the quarks were truly massless, then so would be some charged Nambu-Goldstone bosons, and one might expect a rather unusual “bosonic metal”, in which the low-energy electromagnetic response is dominated by these modes. As we mentioned in Section 2.3, turning on quark masses gives small masses to the Nambu-Goldstone bosons. Electromagnetic radiative corrections further lift the masses of the charged Nambu-Goldstone bosons. As a result, the color-flavor locked material becomes a transparent insulator, with no charged excitations at zero temperature. Altogether, a chunk of color-flavor locked material would resemble a diamond: an ordinary light wave incident upon it would be partially reflected, but some fraction would be admitted as a \tilde{Q} -light wave; the \tilde{Q} -light would travel through the transparent “diamond”, and would partially emerge and be partially internally reflected on the far side. Turning on small but unequal quark masses mars the diamond somewhat:³⁸ maintaining overall electric charge neutrality in this case will require either a nonzero electron density or a condensate of charged kaons,³⁰ and in either case, \tilde{Q} -light will have charged excitations off which to scatter.

Although a quantitative calculation of light reflecting off the facets of a CFL-diamond has not yet been done, the effect of a chunk of color superconducting quark matter (whether in the CFL phase or in the less symmetric phase in which only up and down quarks pair) on a static magnetic field has been described in complete detail.⁴⁰ Some fraction of an externally applied ordinary magnetic field penetrates the superconductor in the form of a \tilde{Q} -magnetic field, while some fraction of the ordinary magnetic field is expelled by the Meissner effect. The fraction of the field which is expelled depends both on α_0 and on the shape of the chunk color superconducting quark matter, but it is small when α_0 is small, as in nature. Most of the flux is admitted, as \tilde{Q} -flux. This \tilde{Q} -magnetic field satisfies Maxwell’s equations and is not restricted to flux tubes.

2.5 Quark-Hadron Continuity

The universal features of the color-flavor locked state: confinement, chiral symmetry breaking leaving a vector $SU(3)$ unbroken, and baryon number superfluidity, are exactly what one expects to find in nuclear matter in three-flavor QCD.⁸ Perhaps this is not immediately obvious in the case of baryon number superfluidity, but let us recall that pairing phenomena, which would go over into neutron superfluidity and proton superconductivity in nuclear matter, are very well established in ordinary nuclei. In three-flavor QCD, there are good reasons⁴¹ to think that the pairing interaction in the flavor singlet dibaryon channel (the so-called H -dibaryon channel) would be quite attractive in three-flavor QCD, and support a robust baryon number superfluidity. Thus, the

symmetries of the color-flavor locked phase are precisely those of nuclear matter in three-flavor QCD, perhaps better referred to as hypernuclear matter.⁸

Furthermore, there is an uncanny resemblance between the low-lying spectrum computed from first principles for QCD at asymptotically high density, and what one expects to find in hypernuclear matter, in a world with three degenerate quark flavors. It is hard to resist the inference that in this theory, there need be no phase transition between nuclear density and high density.⁸ There need be no sharp boundary between hypernuclear matter, where microscopic calculations are difficult but the convenient degrees of freedom are “obviously” hadrons, and the asymptotic high-density phase, where weak-coupling (but non-perturbative) calculations are possible, and the right degrees of freedom are elementary quarks and gluons, together with the collective Nambu-Goldstone modes. We call this quark-hadron continuity.⁸ Perhaps the least surprising aspect of this, by now, is the continuity between the pseudoscalar mesons at nuclear density and those at asymptotically high densities, since in both regimes these are present as a result of the breaking of the same symmetry. It might seem more shocking that a quark can go over continuously into, or “be”, a baryon, since baryons are supposed to contain three quarks, but remember that in the color-flavor locked phase the quarks are immersed in a diquark condensate, and so a one-quark excitation can pick two quarks up from (or lose to quarks to) the condensate at will. The difference between one and three is negotiable. What about the gluons? Within the color-flavor locked phase, similarly, they are quite literally the physical vector mesons. They are massive, as we have discussed, and have the right quantum numbers. Thus the original vision of Yang and Mills – who proposed non-abelian gauge theory as a model of ρ mesons – is here embodied.

Note that the hypothesis of continuity between hypernuclear and dense quark matter certainly does not preclude quantitative change. Far from it. The dispersion relation for a fermion — whether a quark in the CFL phase or a baryon in the hypernuclear phase — is characterized by a gap at the Fermi surface and by a gap at zero momentum, i.e. a mass. As a function of increasing density, gaps at the hyperon Fermi surfaces due to hyperon-hyperon pairing evolve continuously to become the gaps at the quark Fermi surfaces which characterize the color-flavor locked phase.¹³ During this evolution, the gaps are thought to increase significantly. In contrast, the gaps at zero momentum decrease dramatically with increasing density as they evolve from being of order the hyperon masses in hypernuclear matter to being of order the current quark masses at asymptotically high densities.

Note that in order for quark-hadron continuity to be realized, $U(1)_{EM}$ must not be broken by hyperon-hyperon pairing.¹³ At every point during the evolution of the theory as a function of increasing density, there will be an unbroken $U(1)$ and a massless \bar{Q} -photon and the excitations will be integer

charged. As the density is increased, however, the definition of the \tilde{Q} -photon in terms of the vacuum photon and gluon fields rotates. The ordinary photon rotates to become the \tilde{Q} -photon of the CFL phase, defined in (12). Turning to the massive vector bosons, in hypernuclear matter there is both an octet and a singlet. The singlet must become much heavier than the octet as a function of increasing density, since in the low energy description of the color-flavor locked phase one finds the octet alone. We see that if quark-hadron continuity is realized in QCD with three degenerate quarks, it requires various quantitative (but continuous) changes. What is remarkable is that it is even possible to imagine watching all the physical excitations of the theory evolving continuously as one dials the density up and goes from a strongly coupled hadronic world to a weak-coupling world of quarks and gluons.

If the quarks are massless, the Nambu-Goldstone bosons are massless in both hypernuclear and CFL quark matter, and in between. Once nondegenerate quark masses are introduced, however, the evolution of the Nambu-Goldstone masses as a function of increasing density becomes more intricate, as the kaon must go from being heavier than the pion to being lighter.

Note, finally, that the whole story becomes further complicated once the strange quark is made as heavy as in nature.^{13,17} Although the color-flavor locked phase is certainly obtained at asymptotically densities, where quark masses are neglectable, the nuclear matter phase, made of neutrons and protons only, is not continuously connectable with the color-flavor locked phase. If quark-hadron continuity is to be realized in the phase diagram of nature, what must happen is that, as a function of increasing density, one first goes from nuclear matter to hypernuclear matter, with sufficiently high density that all the hyperons have similar Fermi surfaces. This first stage must involve phase transitions, as the symmetries of hypernuclear matter differ from those of ordinary nuclear matter. Then, as the density is increased further, the hypernuclear matter may evolve continuously to become CFL quark matter, with pairing among hyperons becoming CFL pairing among quarks.

We now have a description of the properties of the CFL phase and its excitations, in which much can be described quantitatively if the value of the gap Δ is known. We describe estimates of Δ in Section 4. First, however, we give a full description of the less symmetric variants of color superconductivity which arise in QCD with $N_f \neq 3$. Already, however, in our idealized world (in which we either have three degenerate quarks or such high densities that the quark mass differences can be neglected) let us pause to marvel at our theoretical good fortune. The color-flavor locked phase is a concrete realization of the idea of complementarity: the same phase of a gauge theory can be described simultaneously as one in which the gauge symmetry is spontaneously broken and as one in which color is confined.¹⁵ This means that it provides us with a weak-coupling laboratory within which we can study a confined phase

from first principles at weak coupling. It is furthermore a phase of QCD wherein the physics of chiral symmetry breaking — indeed all the parameters of the chiral effective Lagrangian and all known or conjectured phenomena of the pseudoscalar meson sector, including kaon condensation — are amenable to controlled, weak-coupling calculation.

3 2SC and Other Variants

3.1 Two Flavors

In the previous Section, we have described quark matter in QCD with three degenerate flavors of light quarks. Nature is less symmetric, and in order to bracket nature we now describe the color superconducting phase in QCD with two flavors of light quarks. Pairs of quarks cannot be color singlets, and in QCD with two flavors of massless quarks the Cooper pairs form in the (attractive) color $\bar{\mathbf{3}}$ channel.^{3,4,5,6} The resulting $\langle \epsilon_{\alpha\beta\gamma} \psi_i^\alpha \psi_j^\beta \rangle$ condensate picks a color direction (in this case the 3 or blue direction), creates a gap Δ at the Fermi surfaces of quarks with the other two out of three colors (red and green), and breaks $SU(3)_{\text{color}}$ to an $SU(2)_{\text{color}}$ subgroup, giving mass to five of the gluons by the Anderson-Higgs mechanism. The masses of these vector bosons have been computed in the weak-coupling theory valid at asymptotically high densities,³⁶ and in an instanton liquid model.³⁷ Axial color is not a symmetry of the QCD action, but at asymptotically high densities where the QCD coupling g is weak, explicit axial color breaking is also weak. As a result, the pseudoscalar excitations of the condensate which would be Goldstone bosons arising from axial- $SU(3)_{\text{color}}$ to axial- $SU(2)_{\text{color}}$ breaking if g were zero may be rather light.⁴²

In QCD with two flavors, the Cooper pairs are $ud - du$ flavor singlets and the global flavor symmetry $SU(2)_L \times SU(2)_R$ is intact. There is also an unbroken global symmetry which plays the role of $U(1)_B$. Thus, no global symmetries are broken in this 2SC phase. This means that as a function of increasing density, there must be a phase transition between the hadronic and 2SC phases, at which chiral symmetry is restored. This phase transition is first order^{5,43,44,45} since it involves a competition between chiral condensation and diquark condensation.^{43,45}

Because no global symmetries are broken, there are no light scalar degrees of freedom in the 2SC phase. The 2SC phase is not a superfluid. The potentially light degrees of freedom are the gapless blue quarks, and the gauge bosons associated with unbroken gauge symmetries. The gluons associated with the unbroken $SU(2)_{\text{color}}$ will exhibit strong dynamics on long enough length scales; this aspect of the infrared physics of the 2SC phase is not under perturbative control. Thus, whereas in the CFL phase we expect that any physical quan-

tity can be obtained from a controlled weak-coupling calculation at sufficiently high density, this claim cannot be made for the 2SC phase. Note that the gapless blue quarks are neutral under $SU(2)_{\text{color}}$. As in the CFL phase, there is a massless abelian gauge boson, formed from a suitable linear combination of the photon and one of the eight original gluons. The two blue quarks have charges 0 and 1 under this unbroken, but rotated, \tilde{Q} -electromagnetism.

We expect that the blue quarks, left ungapped by the primary 2SC condensate, will find some way to pair in a higher angular momentum channel. Indeed, the instanton interaction pairs these quarks in a $J = 1$ condensate which breaks rotational invariance. Early work suggested that the associated gap is of order keV,⁵ but this estimate should be revisited.

It is interesting that both the 2SC and CFL phases satisfy anomaly matching constraints, even though it is not yet completely clear whether this must be the case when Lorentz invariance is broken by a nonzero density.⁴⁶ It is not yet clear how high density QCD with larger numbers of flavors,¹⁰ which we discuss below, satisfies anomaly matching constraints. Also, anomaly matching in the 2SC phase requires that the up and down quarks of the third color remain ungapped; this requirement must, therefore, be modified once these quarks pair to form a $J = 1$ condensate, breaking rotational invariance.⁵

3.2 Two+One Flavors

Nature chooses two light quarks and one middle-weight strange quark. If we imagine beginning with the CFL phase and increasing m_s , how do we get to the 2SC phase? This question has been answered in Refs. 13,17. A nonzero m_s weakens those condensates which involve pairing between light and strange quarks. The CFL phase requires nonzero $\langle us \rangle$ and $\langle ds \rangle$ condensates; because these condensates pair quarks with differing Fermi momenta they can only exist if the resulting gaps (call them Δ_{us} and Δ_{ds}) are larger than of order $m_s^2/2\mu$, the difference between the u and s Fermi momenta in the absence of pairing. This means that as a function of increasing m_s at fixed μ (or decreasing μ at fixed m_s) there must be a first order unlocking phase transition.^{13,17} The argument can be phrased thus: the 2SC and CFL phases must be separated by a phase transition, because chiral symmetry is broken in the CFL phase but not in the 2SC phase; suppose this transition were second order; this would require Δ_{us} and Δ_{ds} to be infinitesimally small but nonzero just on the CFL side of the transition; however, these gaps must be greater than of order $m_s^2/2\mu$; a second order phase transition is therefore a logical impossibility, either in mean field theory or beyond; the transition must therefore be first order. Note that the m_s that appears in these estimates is a density dependent effective strange quark mass, somewhat greater than the current quark mass.

Putting in reasonable numbers for quark matter which may arise in com-

pact stars, for $m_s = 200 - 300$ MeV and $\mu = 400 - 500$ MeV we find that the CFL phase is obtained if the interactions are strong enough to generate a gap Δ which is larger than about $40 - 110$ MeV, while the 2SC phase is obtained if Δ is smaller. As we shall see in the next section, $\Delta \sim 40 - 110$ MeV is within the range of current estimates and present calculational methods are therefore not precise enough to determine whether quark matter with these parameters is in the CFL or 2SC phases. At asymptotically high densities, however, the CFL phase is necessarily favored.

3.3 One Flavor

The remaining variant of color superconductivity which may arise in nature is that involving pairing between quarks of a single flavor. If m_s is too large for CFL pairing (i.e. m_s greater than of order $\sqrt{2\mu\Delta}$) but is nevertheless less than μ itself, the 2SC phase will include a nonzero density of strange quarks. Although, by hypothesis, these strange quarks do not pair with the light quarks, they can pair with each other, forming a $\langle ss \rangle$ condensate with angular momentum $J = 1$. This pairing has been analyzed in Ref. 47. (See also Ref. 48.) Interestingly, even though the Cooper pairs have $J = 1$, the condensate does not break rotational invariance.⁴⁷ The Cooper pairs are in the color $\mathbf{\bar{3}}$ channel, and the condensate locks color and spatial rotation: it leaves unbroken a global symmetry associated with simultaneous color and spatial rotation. The resulting gap is much smaller than the $J = 0$ 2SC and CFL gaps. It has been estimated to be of order hundreds of keV,⁴⁷ although applying results of Ref. 49 suggests a somewhat smaller gap, around 10 keV.

3.4 Four or More Flavors

We end this section with brief mention of four variants which are unphysical, but nevertheless instructive: QCD with more than three light flavors, QCD with two colors, QCD with many colors, and QCD with large isospin density and zero baryon density.

Dense quark matter in QCD with more than three flavors was studied in Ref. 10. The main result is that the color-flavor locking phenomenon persists: Condensates form which lock color rotations to flavor rotations, and the $SU(N_f)_L \times SU(N_f)_R$ group is broken down to a vector subgroup. Unlike with $N_f = 3$, however, the unbroken group is not the full $SU(N_f)_{L+R}$ which is unbroken in the vacuum. In the case of $N_f = 4$, for example, one finds $SU(4)_L \times SU(4)_R \rightarrow O(4)_{L+R}$ while in the case of $N_f = 5$, $SU(5)_L \times SU(5)_R \rightarrow SU(2)_{L+R}$.¹⁰ For $N_f = 4, 5$ as for $N_f = 3$, chiral symmetry is broken in dense quark matter. However, because the unbroken vector groups are smaller than $SU(N_f)_V$, there must be a phase transition between hadronic matter and dense

quark matter in these theories.¹⁰

If N_f is a multiple of three, the order parameter takes the form of multiple copies of the $N_f = 3$ order parameter, each locking a block of three flavors to color.¹⁰ All quarks are gapped in this phase, as in the $N_f = 3$ CFL phase. For $N_f = 6$, the resulting symmetry breaking pattern is $SU(6)_L \times SU(6)_R \rightarrow SU(3)_{L+R} \times U(1)_{L+R} \times U(1)_{L-R}$.¹⁰ The unbroken $SU(3)_{L+R}$ is a simultaneous rotation of both three flavor blocks for L and R and a global color rotation. Note that the unbroken $U(1)$'s are subgroups of the original $SU(6)$ groups: they correspond to vector and axial flavor rotations which rotate one three flavor block relative to the other. Note that for $N_f = 6$, unlike for $N_f = 3, 4, 5$, chiral symmetry is not completely broken at high density: an axial $U(1)$ subgroup remains unbroken. As the primary condensate we have just described leaves no quarks ungapped, there is no reason to expect the formation of any subdominant condensate which could break the unbroken chiral symmetry. Both because of this unbroken chiral symmetry and because the unbroken vector symmetry differs from that of the vacuum, there must be a phase transition between hadronic matter and dense quark matter in QCD with $N_f = 6$.¹⁰

3.5 Two Colors

The simplest case of all to analyze is QCD with two colors and two flavors. The condensate is antisymmetric in color and flavor, and is therefore a singlet in both color and flavor. Because it is a singlet in color, dense quark matter in this theory is not a color superconductor. Although the condensate is a singlet under the ordinary $SU(2)_L \times SU(2)_R$ flavor group, it nevertheless does break symmetries because the symmetry of the vacuum in QCD with $N_f = N_c = 2$ is enhanced to $SU(4)$. One reason why $N_c = 2$ QCD is interesting to study at nonzero density is that it provides an example where quark pairing can be studied on the lattice.⁵⁰ The $N_c = 2$ case has also been studied analytically in Refs. 6,51; pairing in this theory is simpler to analyze because quark Cooper pairs are color singlets. We refer the reader to these references for details.

3.6 Many Colors

The $N_c \rightarrow \infty$ limit of QCD is often one in which hard problems become tractable. However, the ground state of $N_c = \infty$ QCD is a chiral density wave, not a color superconductor.⁵² At asymptotically high densities, color superconductivity persists up to N_c 's of order thousands^{53,54} before being supplanted by the phase described in Ref. 52. At any finite N_c , color superconductivity occurs at arbitrarily weak coupling whereas the chiral density wave does not. For $N_c = 3$, color superconductivity is still favored over the chiral density wave (although not by much) even if the interaction is so strong that the color

superconductivity gap is $\sim \mu/2$.⁵⁵

3.7 QCD at Large Isospin Density

The phase of $N_c = 3$ QCD with nonzero isospin density ($\mu_I \neq 0$) and zero baryon density ($\mu = 0$) can be simulated on the lattice.⁵⁶ The sign problems that plague simulations at $\mu \neq 0$ do not arise for $\mu_I \neq 0$. Although not physically realizable, physics with $\mu_I \neq 0$ and $\mu = 0$ is very interesting to consider because phenomena arise which are similar to those occurring at large μ and, in this context, these phenomena are accessible to numerical “experiments”. Such lattice simulations can be used to test calculational methods which have also been applied at large μ , where lattice simulation is unavailable. At low isospin density, this theory describes a dilute gas of Bose-condensed pions. Large μ_I physics features large Fermi surfaces for down quarks and anti-up quarks, Cooper pairing of down and anti-up quarks, and a gap whose g -dependence is as in (108), albeit with a different coefficient of $1/g$ in the exponent.⁵⁶ This condensate has the same quantum numbers as the pion condensate expected at much lower μ_I , which means that a hypothesis of continuity between hadronic — in this case pionic — and quark matter as a function of μ_I . Both the dilute pion gas limit and the asymptotically large μ_I limit can be treated analytically; the possibility of continuity between these two limits can be tested on the lattice.⁵⁶ The transition from a weak coupling superconductor with condensed Cooper pairs to a gas of tightly bound bosons which form a Bose condensate can be studied in a completely controlled fashion.

4 Calculational Methods

In this Section we review the basic theoretical methods used to analyze color superconductivity. To keep the discussion within appropriate bounds, we shall concentrate on the methods used to characterize the ground state. The derivation of effective theories for the low-energy dynamics, electromagnetic response, and transport properties is of course predicated on identification of the ground state, but presents many additional points of interest as we have already seen in Section 2. In that Section, we deferred all discussion of methods by which the gap Δ , which characterizes the ground state, is calculated. Much effort has gone into calculating the magnitude of the gaps in the 2SC and CFL phases,^{4,5,6,7,13,17,43,57,58,59,45,60,9,61,62,63,64,65,66,11,12,67,68,69,70} and in this section we face up to the challenge of describing what has been learned.

It would be ideal if the calculation of the gap were within the scope of lattice gauge theory as is, for example, the calculation of the critical temperature on the vertical axis of the phase diagram. Unfortunately, lattice methods relying on importance sampling have to this point been rendered exponen-

tially impractical at nonzero baryon density by the complex action at nonzero μ . Various lattice methods *can* be applied for $\mu \neq 0$ as long as T/μ is large enough;⁷¹ so far, though, none have proved applicable at temperatures which are low enough that color superconductivity occurs. As we saw in the previous section, lattice simulations are possible in two-color QCD and in QCD at large isospin density. Finally, sophisticated algorithms have recently allowed theories which are simpler than QCD but which have as severe a fermion sign problem as that in QCD at nonzero chemical potential to be simulated.⁷² All of this bodes well for the future.

To date, in the absence of suitable lattice methods, quantitative analyses of color superconductivity have followed two distinct strategies. The first approach is utilitarian and semi-phenomenological, emphasizing the use of simplified models. This will occupy us in Sections 4.1-4.3. The overarching theme here is to define models which incorporate the salient physical effects, yet are tractable using known mathematical techniques of quantum many-body theory. Free parameters within a model of choice are chosen to give reasonable vacuum physics. Examples include analyses in which the interaction between quarks is replaced simply by four-fermion interactions with the quantum numbers of the instanton interaction^{5,6,43} or of one-gluon exchange,^{7,13} random matrix models,⁶⁷ and more sophisticated analyses done using the instanton liquid model.^{45,9,55} Renormalization group methods have also been used to explore the space of all possible effective four-fermion interactions.^{57,58} These methods yield results which are in qualitative agreement: the favored condensates are as described in Sections 2 and 3; the gaps range between several tens of MeV up to of order 100 MeV; the associated critical temperatures (above which the diquark condensates vanish) can be as large as about $T_c \sim 50$ MeV. This agreement between different models reflects the fact that what matters most is simply the strength of the attraction between quarks in the color $\bar{\mathbf{3}}$ channel, and by fixing the parameters of the model interaction to fit, say, the magnitude of the vacuum chiral condensate, one ends up with attractions of similar strengths in different models.

The second, more ambitious approach is fully microscopic. Such an approach is feasible, for high-density QCD, due to asymptotic freedom. Several important results have been obtained from the microscopic approach, perhaps most notably the asymptotic form of the gap.⁵⁹ Very significant challenges remain, however. It is not really known, for example, how to calculate corrections to the leading term in a systematic way. We review the microscopic approach in Sections 4.4-4.5.

These approaches have complementary virtues – simplicity versus rigor, openness to phenomenological input versus quantitative predictive power at asymptotically high density. Fortunately, they broadly agree in their main conclusions as to the patterns of symmetry breaking and the magnitude of the

gap at accessible densities of order $\mu = 400 - 500$ MeV.

4.1 Renormalization Toward the Fermi Surface

The adequacy of weak coupling for describing QCD at high density is by no means obvious. Our strategy will be to adopt it as a working hypothesis, bring out its consequences, and see whether we find a consistent picture. In doing this, we must consider how to work from the fundamental interactions in the perturbative, no-particle state (“Fock vacuum”), which are assumed to be simple, to the effective interactions in the dense medium.

To begin, let us focus on the quark degrees of freedom. In line with our announced strategy, we begin by approximating the ground state with filled Fermi spheres for all the quarks, with Fermi momentum p_F . The low-energy excitations then include states where some modes just below the nominal Fermi surfaces are vacant (hole modes) and some modes just above are occupied (particle modes). There is a continuum of such states. Moreover, states containing pairs of particle or hole modes with three-momenta $(\vec{p}, -\vec{p})$, for various values of the direction of \vec{p} but a common $|\vec{p}|$, are all degenerate. We are therefore faced with a system whose excitations have a large density of states (proportional to the area of the Fermi surface) which can be excited at arbitrarily small free energy cost (for pairs whose $|\vec{p}|$ is arbitrarily close to p_F .) In the absence of interaction, there would be nothing more to say. The effect of interactions, however, is to allow all pairs $(\vec{p}, -\vec{p})$ with a common $|\vec{p}|$ to scatter into one another, consistent with momentum conservation. Thus, we are perturbing a system with a continuum of excitations with arbitrarily low energies. In this situation, with large numbers of nearly degenerate states, straightforward perturbation theory can fail, even for weak coupling.

The Wilsonian renormalization group is often an appropriate tool for analyzing problems of this sort. Following this approach, one attempts to map the original problem onto a problem with fewer degrees of freedom, by integrating out the effect of the higher-energy (or, in a relativistic theory, more virtual) modes. Then one finds a new formulation of the problem, in a smaller space, with new couplings. In favorable cases the reformulated problem is simpler than the original, and one can turn around and solve it.

This use of the renormalization group is in the same spirit as that appropriate for the analysis of long wavelength physics at a second order phase transition, or the long wavelength physics of the QCD vacuum (a.k.a chiral perturbation theory.) In traditional perturbative QCD one runs the logic backwards. The fundamental short-distance theory, with nothing integrated out, is simple and weakly coupled. When one integrates out highly virtual modes, one finds that QCD becomes more strongly coupled. Thus, renormalization group methods are used in two distinct ways in vacuum QCD: first,

they inform us how the fundamentally simple theory of quarks and gluons comes to look complicated at low energy and, second, once rephrased in terms of the correct effective degrees of freedom relevant at low energies, they allow us to make predictions for low energy physics. Renormalization group methods are used in two analogous ways at high density. In this Section we shall use them to inform us at what free energy scale the theory based on the original quark degrees of freedom breaks down, signalling the formation of a gap and the need to switch to new degrees of freedom. These new degrees of freedom include the gapped quasiparticles, which can then be integrated out. If the gapped phase features massless or light Nambu-Goldstone boson excitations of the condensate then, as we have seen in Section 2, we can use renormalization group methods to make predictions for the physics of these effective degrees of freedom at momenta well below the gap.

In both chiral perturbation theory of the QCD vacuum and the Wilsonian effective theory appropriate at high density, one integrates out modes with large free energy, keeping only those with smaller and smaller free energy. In the vacuum, free energy is just energy and this corresponds to keeping modes with momenta closer and closer to zero. At high density, however, the modes with small free energy are those with momenta near the Fermi surface, and it is on these modes that the renormalization group focuses. The application of Wilsonian methods to physics at a Fermi surface was pioneered by Shankar⁷³ and Polchinski⁷⁴

Asymptotic freedom plays a foundational role in the analysis of QCD at asymptotically high density. It allows us to make it plausible that the fundamental couplings among the active modes, near the Fermi surface, are generically weak. Indeed, these modes involve large energy and momenta, and so scattering events which displace them by a fixed finite angle involve large momentum transfer, whereas scattering events with small angle should not much alter the physical properties of the state. This intuitive argument will be refined, and justified, in Section 4.4.

Granting that the fundamental coupling is weak, let us consider the consequences of integrating out modes whose free energy is between ϵ and $\delta\epsilon$ on the effective interactions among the remaining modes, which are those within a band in momentum space centered on the Fermi surface which have free energy less than $\delta\epsilon$. We will obtain renormalized couplings among the remaining modes, due to one-loop diagrams in which external legs are within $\delta\epsilon$ of the Fermi surface while loop momenta are between $\delta\epsilon$ and ϵ . This approach was first applied to high density QCD in Ref. 57 and was generalized in Ref. 58.

The first result of this analysis is that, in general, four-fermion, six-fermion and higher-order interactions are all suppressed as we approach the Fermi surface.^{73,74} This fixed point corresponds to Landau Fermi liquid theory. The only, and crucial, exceptions are those four-fermion operators that involve in-

volve particles or holes with equal and opposite three momenta. These allow pairs of particles on the Fermi surface to scatter, as mentioned above. For couplings G_η of this kind we find

$$\frac{dG_\eta}{d \ln \delta} = -\kappa_\eta G_\eta^2. \quad (15)$$

Here η is a catch-all label that might include color, flavor, angular momentum. The effective couplings will depend on all these indices. In general we will have a matrix equation, with couplings between the different channels (different values of η). But to bring out the main point, it is enough to consider the simplest possible case, with one channel, as we have done in (15). In this single channel calculation, a simple calculation shows that κ is positive. (Note that we have chosen a notation in which attractive interactions correspond to $G > 0$.) This evolution equation is quite simple to integrate, and we find

$$\frac{1}{G_\eta(\delta)} - \frac{1}{G_\eta(1)} = \kappa_\eta \ln \delta. \quad (16)$$

Thus we see that the qualitative behavior of $G_\eta(\delta)$ depends on the sign of $G_\eta(1)$. If this is negative, then as $\delta \rightarrow 0$ one finds that $G_\eta(\delta) \rightarrow 0$ from below. Repulsive interactions are thus irrelevant. On the other hand, if $G_\eta(1) > 0$ (indicating an attractive coupling) then $G_\eta(\delta)$ grows, and formally it diverges when

$$\delta = \exp\left(-\frac{1}{\kappa_\eta G_\eta(1)}\right). \quad (17)$$

Of course once the effective coupling becomes large the working equation (15), which neglects higher-order corrections, is no longer trustworthy. All we may legitimately infer from (17) is that an attractive interaction in any channel, however weak, will, by renormalization toward the Fermi surface, induce a strong effective coupling between particles with equal and opposite momenta, on opposite sides of the Fermi surface.

What we have done here is simply to rephrase Cooper's discovery of the pairing instability in modern language, suitable for generalization. Now let us apply it to four-fermion interactions of the type we expect to occur in QCD.

We will restrict ourselves to massless QCD, a spherical Fermi surface, and local operators invariant under the appropriate chiral symmetry. The cases of three and two flavors are rather different, and we will analyze them separately in turn.

Following Ref. 57, we take the basic four-fermion interactions in $N_f = 3$ QCD to be proportional to the operators

$$\begin{aligned} O_{LL}^0 &= (\bar{\psi}_L \gamma_0 \psi_L)^2, & O_{LR}^0 &= (\bar{\psi}_L \gamma_0 \psi_L)(\bar{\psi}_R \gamma_0 \psi_R), \\ O_{LL}^i &= (\bar{\psi}_L \gamma_i \psi_L)^2, & O_{LR}^i &= (\bar{\psi}_L \vec{\gamma} \psi_L)(\bar{\psi}_R \vec{\gamma} \psi_R). \end{aligned} \quad (18)$$

Each of these operators comes in two color structures, for example color symmetric and color anti-symmetric

$$(\bar{\psi}^a \psi^b)(\bar{\psi}^c \psi^d) (\delta_{ab}\delta_{cd} \pm \delta_{ad}\delta_{bc}). \quad (19)$$

Nothing essentially new emerges upon considering superficially different isospin structures, or different Dirac matrices. All such structures can be reduced to linear combinations of the basic ones (18), or their parity conjugates, by Fierz rearrangements. In total, then, we need to consider eight operators.

As discussed above, these operators are renormalized by quark-quark scattering in the vicinity of the Fermi surface. This means that both incoming and outgoing quarks have momenta $\vec{p}_1, \vec{p}_2 \simeq \pm \vec{p}$ and $\vec{p}_3, \vec{p}_4 \simeq \pm \vec{q}$ with $|\vec{p}|, |\vec{q}| \simeq p_F$. We set the external frequency to be zero. A graph with vertices Γ_1 and Γ_2 then gives⁵⁷

$$G_1 G_2 I (\Gamma_1)_{i' i} (\Gamma_1)_{k' k} \left[-(\gamma_0)_{ij} (\gamma_0)_{kl} - \frac{1}{3} (\vec{\gamma})_{ij} (\vec{\gamma})_{kl} \right] (\Gamma_2)_{jj'} (\Gamma_2)_{ll'} \quad (20)$$

with $I = \frac{i}{8\pi^2} \mu^2 \log(\delta)$. We will denote the density of states on the Fermi surface by $N = \mu^2 / (2\pi^2)$ and the logarithm of the scale as $t = \log(\delta)$. The renormalization group does not mix LL and LR operators, nor different color structures. This means that the evolution equations contain at most 2×2 blocks. A simple calculation now yields⁵⁷

$$\frac{d(G_0^{LL} + G_i^{LL})}{dt} = -\frac{N}{3} (G_0^{LL} + G_i^{LL})^2, \quad (21)$$

$$\frac{d(G_0^{LL} - 3G_i^{LL})}{dt} = -N (G_0^{LL} - 3G_i^{LL})^2, \quad (22)$$

$$\frac{d(G_0^{LR} + 3G_i^{LR})}{dt} = 0, \quad (23)$$

$$\frac{d(G_0^{LR} - G_i^{LR})}{dt} = -\frac{2N}{3} (G_0^{LR} - G_i^{LR})^2. \quad (24)$$

In this basis the evolution equations are already diagonal. The coupling $G_1 = G_0^{LL} + G_i^{LL}$ evolves as

$$G_1(t) = \frac{1}{1 + (N/3)G_1(0)t}, \quad (25)$$

with analogous results for the other operators. Note that the evolution starts at $t = 0$ and moves towards the Fermi surface as $t \rightarrow -\infty$. If the coupling is attractive at the matching scale, $G_1(0) > 0$, it will grow during the evolution, and reach a Landau pole at $t_c = 3/(NG_1(0))$. The location of the pole is controlled by the initial value of the coupling and the coefficient in the evolution

equation. If the initial coupling is negative, the coupling decreases during the evolution. The second operator in (21) has the largest coefficient and will reach the Landau pole first, unless the initial value is very small or negative. In that case, subdominant operators can come to cause the leading instability.

The form of the operators that diagonalize the evolution equations is readily understood.⁵⁸ First, order the operators according to the size of the coefficient in the evolution equations

$$O_{dom} = (\bar{\psi}_L \gamma_0 \psi_L)^2 - (\bar{\psi}_L \vec{\gamma} \psi_L)^2, \quad (26)$$

$$O_{sub,1} = (\bar{\psi}_L \gamma_0 \psi_L)(\bar{\psi}_R \gamma_0 \psi_R) - \frac{1}{3}(\bar{\psi}_L \vec{\gamma} \psi_L)(\bar{\psi}_R \vec{\gamma} \psi_R), \quad (27)$$

$$O_{sub,2} = (\bar{\psi}_L \gamma_0 \psi_L)^2 + \frac{1}{3}(\bar{\psi}_L \vec{\gamma} \psi_L)^2, \quad (28)$$

$$O_{mar} = (\bar{\psi}_L \gamma_0 \psi_L)(\bar{\psi}_R \gamma_0 \psi_R) + (\bar{\psi}_L \vec{\gamma} \psi_L)(\bar{\psi}_R \vec{\gamma} \psi_R). \quad (29)$$

Upon Fierz rearrangement we find

$$O_{dom} = 2(\psi_L C \psi_L)(\bar{\psi}_L C \bar{\psi}_L), \quad (30)$$

$$O_{sub,1} = \frac{1}{3}(\psi_L C \vec{\gamma} \psi_R)(\bar{\psi}_R C \vec{\gamma} \bar{\psi}_L) + \dots, \quad (31)$$

$$O_{sub,2} = \frac{4}{3}(\psi_L C \vec{\Sigma} \psi_L)(\bar{\psi}_L C \vec{\Sigma} \bar{\psi}_L), \quad (32)$$

$$O_{mar} = \frac{1}{2}(\psi_L C \gamma_0 \psi_R)(\bar{\psi}_R C \gamma_0 \bar{\psi}_L) + \dots \quad (33)$$

This demonstrates that the linear combinations in (26-29) correspond to simple structures in the quark-quark channel. (It also means that it might have been more natural to perform the whole calculation directly in a basis of diquark operators.)

The full structure of the (LR) operators is

$$O_{sub,1}, O_{mar} = (\psi C \gamma \tau_{S,A} \psi)(\bar{\psi} C \gamma \tau_{S,A} \bar{\psi}) + (\psi C \gamma \gamma_5 \tau_{A,S} \psi)(\bar{\psi} C \gamma \gamma_5 \tau_{A,S} \bar{\psi}),$$

where $\tau_{S,A}$ are symmetric, respectively anti-symmetric, flavor generators. Note that because these two structures have different flavor symmetry, the flavor structure cannot be factored out.

The dominant operator corresponds to the scalar diquark channel, while the subdominant operators contain vector diquarks. Note that one cannot decide which color channel is preferred from the evolution equation alone. To decide that question, we can appeal to the fact that “reasonable” interactions, including specifically one gluon exchange, will be attractive in the color anti-symmetric but repulsive in the color symmetric channel. Indeed, it is the color anti-symmetric configuration that minimizes the total color flux (and hence

field energy) emanating from the quark pair. If the color wave function is anti-symmetric, the dominant operator fixes the isospin wave function to be anti-symmetric as well.

The form of the dominant operator indicates the existence of potential instabilities, but does not itself indicate how they are resolved. The renormalization group analysis tells us the scale at which the dominant couplings get strong but, strictly speaking, tells us nothing more. In Sections 4.2 and 4.3, we shall see how to learn more, and in particular to confirm that the resolution of the instability is that a gap forms in the dominant attractive channel. Because the renormalization group methods do not allow us to directly describe the formation of the gap (although they indicate its magnitude) they cannot be used to confirm that color-flavor locking is favored. For this, a variational calculation is required as we shall describe in Section 4.2.

The dominant four-fermion operator in three-flavor QCD does not distinguish between scalar and pseudoscalar diquarks. Indeed, for $N_f \geq 3$ all four-quark operators consistent with chiral symmetry exhibit an accidental axial baryon symmetry, under which scalar and pseudoscalar diquarks are equivalent. For $N_f = 3$ this degeneracy is lifted by six-fermion operators,^{7,9,10} which are irrelevant operators in the sense of the renormalization group. In the microscopic theory, these operators will be induced by instantons. Their formal irrelevance does not imply that they are negligible physically, especially since they are the leading terms which break the residual axial baryon number symmetry.

Anticipating that the instability indicated by renormalization toward the Fermi surface is stabilized by the formation of a gap, we conclude that upon further renormalization the couplings cease to run. We therefore expect that, instead of running to zero, the instanton coupling remains at some finite value. Instantons have important physical effects in the condensed phase, even for $N_f = 3$,^{9,10} as already mentioned above. Specifically, they cause quark-antiquark pairs to condense, by inducing the “normal” chirality-violating order parameter (familiar at zero density) from the diquark-antidiquark condensate (which arose, in turn, as a secondary consequence of the primary diquark condensation). The resulting quark-antiquark condensate is very small.^{9,10} The instanton interaction also lifts the degeneracy between the scalar and pseudoscalar diquark condensates, favoring the scalar.

We turn now to QCD with two flavors. This requires us to take into account additional operators. At first hearing it might seem odd that with fewer flavors we encounter more possible interactions. It occurs because for $N_f = 2$, but not for larger values, two quarks of the same chirality can form a chiral $SU(2) \times SU(2)$ singlet. Related to this, for $N_f = 2$ we have $U(1)_A$ violating *four*-fermion operators. In the microscopic theory, these operators will be induced by instantons.

The new operators are

$$O_S = \det_f(\bar{\psi}_R \psi_L), \quad O_T = \det_f(\bar{\psi}_R \vec{\Sigma} \psi_L). \quad (34)$$

Both operators are determinants in flavor space. For quark-quark scattering, this implies that the two quarks have to have different flavors. The fact that the flavor structure is fixed implies that the color structure is fixed, too. For a given (qq) spin, only one of the two color structures contributes. Finally, both quarks have to have the same chirality, and the chirality is flipped by the interaction.

These considerations determine the structure of the evolution equations. Two left handed quarks can interact via one of the instanton operators, become right handed, and then rescatter through an anti-instanton, or through one of the $U(1)_A$ symmetric RR operators. The result will be a renormalization of the LL vertex in the first case, and a renormalization of the instanton in the second. Note that the flavor structure will always remain a determinant. Even though instantons generate all possible Dirac structures in (18), the color-flavor structure is more restricted.

Evidently, instantons do not affect the evolution of the LR couplings at all. The evolution equations of the LL couplings are modified to become (henceforth we drop the subscript LL):⁵⁸

$$\frac{dG_0}{dt} = \frac{N}{2} \left\{ -G_0^2 + 2G_0G_i - 5G_i^2 - K_S^2 + 2K_S K_T - 5K_T^2 \right\}, \quad (35)$$

$$\frac{dG_i}{dt} = \frac{N}{2} \left\{ \frac{1}{3}G_0^2 - \frac{10}{3}G_0G_i + \frac{13}{3}G_i^2 + \frac{1}{3}K_S^2 - \frac{10}{3}K_S K_T + \frac{13}{3}K_T^2 \right\}, \quad (36)$$

$$\frac{dK_S}{dt} = \frac{N}{2} \left\{ 2(-G_0 + G_i) K_S + 2(G_0 - 5G_i) K_T \right\}, \quad (37)$$

$$\frac{dK_T}{dt} = \frac{N}{2} \left\{ \frac{2}{3}(G_0 - 5G_i) K_S + \frac{2}{3}(-5G_0 + 13G_i) K_T \right\}. \quad (38)$$

These equations can be uncoupled in the form

$$\frac{dG_1}{dt} = -\frac{N}{3} (G_1^2 + K_1^2), \quad (39)$$

$$\frac{dK_1}{dt} = -\frac{2N}{3} G_1 K_1, \quad (40)$$

$$\frac{dG_2}{dt} = -N (G_2^2 + K_2^2), \quad (41)$$

$$\frac{dK_2}{dt} = -2N G_2 K_2, \quad (42)$$

where $G_1 = G_0 + G_i$, $K_1 = K_S + K_T$ and $G_2 = G_0 - 3G_i$, $K_2 = K_S - 3K_T$. The equations for G , K uncouple even further. We have

$$\frac{d(G_2 + K_2)}{dt} = -N (G_2 + K_2)^2, \quad (43)$$

$$\frac{d(G_2 - K_2)}{dt} = -N (G_2 - K_2)^2, \quad (44)$$

as well as the analogous equation for G_1 , K_1 .

The differential equations are now easily solved,⁵⁸ leading to

$$G_2(t) = \frac{1}{2} \left\{ \frac{1}{a + Nt} + \frac{1}{b + Nt} \right\}, \quad (45)$$

$$K_2(t) = \frac{1}{2} \left\{ \frac{1}{a + Nt} - \frac{1}{b + Nt} \right\}, \quad (46)$$

together with the analogous results for G_1 , K_1 . Here, $a, b = (G_2(0) \pm K_2(0))^{-1}$. We see that G_2 and K_2 will grow and eventually reach a Landau pole if either a or b is positive. The location of the pole is determined by the smaller of the values, $t_c = -a/N$ or $t_c = -b/N$. The same is true for G_1 and K_1 , but the couplings evolve more slowly, and the Landau pole is reached later.

At this level a number of qualitatively different scenarios are possible, depending on the sign and relative magnitude of $G(0)$ and $K(0)$.⁵⁸ (Henceforth we drop all subscripts.) If $G(0)$ and $K(0)$ are both positive then they will both grow, and the location of the nearest Landau pole is determined by $G(0) + K(0)$. The asymptotic ratio of the two couplings is 1. If $G(0)$ and $K(0)$ are both negative, and the magnitude of $G(0)$ is bigger than the magnitude of $K(0)$, then the evolution drives both couplings to zero. These are the standard cases. Attraction leads to an instability, and repulsive forces are suppressed.

More interesting cases arise when the sign of the two couplings is different. The case $G(0), K(0) < 0$ and $|K(0)| > |G(0)|$ is especially weird.⁵⁸ Both $G(0), K(0)$ are repulsive, but the evolution drives $G(0)$ to positive values. Both couplings reach a Landau pole, and near the pole their asymptotic ratio approaches minus one. Similarly, we can have a negative $G(0)$ and positive $K(0)$ with $K(0) > |G(0)|$. Again, the evolution will drive $G(0)$ to positive values.⁵⁸

The dominant and sub-dominant instanton operators are

$$O_{dom} = \det_f \left[(\bar{\psi}_R \psi_L)^2 - (\bar{\psi}_R \vec{\Sigma} \psi_L)^2 \right], \quad (47)$$

$$O_{sub} = \det_f \left[(\bar{\psi}_R \psi_L)^2 + \frac{1}{3} (\bar{\psi}_R \vec{\Sigma} \psi_L)^2 \right]. \quad (48)$$

Upon Fierz rearrangement, we find

$$O_{dom} = 2(\psi_L C \tau_2 \psi_L)(\bar{\psi}_R C \tau_2 \bar{\psi}_R), \quad (49)$$

$$O_{sub} = \frac{2}{3}(\psi_L C \tau_2 \vec{\Sigma} \psi_L)(\bar{\psi}_R C \tau_2 \vec{\Sigma} \bar{\psi}_R), \quad (50)$$

corresponding to scalar and tensor diquarks. Both operators are flavor singlet. Overall symmetry then fixes the color wave functions, anti-symmetric $\bar{3}$ for the scalar, and symmetric 6 for the tensor. The dominant pairing induced by instantons is in the scalar diquark channel, the only other attractive channel is the tensor. All this neatly confirms the scenario discussed in Refs. 5,6 and Section 3.1.

Just as we found for $N_f \geq 3$, there is an appealing heuristic understanding for the amazingly simple behavior of the evolution equations, obtained by focussing on the diquark channels. Instantons distinguish between scalar diquarks with positive and negative parity. $G + K$ corresponds to the positive parity operator ($\psi C \gamma_5 \psi$) and $G - K$ to the negative parity ($\psi C \psi$). The asymptotic approach of $G/K \rightarrow 1$, then corresponds to the fact that scalar diquark condensation is favored over pseudoscalar diquark condensation. This is always the case if $K(0) > 0$.

We can also understand the strange case $G(0), K(0) < 0$ and $|K(0)| > |G(0)|$. In this case the interaction for scalar diquarks is repulsive, but the interaction in the pseudoscalar channel is attractive and leads to an instability. Note that this can only happen if we have the “wrong” sign of the instanton interaction, *i.e.* for $\theta = \pi$. Similarly, we can understand why the asymptotic ratio of the molecular (instanton-anti-instanton) and direct instanton couplings approaches $G/K = \pm 1$. Instantons induce a repulsive interaction for pseudoscalar diquarks. During the evolution, this coupling will be suppressed, whereas the attractive scalar interaction grows. But this means that in the pseudoscalar channel, the repulsive (instanton) and attractive (molecular) forces have to cancel in the asymptotic limit, so the effective couplings become equal.

To match all the instanton coupling constants to microscopic QCD would require control of the instanton density, the relevant value of α_s , and the screening mechanism, and does not seem practicable. Some simple qualitative conclusions may be inferred, however. From the form of the instanton vertex we can fix the ratio of the two instanton-like couplings, $K_T/K_S = 1/(2N_c - 1)$.^{75,76} This emphasizes that the tensor channel coupling is expected to be small.

Also, both one gluon exchange and ideas based on instantons (e.g., the instanton liquid model) yield $G_0^{LL} > 0$, $-G_i^{LL} > 0$. Thus the favored scenario is that both instanton and $U(1)_A$ symmetric couplings flow at the same rate. In any case, the leading instability occurs in a scalar diquark channel.

The simplified analysis presented here is incomplete, in that we have retained only instantaneous s-wave interactions. Realistic interactions, such as those generated by gluon exchange or instantons, are momentum- and frequency-dependent. Nevertheless the simplified analysis is valuable, in that

it indicates the internal quantum numbers of the channels likely to be most unstable. Moreover, other things being equal, s-wave instabilities seem likely to dominate, since they add constructively over the Fermi surface. (This intuition is borne out by variational calculations of gaps and pairing energies associated with higher angular momentum condensates, which turn out to be very small.^{5,47,49})

4.2 Model Hamiltonian by Variational Methods

The renormalization group determines the running of couplings from the matching point downwards, towards the Fermi surface. The catastrophic growth of an attractive interaction we have encountered indicates an instability of the system, indicates in what channel(s) the instability is most pronounced, and indicates the energy scale at which the instability develops. At the scale at which the instability sets in, however, the perturbative renormalization procedure breaks down. The great achievement of Bardeen, Cooper, and Schrieffer (BCS)⁷⁷ was to demonstrate how Fermi-surface instabilities of this type are resolved by pairing, to produce a superconducting ground state. This ground state is characterized by a gap Δ , whose magnitude does indeed turn out to be of the same order as the energy scale indicated by the renormalization group analysis. The instability arose in a renormalization group analysis done in terms of fermionic excitations (about the naive ground state with no pairing) which have zero free energy at the Fermi surface. In the gapped state, which the BCS analysis determines is formed, the resolution of the instability is simply that the correct fermionic degrees of freedom are quasiparticle excitations which have a gap in their spectrum. In this section we outline the BCS argument that the resolution of the instability is a paired state, and give the associated calculation of Δ .

As an aside, note that once Δ is known and the ground state has been characterized, if (as in the CFL phase) there are bosonic excitations of this ground state with energy less than Δ , a renormalization group analysis framed in terms of these new degrees of freedom can be employed in their description. The results of such analyses were presented in Section 2.3.

The original BCS theory was founded on a variational calculation using a model Hamiltonian. Their model Hamiltonian retained only an idealized form of the effective attraction near the Fermi surface, that encouraged condensation in the s-wave, spin-singlet channel. The pioneering work of Nambu and Jona-Lasinio,⁷⁸ who first applied the ideas behind BCS theory to particle–anti-particle pairing in quantum field theories describing elementary particle interactions, followed a similar approach. We shall follow the literature in referring to models of this class as NJL models, but shall apply them à la BCS, to quark-quark pairing.

In QCD there are many more fermion species (colors and flavors) than in conventional superconductors, and the form of the condensate is a major focus of interest. Renormalization group calculations, as presented in Section 4.1, provide important guidance. The dominant operator indicates the existence of potential instabilities that are amplified by renormalization, but does not indicate how they are resolved. To decide the most favorable form of pairing, we must compare the energies associated with different possibilities. For this qualitative purpose, and of course to estimate the quantitative relationship between the size of the pairing gap and the microscopic parameters, we still require detailed dynamical calculations. NJL models provide an appropriate, tractable starting point.^{5,6} One chooses a simple four-quark interaction, which provides attraction in the channel which the renormalization group analysis indicates is dominant. One first normalizes the parameters in such a toy model to give reasonable vacuum physics, and then uses the model to estimate the gap. Here we shall exemplify the use of such models by using them to estimate the size of the gaps in the 2SC and CFL phases and to argue that the CFL condensate is indeed the favored pattern of condensation in three-flavor QCD.

We use an NJL model with free energy

$$\Omega = \int d^3x \bar{\psi}(x)(\not{\nabla} - \mu\gamma_0)\psi(x) + H_I, \quad (51)$$

where the interaction Hamiltonian

$$H_I = \frac{3}{8}G \int d^3x \mathcal{F}(\bar{\psi}(x)\gamma_\mu T^A\psi(x))(\bar{\psi}(x)\gamma^\mu T^A\psi(x)) \quad (52)$$

describes a four-fermion interaction with the color, flavor, and spinor structure of single-gluon exchange.

In microscopic QCD the interactions become weak at high momentum. Here this feature is caricatured with a form factor \mathcal{F} . In detail, when we expand H_I in momentum modes we are instructed to include a form factor $F(p)$ on each leg of the interaction vertex. Examples which have been used in the literature include power-law and smoothed-step profiles for F :^{5,7,13}

$$F(p) = \left(\frac{\Lambda^2}{p^2 + \Lambda^2}\right)^\nu, \quad \text{or} \quad F(p) = \left(1 + \exp\left[\frac{p - \Lambda}{w}\right]\right)^{-1}. \quad (53)$$

One of the important results found in these investigations is that if, for any given $F(p)$, the coupling constant G is chosen to yield a reasonable vacuum chiral condensate (say with a constituent quark mass of 400 MeV) then the resulting superconducting gap is reasonably insensitive to the choice of $F(p)$. Varying the scale Λ and the shape of the form factor while tuning the coupling to keep some physical property of the vacuum fixed affects the gap very little.

This robustness indicates that the magnitude of the gap is largely determined just by the strength of the interaction (normalized with respect to a physical observable) and does not depend sensitively on other details. For this reason, and following Ref. 13,49 we make the simplifying choice of replacing the smooth form factor $F(p)$ by a step function: $F(p) = 1$ for $p < \Lambda$ and $F(p) = 0$ for $p > \Lambda$.

We begin with two flavors and follow the analysis presented in Refs. 5,49. We seek a condensate of the 2SC form by making the BCS ansatz

$$\begin{aligned} |\Psi\rangle &= A_L^\dagger A_R^\dagger |0\rangle, \\ A_L^\dagger &= \prod_{\mathbf{p}, \alpha, \beta} \left(\cos \theta_L(\mathbf{p}) + \epsilon^{\alpha\beta 3} e^{i\xi_L(\mathbf{p})} \sin \theta_L(\mathbf{p}) a_{Lu\alpha}^\dagger(\mathbf{p}) a_{Ld\beta}^\dagger(-\mathbf{p}) \right), \quad (54) \\ A_R^\dagger &= \text{as above, } L \rightarrow R, \end{aligned}$$

for the ground state wave function. Here, α and β are color indices, u and d label flavors explicitly, and a^\dagger is the particle creation operator (for example, $a_{Ld\alpha}^\dagger$ creates a left-handed down quark with color α). The Cooper pairs described by this ansatz are evidently antisymmetric in color; that they are also antisymmetric in flavor follows from the anticommutation relations satisfied by the creation operators. The θ 's and ξ 's are the variational parameters of our ansatz: they are to be chosen to minimize the free energy of this BCS state. Note that we really should have included pairing among antiparticles in our ansatz also. However, this doubles the length of the equations and makes little difference in the end. We therefore leave the antiparticles out until the end of the derivation, and restore them in the gap equation itself. Note also that $|0\rangle$ is the no-particle state. At nonzero chemical potential, in the absence of any interactions, the ansatz (54) describes filled Fermi seas if $\theta_L(\mathbf{p}) = \theta_R(\mathbf{p}) = \pi/2$ for $|\mathbf{p}| < \mu$, and $\theta_L(\mathbf{p}) = \theta_R(\mathbf{p}) = 0$ otherwise. Throughout this section, we assume μ is the same for all flavors of quarks. The consequences of relaxing this assumption are described in Ref. 49 and sketched in Section 6.

Explicit computation demonstrates that the condensate

$$\Gamma_L \equiv -\frac{1}{2} \langle \Psi | \epsilon_{ij} \epsilon_{\alpha\beta 3} \psi^{i\alpha}(\mathbf{r}) C L \psi^{j\beta}(\mathbf{r}) | \Psi \rangle \quad (55)$$

is nonvanishing. Here, $C = i\gamma^0\gamma^2$ and $L = (1 - \gamma_5)/2$ is the usual left-handed projection operator. Γ_L can be expressed in terms of the variational parameters as:

$$\Gamma_L = \frac{4}{V} \sum_{\mathbf{p}} \sin \theta_L(\mathbf{p}) \cos \theta_L(\mathbf{p}) e^{i(\xi_L(\mathbf{p}) - \phi(\mathbf{p}))}. \quad (56)$$

Here V is the spatial volume of the system and the dependence on the azimuthal angle ϕ follows from our use of the spinor conventions described in

Refs. 5,7,79. The expression for Γ_R is the same as that in (56) except that $\phi(\mathbf{p})$ is replaced by $\pi - \phi(\mathbf{p})$. In Eq. (56) and throughout, $(1/V)\sum_{\mathbf{p}}$ becomes $\int d^3p/(2\pi)^3$ in an infinite system. Our simplified choice of form factor corresponds to restricting the range of this integral to $|\mathbf{p}| < \Lambda$.

We must now minimize the expectation value of the free energy (51) in the state $|\Psi\rangle$:

$$\langle\Psi|\Omega|\Psi\rangle = 4\sum_{\mathbf{p}}(|\mathbf{p}| - \mu)\sin^2\theta_L(\mathbf{p}) + 4\sum_{\mathbf{p}}(|\mathbf{p}| - \mu)\sin^2\theta_L(\mathbf{p}) + \langle H_I\rangle \quad (57)$$

where

$$\langle H_I\rangle = -\frac{GV}{2}(|\Gamma_L|^2 + |\Gamma_R|^2) \quad (58)$$

in terms of the condensates which are in turn specified in terms of the variational parameters by (56). We have neglected the contribution to $\langle\Omega\rangle$ made by the third color quarks, which do not pair.

Upon variation with respect to the ξ 's, we find that they must be chosen to cancel the azimuthal phases $\phi(\mathbf{p})$ in (56). In this way, we obtain maximum coherence in the sums over \mathbf{p} , giving the largest possible magnitudes for the condensates and gap parameters. We have

$$\xi_L(\mathbf{p}) = \phi(\mathbf{p}) + \varphi_L, \quad \xi_R(\mathbf{p}) = \pi - \phi(\mathbf{p}) + \varphi_R, \quad (59)$$

where φ_L and φ_R are arbitrary \mathbf{p} -independent angles. These constant phases do not affect the free energy — they correspond to the Goldstone bosons for the broken left-handed and right-handed baryon number symmetries — and are therefore not constrained by the variational procedure. For convenience, we set $\varphi_L = \varphi_R = 0$ and obtain condensates and gap parameters that are purely real.

The relative phase $\varphi_L - \varphi_R$ determines how the condensate transforms under a parity transformation. Its value determines whether the condensate is scalar, pseudoscalar, or an arbitrary combination of the two. Because single gluon exchange cannot change the handedness of a massless quark, the left- and right-handed condensates are not coupled in the free energy Ω . Our choice of interaction Hamiltonian therefore allows an arbitrary choice of $\varphi_L - \varphi_R$. A global $U(1)_A$ transformation changes $\varphi_L - \varphi_R$, and indeed this is a symmetry of our toy model. If we included $U(1)_A$ -breaking interactions in our Hamiltonian, to obtain a more complete description of QCD, we would find that the free energy depends on $\varphi_L - \varphi_R$, and thus selects a preferred value. For example, had we taken H_I to be the two-flavor instanton interaction as in Refs. 5,6, the interaction energy would appear as $\Gamma_L^*\Gamma_R + \Gamma_L\Gamma_R^*$ instead of as in (58). This would enforce a fixed phase relation $\varphi_L - \varphi_R = 0$, favoring the parity conserving $\langle\psi C\gamma_5\psi\rangle$ condensate.^{5,6}

We now apply the variational method to determine the angles $\theta(\mathbf{p})$ in our trial wavefunction, by minimizing the free energy: $\partial\langle\Omega\rangle/\partial\theta(\mathbf{p}) = 0$. Everything is the same for left and right condensates so we hereafter drop the L and R labels. Upon variation with respect to $\theta(\mathbf{p})$, we obtain

$$\tan 2\theta(\mathbf{p}) = \frac{\Delta}{|\mathbf{p}| - \mu}, \quad (60)$$

where $\Delta_{L,R} = G\Gamma_{L,R}$. With the θ angles now expressed in terms of Δ , we can use the wave function $|\Psi\rangle$ to obtain expressions for the quasiparticle dispersion relation:

$$E(\mathbf{p}) = \sqrt{(|\mathbf{p}| - \mu)^2 + \Delta^2}. \quad (61)$$

Here, E is the free energy cost of removing a pair and replacing it with either an up quark with momentum \mathbf{p} or a down quark with momentum $-\mathbf{p}$. This result confirms that Δ is the gap in the spectrum of fermionic excitations. Note, however, that in the 2SC phase the third color (“blue”) quarks remain gapless in the ansatz within which we are working. As mentioned in Section 3, it is likely that they form an angular momentum $J = 1$ condensate with a gap which is many orders of magnitude smaller than the gap Δ for the red and green quarks.

Substituting the expression (60) for the θ angles into the expression (56) for the Γ condensate, and using the relation $\Delta = G\Gamma$, we obtain a self-consistency equation for Δ :

$$1 = \frac{2G}{V} \sum_{\mathbf{p}} \left\{ \frac{1}{\sqrt{(|\mathbf{p}| - \mu)^2 + \Delta^2}} + \frac{1}{\sqrt{(|\mathbf{p}| + \mu)^2 + \Delta^2}} \right\}. \quad (62)$$

The first term on the right-hand side of the gap equation (62) yields a logarithmic divergence at the Fermi surface if Δ is small. This term is the contribution to the gap equation from particles and holes, and the logarithmic divergence is the manifestation of the BCS instability. Because the right hand side diverges for $\Delta \rightarrow 0$, there must be a solution to the gap equation with $\Delta \neq 0$ even for an arbitrarily small coupling G , as long as G is positive (attractive). The second term, with $(|\mathbf{p}| + \mu)$ in the denominator, is the contribution from antiparticles, which we have suppressed above and restored here. Note that even though the same value of Δ appears in both the antiparticle and particle/hole contributions, the antiparticle contribution to the gap equation is small because its denominator is everywhere greater than μ .

We shall rederive the gap equation (62) diagrammatically in Section 4.3. The variational method we have used above has the virtue of providing us in addition with an expression for the corresponding wave function itself.

In order to use this gap equation to estimate Δ , we need to fix the coupling G . To do this, we evaluate the vacuum chiral gap (or constituent quark mass) and set it to $M = 400$ MeV. In vacuum, M satisfies the gap equation

$$1 = \frac{8G}{V} \sum_{\mathbf{p}} \frac{1}{\sqrt{|\mathbf{p}|^2 + M^2}}, \quad (63)$$

which may be derived along very similar lines to the above, working at zero chemical potential and postulating a chiral symmetry breaking condensate in which quarks and anti-quarks pair in the standard fashion. Note that for $M \rightarrow 0$, the right-hand side of the chiral gap equation has no logarithmic divergence; no BCS Fermi surface instability. This means that $M \neq 0$ only if G is above some threshold. Let us choose $\Lambda = 800$ MeV and fix G such that $M = 400$ MeV. Upon solving the BCS gap equation (62) we then find that $\Delta = 106$ MeV when $\mu = 400$ MeV and $\Delta = 145$ MeV when $\mu = 500$ MeV.

Note that if, instead, we had used the four-fermion interaction with the quantum numbers of the instanton vertex, as in Ref. 5, we would have obtained *precisely* the same results. That is, had we made the same choice for the form factor and for Λ , and then chosen the coupling constant for the instanton vertex such that the vacuum constituent quark mass is 400 MeV, it turns out that the resulting Δ is exactly that which we have obtained using the single-gluon exchange interaction.

Varying Λ , or using a smooth form factor instead of a sharp cutoff, yields similar results for Δ , ranging from about 50 MeV to somewhat more than 100 MeV^{5,43} The authors of Ref. 6 also use the instanton interaction, and also normalize it such that $M = 400$ MeV in vacuum, but they model the fact that instanton effects decrease at nonzero density by introducing a density-dependent coupling constant. They find gaps ranging from 20 MeV to 90 MeV. More sophisticated treatments of the instanton interaction, including form factors obtained from suitable Fourier transforms of instanton profiles, tend to yield larger gaps, perhaps as large as 200 MeV.^{45,55}

The models we are discussing in this subsection can only be used for qualitative guidance, but it is very pleasing to see so many of them agreeing on the order of magnitude of the gap.

The 2SC phase has also been studied at nonzero temperature using the instanton interaction.^{6,43} The critical temperature above which the condensate vanishes (in mean field theory) turns out to be within a few percent of that expected from BCS theory: $T_c = 0.57\Delta(T=0)$.⁴³ The standard BCS result is valid in the $\Delta/\mu \rightarrow 0$ limit, and the interaction in QCD is strong enough that $\Delta/\mu \sim 1/4$ at the densities we are discussing, so a few percent discrepancy is to be expected. Note that based on our estimate of the gap, the critical temperature we estimate for the color superconducting phase is of order many

tens of MeV. This makes it almost certain that this phase is inaccessible in heavy ion collisions, which are much hotter. Although T_c is low relative to heavy ion collision temperatures, color superconductors are in three senses high temperature superconductors. First, $T_c \sim 10^{12}$ Kelvin. Second, and more seriously, T_c can easily be of order 10% of the Fermi energy. This makes these materials high temperature superconductors by any definition, even relative to the cuprates. This robustness of the phenomenon of color superconductivity in the face of nonzero temperature directly reflects the strength of the attraction between quarks in QCD. Third, T_c is much hotter than the temperature in a neutron star which is more than a few seconds old, making it clear that if quark matter exists in the core of a neutron star, it must be a color superconductor.

We turn now to QCD with three flavors, and derive a gap equation appropriate for the CFL phase. We use the same single gluon exchange interaction Hamiltonian H_I as above. This time, however, we present a derivation which follows the ideas of Bogoliubov and Valatin.⁸⁰ We focus from the beginning only on the condensate of left-handed quarks. (As above, since we do not include any $U(1)_A$ breaking interaction the left- and right-handed condensates can be rotated one into the other. Introducing instanton effects, done in the CFL phase in Refs. 9,10, favors the Lorentz scalar combination.)

We rewrite the interaction Hamiltonian in terms of Weyl spinors, keeping only the left-handed fields:

$$H_I = \frac{G}{2} \int d^3x \mathcal{F} (3\delta_\delta^\alpha \delta_\beta^\gamma - \delta_\beta^\alpha \delta_\delta^\gamma) (\psi_{\alpha\dot{a}}^\dagger \psi_{\gamma\dot{c}}^\dagger \epsilon^{\dot{a}\dot{c}} \psi_{ib}^\beta \psi_{jd}^\delta \epsilon^{bd}), \quad (64)$$

We have explicitly displayed color ($\alpha, \beta \dots$), flavor ($i, j \dots$), and spinor ($a, \dot{a} \dots$) indices, and rewritten the color and flavor generators.

We now make the mean-field ansatz that in the true ground state $|\Psi\rangle$ at a given chemical potential,

$$\begin{aligned} \langle \Psi | \psi_{\alpha\dot{a}}^\dagger \psi_{\gamma\dot{c}}^\dagger \epsilon^{\dot{a}\dot{c}} | \Psi \rangle &= \frac{1}{G} P_{\alpha\gamma}^{ij}, \\ P_{\alpha\gamma}^{ij} &= \frac{1}{3} (\Delta_8 + \frac{1}{8} \Delta_1) \delta_\alpha^i \delta_\gamma^j + \frac{1}{8} \Delta_1 \delta_\gamma^i \delta_\alpha^j, \end{aligned} \quad (65)$$

where the numerical factors have been chosen so that Δ_1 and Δ_8 , which parameterize P , will turn out to be the gaps for singlet and octet quark excitations, respectively (see below). This ansatz takes the color $\bar{\mathbf{3}}$ form (1) if $\Delta_1 = -2\Delta_8$. Solutions to the gap equation turn out to be within a few percent of satisfying this, meaning that there is only a small admixture of the color $\mathbf{6}$ condensate. In the mean field approximation, the interaction Hamiltonian becomes

$$\begin{aligned} H_I &= \frac{1}{2} \int d^3x \mathcal{F} Q_{\beta\delta}^{ij} \psi_{ib}^\beta \psi_{jd}^\delta \epsilon^{bd} + \text{c.c.}, \\ Q_{\beta\delta}^{ij} &= \Delta_8 \delta_\delta^i \delta_\beta^j + \frac{1}{3} (\Delta_1 - \Delta_8) \delta_\beta^i \delta_\delta^j. \end{aligned} \quad (66)$$

Replacing indices i, β with a single color-flavor index ρ , we can simultaneously diagonalize the 9×9 matrices Q and P , and find that they have two eigenvalues,

$$\begin{aligned} P_1 &= \Delta_8 + \frac{1}{4}\Delta_1, & P_2 \cdots P_9 &= \pm \frac{1}{8}\Delta_1, \\ Q_1 &= \Delta_1, & Q_2 \cdots Q_9 &= \pm \Delta_8. \end{aligned} \quad (67)$$

That is, eight of the nine quarks in the theory have a gap parameter given by Δ_8 , while the remaining linear combination of the quarks has a gap parameter Δ_1 .

The Hamiltonian can be rewritten in this color-flavor basis in terms of particle/antiparticle creation/annihilation operators $\bar{a}_\rho, \bar{b}_\rho$. (This time, we keep the antiparticles throughout the derivation.) We also expand in momentum modes (see Refs. 7,79 for our spinor conventions) and now explicitly include the form factors $F(p)$,

$$\begin{aligned} H &= \sum_{\rho, k > \mu} (k - \mu) \bar{a}_\rho^\dagger(\mathbf{k}) \bar{a}_\rho(\mathbf{k}) + \sum_{\rho, k < \mu} (\mu - k) \bar{a}_\rho^\dagger(\mathbf{k}) \bar{a}_\rho(\mathbf{k}) \\ &\quad + \sum_{\rho, \mathbf{k}} (k + \mu) \bar{b}_\rho^\dagger(\mathbf{k}) \bar{b}_\rho(\mathbf{k}) \\ &\quad + \frac{1}{2} \sum_{\rho, \mathbf{p}} F(p)^2 Q_\rho e^{-i\phi(\mathbf{p})} \left(\bar{a}_\rho(\mathbf{p}) \bar{a}_\rho(-\mathbf{p}) + \bar{b}_\rho^\dagger(\mathbf{p}) \bar{b}_\rho^\dagger(-\mathbf{p}) \right) + \text{c.c.}, \end{aligned} \quad (68)$$

where the perturbative ground state, annihilated by \bar{a}_ρ and \bar{b}_ρ is the Fermi sea, with states up to $p_F = \mu$ occupied. Finally, we change basis to creation/annihilation operators y and z for quasiparticles,

$$\begin{aligned} y_\rho(\mathbf{k}) &= \cos(\theta_\rho^y(\mathbf{k})) \bar{a}_\rho(\mathbf{k}) + \sin(\theta_\rho^y(\mathbf{k})) \exp(i\xi_\rho^y(\mathbf{k})) \bar{a}_\rho^\dagger(-\mathbf{k}), \\ z_\rho(\mathbf{k}) &= \cos(\theta_\rho^z(\mathbf{k})) \bar{b}_\rho(\mathbf{k}) + \sin(\theta_\rho^z(\mathbf{k})) \exp(i\xi_\rho^z(\mathbf{k})) \bar{b}_\rho^\dagger(-\mathbf{k}), \end{aligned} \quad (69)$$

where

$$\begin{aligned} \cos(2\theta_\rho^y(\mathbf{k})) &= \frac{|k - \mu|}{\sqrt{(k - \mu)^2 + F(k)^4 Q_\rho^2}}, & \xi_\rho^y(\mathbf{k}) &= \phi(\mathbf{k}) + \pi, \\ \cos(2\theta_\rho^z(\mathbf{k})) &= \frac{k + \mu}{\sqrt{(k + \mu)^2 + F(k)^4 Q_\rho^2}}, & \xi_\rho^z(\mathbf{k}) &= -\phi(\mathbf{k}). \end{aligned} \quad (70)$$

These values are chosen so that H has the form of a free Hamiltonian for

quasiparticles:

$$H = \sum_{\mathbf{k}, \rho} \left\{ \begin{aligned} & \sqrt{(k - \mu)^2 + F(k)^4 Q_\rho^2} y_\rho^\dagger(\mathbf{k}) y_\rho(\mathbf{k}) \\ & + \sqrt{(k + \mu)^2 + F(k)^4 Q_\rho^2} z_\rho^\dagger(\mathbf{k}) z_\rho(\mathbf{k}) \end{aligned} \right\}. \quad (71)$$

Clearly then the ground state $|\psi\rangle$ contains no quasiparticles:

$$y_\rho(\mathbf{k})|\psi\rangle = z_\rho(\mathbf{k})|\psi\rangle = 0. \quad (72)$$

The gap equations follow from requiring that the mean field ansatz (65) hold in the quasiparticle basis. In other words, we use (69) and (70) to rewrite (65) in terms of quasiparticle creation/annihilation operators, and then evaluate the expectation value using (72). We get two gap equations:

$$\begin{aligned} \Delta_8 + \frac{1}{4}\Delta_1 &= GK(\Delta_1), \\ \frac{1}{8}\Delta_1 &= GK(\Delta_8), \end{aligned} \quad (73)$$

where

$$K(\Delta) = -\frac{1}{2} \sum_{\mathbf{k}} \left\{ \frac{F(k)^4 \Delta}{\sqrt{(k - \mu)^2 + F(k)^4 \Delta^2}} + \frac{F(k)^4 \Delta}{\sqrt{(k + \mu)^2 + F(k)^4 \Delta^2}} \right\}. \quad (74)$$

From (71) we see that the physical gap, namely the minimum energy of the quasiparticles, is $F(\mu)^2 |\Delta|$. Creating a quasiparticle-quasihole pair requires at least twice this energy. If we take $F(p)$ to be a step function as above, then the gaps are simply $|\Delta_1|$ and $|\Delta_8|$.

In this derivation, the variational nature of the procedure is somewhat hidden. The point is that the θ angles were chosen to guarantee the absence of linear terms in the effective Hamiltonian. Such terms would indicate the instability of the no-“particle” state, where particles are defined by the action of the operators (69). This state varies with the θ angles. Thus in searching for a θ -dependent Hamiltonian free of linear terms we are in effect looking for the stationary point of the expectation value of the energy, within a continuous manifold of candidate states.

For the same choice of parameters as we used in the 2SC case (namely $\Lambda = 800$ MeV, G chosen so that the vacuum constituent quark mass is $M = 400$ MeV, and $\mu = 400$ MeV) solving the coupled gap equations (73) yields $\Delta_8 = 80$ MeV and $\Delta_1 = -176$ MeV. As promised, this is not far from the ratio $\Delta_1 = -2\Delta_8$ required if the condensate were entirely in the color $\mathbf{\bar{3}}$ channel. The color $\mathbf{6}$ condensate is nonzero but small, as is also the case in the CFL

phase at asymptotically high densities.^{10,11} If μ is increased to 500 MeV, we find $\Delta_8 = 109$ MeV and $\Delta_1 = -249$ MeV. These estimates of Δ may be a bit of an overestimate, because it is likely that the instanton interaction contributes significantly to M in vacuum but, because it is a six-fermion interaction, it does not contribute significantly to Δ . For this reason, we are overestimating G by assuming that M in vacuum is due entirely to the one-gluon exchange interaction. (This uncertainty did not arise with two flavors because in that case, the instanton and one-gluon exchange four-fermion interactions both contribute to M and to Δ in the same way.) Reducing G by a factor of two results in $\Delta_8 = 16$ MeV and $\Delta_1 = -34$ MeV at $\mu = 500$ MeV. The magnitude of the gap *is* sensitive to the strength of the interaction, even though it is insensitive to details of the form factor as we described above. This reminds us that we should use these models as a qualitative guide only.

In three-flavor QCD, the instanton interaction is a six-fermion interaction. As we have discussed in Section 2, its effects are small but are nevertheless important because they are the leading source of $U(1)_A$ breaking. It is also interesting to note that the four-fermion interaction introduced by instanton–anti-instanton pairs contributes to both M and Δ . In the analysis of Ref. 9, this interaction is employed in an analogous fashion to the way we have employed single-gluon exchange, and quite similar gaps are obtained.

We can now outline the argument that the CFL phase is indeed the favored pattern of condensation. First, the interaction favors antisymmetry in color. Second, pairing with zero angular momentum is favored because it allows condensation which utilizes the entire Fermi surface. This has been confirmed in a variety of explicit calculations. Pauli then requires flavor antisymmetry. These arguments favor a condensate of the form

$$\langle \psi_i^\alpha C \gamma_5 \psi_j^\beta \rangle \sim \epsilon^{\alpha\beta A} \epsilon_{ijB} \equiv \phi_B^A . \quad (75)$$

Color-flavor locking corresponds to $\phi_B^A \sim \text{diag}(1, 1, 1)$, in which all nine quarks pair. The antithetical possibility is $\phi_B^A \sim \text{diag}(0, 0, 1)$, but this is just the 2SC phase, whose gap equation we have also solved! For $\mu = 400$ MeV and G fixed so that $M = 400$ MeV in vacuum, we found that in the CFL phase (with $\phi_B^A \sim \text{diag}(1, 1, 1)$) there are 8 quasiparticles with gap 80 MeV and one with gap 176 MeV. For $\phi_B^A \sim \text{diag}(0, 0, 1)$, on the other hand, we find four quasiparticles with gap 106 MeV and 5 quarks (strange quarks; blue up and blue down quarks) with zero gap. Clearly, the condensation energy (i.e. $\langle \Omega \rangle$ relative to that in the unpaired state) will be greater with $\phi_B^A \sim \text{diag}(1, 1, 1)$. Explicit evaluation of $\langle \Psi | \Omega | \Psi \rangle$ using the variational wave functions for the 2SC and CFL phases confirms this.

These calculations are strongly suggestive that $\phi_B^A \sim \text{diag}(1, 1, 1)$ is the choice with the lowest free energy, although they do also demonstrate that a

small admixture of the color **6** condensate which is symmetric in both color and flavor is mandatory. This means that a complete demonstration is more complicated. Schäfer has, however, constructed an effective potential for ϕ_B^A (and the color **6** condensate) within a particular NJL model but making the most general assumptions for the form of the condensate. He finds that the CFL phase, with $\phi_B^A \sim \text{diag}(1, 1, 1)$, minimizes $\langle \Omega \rangle$. The authors of Refs. 62,12 have addressed this question in analyses done using the interaction generated by the exchange of a propagating gluon, rather than in a model with point-like interactions. They confirm that $\phi_B^A \sim \text{diag}(1, 1, 1)$ is favored, thus explicitly confirming that the CFL phase is favored at arbitrarily high density. The essence of all of these different analyses is that in the CFL phase all quarks are able to pair, and the condensation energy is therefore larger than that for any less symmetric condensate. This simple argument could in principle be outweighed if a less symmetric condensate were found whose gaps were much larger in magnitude than those of the CFL phase. With all parameters fixed, though, different choices for ϕ_B^A turn out to yield comparable gaps. Although $\phi_B^A \sim \text{diag}(0, 0, 1)$ does yield somewhat larger gaps, this advantage is not close to outweighing the 9/4 numerical advantage enjoyed by the CFL phase.

4.3 Model Hamiltonian by Diagrammatic Methods

In this brief subsection, we use diagrammatic methods, sometimes named after Dyson and Schwinger or, in this context, Nambu and Gorkov, to rederive the gap equation (62) for the 2SC phase, still in a model in which the QCD interaction between quarks has been replaced by a point-like four-fermion interaction. We do so both because these methods may be more familiar to some readers and because they serve as a warmup for the weak-coupling calculations of the next subsection. To that end, we also discuss the $G \rightarrow 0$ limit of the model.

We follow the standard Nambu-Gorkov formalism and introduce an eight-component field $(\psi, \bar{\psi}^T)$. In this basis, the inverse quark propagator takes the form

$$S^{-1}(p) = \begin{pmatrix} \not{p} + \mu\gamma_0 & \bar{\Delta} \\ \Delta & (\not{p} - \mu\gamma_0)^T \end{pmatrix}, \quad (76)$$

where $\bar{\Delta} = \gamma_0 \Delta^\dagger \gamma_0$ and where in this expression Δ is a matrix with color, flavor and Dirac indices which have all been suppressed. The diagonal blocks correspond to ordinary propagation of massless quarks and the off-diagonal blocks reflect the possibility for “anomalous propagation” in the presence of a diquark condensate. The 2SC ansatz for the form of the gap matrix is

$$\Delta_{ij}^{\alpha\beta}(p) = \epsilon^{\alpha\beta 3} \epsilon_{ij} C \gamma_5 \Delta, \quad (77)$$

where Δ on the right-hand side is now the gap parameter, and all matrix structure has been written explicitly.

gap equation. The first term, due to particles and holes, yields a logarithmic divergence in the $|\bar{p}|$ integral if $\Delta \rightarrow 0$. As we have seen, this divergence at the Fermi surface is the hallmark of the BCS phenomenon.

In the variational approach, once we have solved the gap equation we know the variational wave function and with this in hand we can evaluate the expectation value of the free energy Ω . If, instead, we have obtained the gap equation diagrammatically, we can still obtain the free energy upon realizing that the gap equation can be seen as the statement that the free energy is stationary with respect to the gap parameter. That is, we integrate the gap equation:

$$\Omega = \Omega_{\text{free}} + V \int_0^{\Delta_{\text{solution}}} d\Delta \left(-\frac{2\Delta}{G} + 8 \int \frac{d^4p}{(2\pi)^4} \text{integrand} \right), \quad (82)$$

where the “integrand” is that on the right hand side of the gap equation (81), where Δ_{solution} is the value of Δ which solves the gap equation, and where Ω_{free} is that for noninteracting fermions.

Our next goal is the study of color superconductivity in the limit of asymptotically high density and thus, because of asymptotic freedom, at weak coupling. It goes against the spirit of the phenomenologically motivated models which we have used in Sections 4.2 and 4.3 to apply them at these densities. Our approach has been to use such models to investigate how the quarks resolve the instability revealed by the renormalization group analysis of Section 4.1 (they pair) and then to use the models as devices which allow us to make a phenomenological normalization of the strength of the attraction between quarks, and thus to obtain a qualitative measure of the magnitude of the gap. At asymptotically high densities, instead of attempting to normalize the interaction via vacuum phenomenology, we should use the weak-coupling QCD interaction itself. This is the subject of Section 4.4. Before beginning, and in order to provide a contrast, let us see what does happen if we take the four-fermion coupling $G \rightarrow 0$, and thus take $\Delta \ll \mu, \Lambda$. Solving the gap equation (62) explicitly in this limit yields

$$\Delta = 2\sqrt{\Lambda^2 - \mu^2} \exp\left(\frac{\Lambda^2 - 3\mu^2}{2\mu^2}\right) \exp\left(-\frac{\pi^2}{2\mu^2 G}\right). \quad (83)$$

As expected from BCS theory, the factor $2\mu^2/\pi^2$ which multiplies G in the exponent is the density of states (for red and green u and d quarks of a single chirality) at the Fermi surface in the absence of interactions. The Λ -dependent prefactor is clearly model-dependent. However, since the four-fermion interaction with coupling G models single gluon exchange, the result (83) could suggest that for $\mu \rightarrow \infty$ in QCD, we may find $\Delta \sim \exp(-\text{const}/g^2)$. We shall see in the next section that this is *not* correct.

Upon replacing gluon exchange by a contact interaction, we have already seen that we obtain a gap equation of the form

$$\Delta \propto g^2 \int d\epsilon \frac{\Delta}{\sqrt{\epsilon^2 + \Delta^2}}. \quad (85)$$

where $\epsilon = (|\vec{q}| - \mu)$ is the distance to the Fermi surface. The integral diverges at small ϵ , so that as long as the proportionality constant is positive one will have non-trivial solutions for Δ , no matter how small is g . Indeed, for small g the solution is $\Delta \sim e^{-\text{const}/g^2}$.

At asymptotically large μ , models with short-range interactions are bound to fail because the dominant interaction is that due to the long-range magnetic interaction coming from single gluon exchange.^{44,59} When we now restore the gluon propagator, we find a nontrivial angular integral which diverges logarithmically for forward scattering in the absence of any mechanism which screens the long-range magnetic interaction. We suspect, however, that in the superconducting phase this divergence will at the very least be precluded by the generation of a gluon mass $\propto \Delta$ by the Meissner-Higgs mechanism.^b We therefore expect a gap equation of the form

$$\Delta \propto g^2 \int d\epsilon \frac{\Delta}{\sqrt{\epsilon^2 + \Delta^2}} d\theta \frac{\mu^2}{\theta \mu^2 + \Delta^2}, \quad (86)$$

where θ is the angle between the external momentum and the loop momentum and where the integral is dominated by small ϵ and small θ . This gap equation yields $\Delta \sim g^2 \Delta (\log \Delta)^2$ and hence $\Delta \sim e^{-\text{const}/g}$!

The proper discussion of the microscopic gap equation is considerably more involved than (86). For example, it turns out that the collinear logarithmic divergence is cutoff by dynamical screening (Landau damping) and not by the Meissner effect.⁵⁹ As a result, the prefactor of $1/g$ in the exponent turns out to differ from that which one would derive from (86). It nevertheless turns out that the conclusion that at weak coupling the gap goes exponentially in the inverse coupling (rather than its square) still emerges.⁵⁹ As a result, the gap is parametrically larger at $\mu \rightarrow \infty$ than it would be for any point-like four-fermion interaction. This has the amusing consequence, that at asymptotically high densities the gap becomes arbitrarily large! This is because asymptotic freedom ensures that it is the microscopic coupling $1/g(\mu)^2$ which vanishes logarithmically, so that $e^{-\text{const}/g(\mu)}$ does not shrink as fast as $1/\mu$. Since the ‘‘dimensional analysis’’ scale of the gap is set by μ , Δ grows asymptotically even though Δ/μ shrinks.

^bThe Meissner mass is of order $g\mu$,^{21,36,37,28,34} but the gluon wave function renormalization is of order $g\mu/\Delta$ and the physical screening length, which is the ratio of the two, is therefore of order $1/\Delta$.³⁴

We shall discuss the asymptotic analysis by example, focussing on the 2SC phase and following the presentation of Ref. 64. After describing the results, we shall quote the analogous results for the CFL phase. We use the 2SC phase as our example only because the algebra is simpler with only two flavors. The physics is under much better control in the CFL phase. In the calculation we outline, we determine the dominant gap in the 2SC phase, describing the pairing of red and green u and d quarks. This leaves the blue and strange quarks unpaired, and thus leaves open the possibility of further infrared divergences at the Fermi surface, leading to small gaps via the formation of Cooper pairs with nonzero angular momentum. Also, three gluons are left unscreened raising the spectre of further infrared complications. In the CFL phase, the dominant condensate gives a gap to all nine quarks and gives a mass to all eight gluons, and there are no further infrared difficulties to be resolved.

As in Section 4.3, we introduce an eight-component field $(\psi, \bar{\psi}^T)$ and the inverse quark propagator (76). We assume that the gap matrix is anti-symmetric in both color and flavor, which is the channel in which single-gluon exchange is attractive. We also assume that the condensation is in the channel with total angular momentum $J = 0$. In the case of short range interactions, all these assumptions can be justified by reference to the renormalization group equations for a general four-fermion interaction,^{57,58} as described in Section 4.1. The single-gluon exchange interaction is long range, however, and other forms of pairing might take place in addition. In particular, since the interaction is dominated by almost collinear scattering, it includes substantial strength in all partial waves, and one might expect some condensation in the higher partial waves.^{59,61} It turns out that these condensates have the same leading g -dependence as the $J = 0$ condensate,^{59,61,65} but they are suppressed by numerical factors of order 1/100 to 1/1000.⁶⁵ We therefore neglect them, and concentrate on the $J = 0$ gap.

We also assume that the gap has positive parity. As we discussed in Sections 4.1 and 4.2, single-gluon exchange does not distinguish between the positive parity $\langle \psi C \gamma_5 \psi \rangle$ condensate and the negative parity $\langle \psi C \psi \rangle$ condensate. This degeneracy is lifted by instantons, which favor the positive parity channel.^{5,6,58} At large chemical potential instanton effects are exponentially suppressed. In the following, we will therefore assume that the only instanton effect is to determine the parity of the gap. Finally, we neglect quark mass effects and chiral symmetry breaking LR condensates. As shown in Ref. 58 and described in Section 4.1, there is no BCS instability in the case of pairing between left and right handed quarks. The formation of LR condensates is therefore suppressed by m/μ .⁶¹

Given all these assumptions and specializations, the gap matrix takes the form^{4,61,64}

$$\Delta_{ij}^{\alpha\beta}(p) = (\lambda_2)^{\alpha\beta}(\tau_2)_{ij}C\gamma_5(\Delta_1(p_0)P_+(p) + \Delta_2(p_0)P_-(p)) , \quad (87)$$

where the projection operators are given by

$$\begin{aligned} P_+(p) &= \frac{1}{2}(1 + \gamma_0\vec{\gamma}\cdot\hat{p}) , \\ P_-(p) &= \frac{1}{2}(1 - \gamma_0\vec{\gamma}\cdot\hat{p}) . \end{aligned} \quad (88)$$

We have neglected the dependence of the gap on the magnitude of the momentum $|\vec{p}|$, but kept the dependence on frequency p_0 . The $|\vec{p}|$ -dependence can be dropped because, in the weak coupling limit, all momenta are close to the Fermi surface. For short-range interactions, the dependence on frequency can also be neglected. Thus, in Section 4.3 we chose the ansatz (77) in which $\Delta_1(p_0) = \Delta_2(p_0)$ and both were given by the constant Δ . This was appropriate in that context, and we had no difficulty finding a solution to the gap equation upon making this ansatz. Now, however, because long range interactions are important, retardation effects cannot be neglected.

P_+ and P_- are projection operators which project onto particles and antiparticles respectively. This means that $\Delta_1(p_0)$ describes the modification of the propagator due to particle-particle and hole-hole pairing whereas $\Delta_2(p_0)$ describes that due to antiparticle-antiparticle pairing. The gap in the quasi-particle spectrum at the Fermi surface is given by $\Delta_1(\Delta_1)$, and we are therefore primarily interested in deriving a gap equation for $\Delta_1(p_0)$. We expect that at weak coupling, quarks near the Fermi surface should dominate and the contribution of Δ_2 to the gap equation for Δ_1 should vanish. (This is what we found in our analysis of the gap equation (62), for example.) This emerges explicitly as a consequence of the fact that in the weak coupling limit, we can replace $\gamma_0\vec{\gamma}\cdot\hat{p}$ by the unit matrix using the equations of motion. Note that this does not mean that Δ_2 is in any sense smaller than Δ_1 . It only means that the contribution of Δ_2 to the gap equation for Δ_1 becomes small.

The self energy in the Nambu-Gorkov formalism obeys the Dyson-Schwinger equation⁴

$$\Sigma(k) = ig^2 \int \frac{d^4p}{(2\pi)^4} \Gamma_\mu^A S(p) \Gamma_\nu^A D_{\mu\nu}(k-p) . \quad (89)$$

Here, $\Sigma(k)$ is the proper self energy defined via (78), Γ_μ^A is the quark-gluon vertex and $D_{\mu\nu}(k-p)$ is the gluon propagator. We have written (89) in Minkowski space. To leading order in the perturbative expansion, we can use the free vertex (80). To leading order, we can also neglect the diagonal part of the proper self energy, namely the fermion wave function renormalization.⁵⁹ We shall see below that although we obtain the asymptotic form for the gap,

the results we obtain are uncontrolled for $g > g_c \sim 0.8$, corresponding to a rather large value of $\mu \sim 10^8$ MeV.⁶⁹ This breakdown could in principle reflect a failure in any of our assumptions. We expect, however, that it arises because contributions which have been truncated in writing the one-loop Schwinger-Dyson equation (89) with (80) are large for $g > g_c$. That is, we expect that this truncation (for example the neglect of vertex corrections), and not any of the simplifications we introduced in making the ansatz (87) for Δ , is the most significant assumption we make in this analysis.

The Dyson-Schwinger equation (89) reduces to an equation for the gap matrix,

$$\Delta(k) = -ig^2 \int \frac{d^4p}{(2\pi)^4} \left(\gamma_\mu \frac{\lambda^a}{2} \right)^T S_{21}(p) \left(\gamma_\nu \frac{\lambda^a}{2} \right) D_{\mu\nu}(k-p). \quad (90)$$

Here, $S_{21}(p)$ is the 21-component of the fermion propagator in the Nambu-Gorkov representation. $S_{21}(p)$ is determined from the inverse of (76). We have

$$S_{21}(p) = -\frac{1}{(\not{p} - \not{\mu})^T} \Delta \frac{1}{(\not{p} + \not{\mu}) - \bar{\Delta}[(\not{p} - \not{\mu})^T]^{-1} \Delta}. \quad (91)$$

Inserting the ansatz (87) for the gap gives

$$S_{21}(p) = -\lambda_2 \tau_2 C \gamma_5 \left(\frac{\Delta_1(p_0) P_-(p)}{p_0^2 - (|\vec{p}| - \mu)^2 - \Delta_1(p_0)^2} + \frac{\Delta_2(p_0) P_+(p)}{p_0^2 - (|\vec{p}| + \mu)^2 - \Delta_2(p_0)^2} \right). \quad (92)$$

Both the RHS and the LHS of the gap equation are proportional to τ_2 , so the flavor structure simply drops out. The color coefficient is given by

$$\frac{1}{4} (\lambda_a)^T \lambda_2 \lambda_a = -\frac{N_c + 1}{2N_c} \lambda_2 = -\frac{2}{3} \lambda_2 \quad (N_c = 3), \quad (93)$$

where we have used the Fierz identity $(\lambda^a)_{ij} (\lambda^a)_{kl} = -(2/N_c) \delta_{ij} \delta_{kl} + 2\delta_{il} \delta_{jk}$ and the factor $1/4$ comes from the color generators $t^a = \lambda^a/2$. Projecting (90) on $\Delta_{1,2}$ gives two coupled gap equations

$$\begin{aligned} \Delta_{1,2}(k_0) = & \frac{2ig^2}{3} \int \frac{d^4p}{(2\pi)^4} \left\{ \frac{1}{2} \text{tr} (\gamma_\mu P_-(p) \gamma_\nu P_\pm(k)) \frac{\Delta_1(p_0)}{p_0^2 - (|\vec{p}| - \mu)^2 - \Delta_1(p_0)^2} \right. \\ & \left. + \frac{1}{2} \text{tr} (\gamma_\mu P_+(p) \gamma_\nu P_\mp(k)) \frac{\Delta_2(p_0)}{p_0^2 - (|\vec{p}| + \mu)^2 - \Delta_2(p_0)^2} \right\} D_{\mu\nu}(k-p), \quad (94) \end{aligned}$$

where the upper and lower signs on the RHS correspond to Δ_1 and Δ_2 on the LHS.

We now must specify the gluon propagator. The gluon propagator in a general covariant gauge is given by

$$D_{\mu\nu}(q) = \frac{P_{\mu\nu}^T}{q^2 - G(q)} + \frac{P_{\mu\nu}^L}{q^2 - F(q)} - \xi \frac{q_\mu q_\nu}{q^4}, \quad (95)$$

where the projectors $P_{\mu\nu}^{T,L}$ are defined by

$$P_{ij}^T = \delta_{ij} - \hat{q}_i \hat{q}_j, \quad P_{00}^T = P_{0i}^T = 0, \quad P_{\mu\nu}^L = -g_{\mu\nu} + \frac{q_\mu q_\nu}{q^2} - P_{\mu\nu}^T. \quad (96)$$

The functions $F(q)$ and $G(q)$ describe the effects of the medium on gluon propagation. If we neglect the Meissner effect (that is if we neglect the modification of $F(q)$ and $G(q)$ due to the gap Δ in the fermion propagator) then $F(q)$ describes Thomas-Fermi screening, $G(q)$ describes dynamical screening (Landau damping), and they are given in the hard dense loop approximation by⁸¹

$$F(q) = 2m^2 \frac{q^2}{q^2} \left(1 - \frac{iq_0}{|\vec{q}|} Q_0 \left(\frac{iq_0}{|\vec{q}|} \right) \right), \quad Q_0(x) = \frac{1}{2} \log \left(\frac{x+1}{x-1} \right), \quad (97)$$

$$G(q) = m^2 \frac{iq_0}{|\vec{q}|} \left[\left(1 - \left(\frac{iq_0}{|\vec{q}|} \right)^2 \right) Q_0 \left(\frac{iq_0}{|\vec{q}|} \right) + \frac{iq_0}{|\vec{q}|} \right], \quad (98)$$

where $m^2 = N_f g^2 \mu^2 / (4\pi^2)$ and we are working with $N_f = 2$ flavors. Note that $G \rightarrow 0$ for $q_0 \rightarrow 0$: static magnetic modes are not screened. Nonstatic modes are dynamically screened due to Landau damping. Note that the gluon propagator contains the gauge parameter ξ , which must not appear in physical results.

In the weak coupling limit, q_0 is small as compared to $|\vec{q}|$. In this case we can expand the projectors $P_{\mu\nu}^L \simeq \delta_{\mu 0} \delta_{\nu 0}$ and $q_i q_j / q^2 \simeq \hat{q}_i \hat{q}_j$. (See Ref. 69 for an analysis in which these simplifying kinematic approximations and others which follow are not made.) The gap equation now becomes

$$\begin{aligned} \Delta_1(k_0) = & -\frac{2ig^2}{3} \int \frac{d^4 p}{(2\pi)^4} \left\{ \frac{\Delta_1(p_0)}{p_0^2 - (|\vec{p}| - \mu)^2 - \Delta_1(p_0)^2} \right. \\ & \times \left(\frac{\frac{3}{2} - \frac{1}{2} \hat{k} \cdot \hat{p}}{(k-p)^2 - G(k-p)} + \frac{\frac{1}{2} + \frac{1}{2} \hat{k} \cdot \hat{p}}{(k-p)^2 - F(k-p)} \right) \\ & + \frac{\Delta_2(p_0)}{p_0^2 - (|\vec{p}| + \mu)^2 - \Delta_2(p_0)^2} \\ & \left. \times \left(\frac{\frac{1}{2} + \frac{1}{2} \hat{k} \cdot \hat{p}}{(k-p)^2 - G(k-p)} + \frac{\frac{1}{2} - \frac{1}{2} \hat{k} \cdot \hat{p}}{(k-p)^2 - F(k-p)} + \frac{\xi}{(k-p)^2} \right) \right\}. \quad (99) \end{aligned}$$

There is a similar equation for Δ_2 in which the two terms in the round brackets are interchanged. Only the first term in (99) has a singularity on the Fermi surface. In the weak coupling limit, we can therefore drop the second term, and we are left with an equation for $\Delta(k_0) \equiv \Delta_1(k_0)$. This equation is independent of the gauge parameter ξ . The ξ -independence of the Δ_1 term in (99) arises because of the kinematic approximations made in deriving it. If one goes beyond these approximations, Δ_1 is ξ -dependent.⁶⁹ The second gap parameter Δ_2 is not suppressed in magnitude and its gauge-dependence is not kinematically suppressed. However, Δ_2 does not lead to a gap on the Fermi surface.

The fact that the gap is gauge independent in the present weak-coupling approximation is a consequence of the fact that the gap is determined by the scattering of quarks that are almost on shell. For on-shell quarks, the fact that the gauge dependent part of the propagator does not contribute follows directly from the equations of motion for the quark fields. This argument is adequate only to lowest order, as appeared in the specific diagrammatic cancellation (and non-cancellation) above.

For large chemical potential the integral over p is dominated by momenta in the vicinity of the Fermi surface, $|\vec{p}| \simeq \mu$ and $p_0 \ll \mu$. We can expand all momenta as $\vec{p} = \vec{p}_F + \vec{l}$, where \vec{p}_F is on the Fermi surface, and \vec{l} is orthogonal to it. Asymptotically, $|\vec{l}| \ll |\vec{p}_F|$ and the integration measure becomes $dp_0 \mu^2 dl d\cos\theta d\phi$. We also have $|\vec{k} - \vec{p}| \simeq \sqrt{2}\mu(1 - \cos\theta)$. The integral over ϕ is performed trivially. We analytically continue to imaginary p_0 , and perform the integral over \vec{l} by picking up the pole in the diquark propagator. We find

$$\Delta(k_0) = \frac{g^2}{12\pi^2} \int dp_0 \int d\cos\theta \left(\frac{\frac{3}{2} - \frac{1}{2}\cos\theta}{1 - \cos\theta + (G + (k_0 - p_0)^2)/(2\mu^2)} + \frac{\frac{1}{2} + \frac{1}{2}\cos\theta}{1 - \cos\theta + (F + (k_0 - p_0)^2)/(2\mu^2)} \right) \frac{\Delta(p_0)}{\sqrt{p_0^2 + \Delta(p_0)^2}}. \quad (100)$$

The integral over $\cos\theta$ is dominated by small θ , corresponding to almost collinear scattering. We must, therefore, take careful account of the medium modifications of the gluon propagator described by $F(q)$ and $G(q)$ given in (97). In the gap equation (100) $F(q)$ and $G(q)$ are to be evaluated at $q_0 = k_0 - p_0$ and $|\vec{q}| = |\vec{k} - \vec{p}| \simeq \sqrt{2}\mu(1 - \cos\theta)$, and are therefore functions of $k_0 - p_0$ and $\cos\theta$. For $q_0 \ll \vec{q} \rightarrow 0$ the expressions (97) for $F(q)$ and $G(q)$ simplify, yielding

$$F(q) = 2m^2, \quad G(q) = \frac{\pi}{2} m^2 \frac{q_0}{|\vec{q}|}. \quad (101)$$

In the longitudinal part, $m_D^2 = 2m^2$ is the familiar Debye screening mass. In the transverse part, nonstatic modes are dynamically screened. In our case,

typical frequencies are on the order of the gap, $q_0 \simeq \Delta$. This means that the electric part of the interaction is screened at $q_E \simeq m_D^{1/2}$ whereas the magnetic interaction is screened at $q_M \simeq (\pi/4 \cdot m_D^2 \Delta)^{1/3}$.

Asymptotically, $q_M \ll q_E$, and magnetic gluon exchange dominates over electric gluon exchange. We therefore begin by analyzing the gap equation taking into account the magnetic part of the interaction only. We will also approximate $\cos \theta \simeq 1$ in the denominator and drop $(k_0 - p_0)^2$ in the denominator. All of these terms will be reinstated later. The integration over $\cos \theta$ is now straightforward. We have

$$\Delta(k_0) = \frac{g^2}{18\pi^2} \int dp_0 \log \left(1 + \frac{64\pi\mu}{N_f g^2 |k_0 - p_0|} \right) \frac{\Delta(p_0)}{\sqrt{p_0^2 + \Delta(p_0)^2}} . \quad (102)$$

If we are only interested in the leading exponential behavior of the gap we can drop the numerical factors and the powers of g in the logarithm. We then arrive at

$$\Delta(k_0) = \frac{g^2}{18\pi^2} \int dp_0 \log \left(\frac{c\mu}{|k_0 - p_0|} \right) \frac{\Delta(p_0)}{\sqrt{p_0^2 + \Delta(p_0)^2}} , \quad (103)$$

where c is a factor to be determined more fully below. This equation was first derived by Son.⁵⁹ (In ordinary superconductivity, the corresponding equation was first derived by Eliashberg.⁸²) What we have shown here (following Ref. 64) is that one can derive this equation directly from the Dyson-Schwinger equation in the weak coupling limit, and that upon making the approximations we have made the result is independent of the gauge parameter. The integral equation (103) can be converted to a differential equation,⁵⁹ and in the weak coupling limit an approximate solution is given by^{59,61,64,65}

$$\Delta(k_0) \simeq \Delta_0 \sin \left(\frac{g}{3\sqrt{2}\pi} \log \left(\frac{c\mu}{k_0} \right) \right) , \quad k_0 > \Delta_0 , \quad (104)$$

where

$$\Delta_0 = 2c\mu \exp \left(-\frac{3\pi^2}{\sqrt{2}g} \right) . \quad (105)$$

At this point a few comments are in order. First, we note that the use of perturbation theory to determine the dynamic screening is self-consistent. Since $\Delta \sim \mu \exp(-\text{constant}/g)$, the gap grows as $\mu \rightarrow \infty$ and $q_M \gg \Lambda_{QCD}$. Second, we note that it is essential to keep the frequency dependence of the gap. For small frequencies, $\Delta(k_0)$ varies over scales on the order of $k_0 \sim \Delta_0$ itself. Therefore, $\Delta(k_0)$ cannot be replaced by a constant. Were we to approximate $\Delta(k_0) \simeq \Delta_0$, we would obtain a gap equation for Δ_0 that has the correct double logarithmic structure and gives $\Delta_0 \simeq \mu \exp(-\text{constant}/g)$, but the constant in the exponent would not be correct.

We now come to the role of electric gluon exchanges. We include the second term in (100) with $F = m_D^2$. We again use the approximation $\cos \theta \simeq 1$ in the numerator and drop the $(k_0 - p_0)^2$ term in the denominator. Let us note that in the forward direction, electric and magnetic gluon exchanges have the same overall factor. Performing the integral over $\cos \theta$, we find

$$\Delta(k_0) = \frac{g^2}{18\pi^2} \int dp_0 \left\{ \log \left(1 + \frac{64\pi\mu}{N_f g^2 |k_0 - p_0|} \right) + \frac{3}{2} \log \left(1 + \frac{8\pi^2}{N_f g^2} \right) \right\} \times \frac{\Delta(p_0)}{\sqrt{p_0^2 + \Delta(p_0)^2}}, \quad (106)$$

where the factor 3/2 in front of the second term comes from the difference between dynamic screening, $q_M \sim |\vec{q}|^{1/3}$, and static screening, $q_E \sim |\vec{q}|$. In the weak coupling limit, the gap equation (106) reduces to the form (103) with approximate solution (104), where we now see that we can estimate the constant $2c$ to be

$$2c = 2048\sqrt{2}\pi^4 N_f^{-5/2} g^{-5} = 512\pi^4 g^{-5} \simeq 5.0 \times 10^4 g^{-5} \quad (N_f = 2). \quad (107)$$

We have obtained the result (107) for the prefactor $2c$ in the expression for the gap Δ_0 by collecting the leading logarithms from both electric and magnetic gluon exchange. To do better, Schäfer and Wilczek solve the gap equation (100), which incorporates both electric and magnetic exchange, numerically.⁶⁴ They also keep the $\cos \theta$ dependence in the numerator, and the terms $(k_0 - p_0)^2$ in the denominator. Finally, they use the exact forms of $G(q)$ and $F(q)$ in the hard dense loop approximation, (97). This takes into account that there is no dynamic screening for $|\vec{q}| < q_0$. Asymptotically (i.e. for small g) the numerical solution to the gap equation is well described by (104,105) with $2c \simeq 1.4 \times 10^4 g^{-5}$, at least for $k_0 < \sqrt{N_f/(8\pi)} g\mu$. At larger k_0 , the retardation terms $\sim (k_0 - p_0)^2$ dominate over screening and Δ falls off more quickly with increasing k_0 than in (104). We are interested in $k_0 = \Delta_0$, however, and in this regime (104) describes the shape of the numerical solution quite well.

In order to use the weak-coupling results, we must choose an energy scale at which to evaluate the running QCD coupling. Schäfer and Wilczek chose to use the one-loop running coupling constant evaluated at the Fermi momentum $p_F = \mu$, which is an average over the momenta of the exchanged gluons, which are in the range $[q_M, 2\mu]$. Strictly speaking, only a higher order calculation can fix the scale in the running coupling. It turns out, however, that with g evaluated at μ , the gap Δ_0 only depends rather weakly on μ . We return to this below. The numerical solution yields $\Delta_0 \simeq 40$ MeV at $\mu = 10^{10}$ MeV, corresponding to $\Delta_0/\mu = 4 \times 10^{-9}$ at $g = 0.67$ and a value of $2c$ which is about 2/5 that in (107), and $\Delta_0 \simeq 90$ MeV at $\mu = 400$ MeV, corresponding to

$\Delta_0/\mu = 0.23$ at $g = 3.43$ and a value of $2c$ which happens to be almost exactly that in (107). As μ increases from 400 MeV to about 10^6 MeV, Δ drops from 90 MeV to about 10 MeV; as μ increases further, Δ then begins its inexorable, but logarithmic, rise.

Clearly, with $\mu = 400$ MeV and $g = 3.43$, the calculation of the gap is determined by momenta which are not large compared to Λ_{QCD} , and all of the approximations we have used have broken down. More on this below, but before plunging into caveats let us note that it is gratifying to see that the order of magnitude of the result agrees with that obtained in the calculations described in Sections 4.2 and 4.3, based on more phenomenological effective interactions, which were normalized to the strength of chiral symmetry breaking at zero density, rather than to the calculable asymptotics of the running coupling.

Son's result⁵⁹

$$\frac{\Delta}{\mu} \sim \frac{b}{g^5} \exp\left(-\frac{3\pi^2}{\sqrt{2}g}\right) \quad (108)$$

has now been confirmed using a variety of methods.^{61,62,63,64,65,66,12,68,69} However, even the $\mathcal{O}(g^0)$ contribution to the prefactor b in (108) is not yet fully understood, and certainly nobody has proposed a controlled calculational scheme which could be used to push the calculation of b to arbitrarily high accuracy. We have worked through the analysis of Schäfer and Wilczek,⁶⁴ which leads to the estimate that $b \sim 512\pi^4$ in the 2SC phase, a result which is supported by their numerical work and by the work of other authors.^{61,65,66,12,68} A similar analysis yields the estimate that $b \sim 512\pi^4 2^{-1/3} (2/3)^{5/2}$ in the CFL phase, with the $(2/3)^{5/2}$ coming from the N_f -dependence of the Debye mass and the $2^{-1/3}$ coming from an analysis of the color-flavor structure of the CFL gap equation,¹⁰ along the lines of that we have presented in Section 4.2 in the context of models with four-fermion interactions. Numerical solutions of the weak-coupling CFL gap equation by Evans *et al.* are in good agreement with this estimate, and these authors also confirm that including Meissner effects in the gluon propagator makes little difference to the final result.¹²

The argument that the CFL phase is favored at asymptotically high density in QCD with three flavors of quarks is similar to that given at the end of Section 4.2. 2SC pairing would yield a gap given by (108) with $b \sim 512\pi^4 (2/3)^{5/2}$, whereas in the CFL phase the gap is smaller by a factor of $2^{-1/3}$. In the asymptotic regime, the condensation energy is proportional to $\Delta^2 \mu^2$ up to logarithmic corrections.^{10,12} As expected, the expression (82) derived by taking $G \rightarrow 0$ in the analysis done using a four-fermion interaction is a good guide. In the 2SC phase, four quarks pair with gap Δ and the condensation energy is $\sim 4(\Delta^2 \mu^2 / 4\pi^2)$. In the CFL phase at asymptotically high density, the color **6** condensate is suppressed relative to the color **3** condensate by a factor $g\sqrt{2} \log(2)/36\pi$,¹⁰ and so to leading order one has eight quarks with

gap Δ and one with gap 2Δ , and a condensation energy which is therefore $\sim 12(\Delta^2\mu^2/4\pi^2)$. Although the CFL gap is smaller than the 2SC gap by a factor of $2^{-1/3}$, this does not outweigh the advantage the CFL phase enjoys because it allows all nine quarks to pair. As a result, the CFL phase is favored. As we saw in Section 3, this conclusion continues to hold even when the strange quark mass m_s is nonzero, as long as $m_s^2/2\mu$ is small compared to Δ .

There are several contributions to b which we have not taken into account above. They modify the magnitude of the gap, but do so in the same way for CFL or 2SC pairing. For example, modifications to the quasiparticle dispersion relations in the normal (nonsuperconducting; high temperature) phase^{65,83,84} and quasiparticle damping effects in the superconducting phase⁷⁰ do affect the gap, and both tend to reduce b . In the normal phase, the effects of wave function renormalization are only important within $\sim \exp(-1/g^2)$ of the Fermi surface,⁸⁴ which supports Son's conclusion that in the superconducting phase these effects result only in a subleading correction to Δ .⁵⁹ This correction does, however, reduce b by about a factor of 5.⁶⁵

The value of b is also affected by the choice of the scale at which g is evaluated in (108). The consequent modifications to Δ have been considered by Beane *et al.*⁶⁸ They do a renormalization group analysis within the effective theory constructed by Hong,⁶² who noted that the antiparticles can safely be integrated out. Beane *et al* use the renormalization group to compute and resum contributions of the form $\alpha^{n+1}\beta_0^n \log^n(\Delta/\mu)$ to the gap equation, where β_0 is the first coefficient in the QCD β -function. Their results demonstrate that g should be evaluated at a μ -dependent scale which is much lower than μ .⁶⁸ Upon assuming that the QCD coupling runs according to the vacuum β -function all the way down to the magnetic scale q_M — an assumption which is not justified but which has not yet been superseded — they find that if, by convention, g is taken as $g(\mu)$, then b is enhanced by a factor of about 20.

Finally, we return to the question of the gauge dependence of b . Both the analysis of Schäfer and Wilczek presented above and that of Pisarski and Rischke⁶¹ demonstrate that the $\mathcal{O}(g^0)$ contribution to b is gauge-independent. However, Rajagopal and Shuster have gone back to (94), eliminated Δ_2 in the gap equation for Δ_1 , but made no further kinematic simplifications. The resulting gap equation for Δ_1 is gauge-dependent. Examination of the gauge-dependent (and g -dependent) contributions to b obtained by solving this equation reveals that these do decrease with decreasing g , but that they only begin to decrease for $g < 0.8$.⁶⁹ This means that effects like vertex corrections which have to date been neglected in all calculations based on the one-loop Schwinger-Dyson equation (e.g. those of Refs. 61,63,64,66) are small corrections to b only for $\mu \gg 10^8$ MeV.

All these caveats should by now have made it clear that although we are confident of the leading g -dependence of the gap Δ at asymptotically large

μ , there remains physics which has not been satisfactorily treated which contributes at order g^0 to the prefactor b . Furthermore, effects which are higher order in g are large enough that they can only be neglected for $\mu \gg 10^8$ MeV.

The asymptotic results nevertheless have very important consequences. We have seen in Section 3 that the outcome of the competition between the CFL and 2SC phases depends on the relative magnitudes of Δ and $m_s^2/2\mu$. The latter decreases at large μ , while the result (108) demonstrates that Δ increases logarithmically as $\mu \rightarrow \infty$. This means that the CFL phase is favored over the 2SC phase for $\mu \rightarrow \infty$ for any $m_s \neq \infty$.¹³ Even though the asymptotic regime where Δ can be calculated from first principles with confidence is not accessed in nature, it is of great theoretical interest. The weak-coupling calculation of the gap in the CFL phase is the first step toward the weak-coupling calculation of other properties of this phase, in which chiral symmetry is broken and the spectrum of excitations is as in a confined phase. As we have described in Section 2, for example, the masses and decay constants of the pseudoscalar mesons can be calculated from first principles once Δ is known.

Although the value of Δ is under control asymptotically, it seems fair to say that applying these asymptotic results at $\mu = 400$ MeV is currently at least as uncertain a proposition as applying estimates made using phenomenologically normalized models with point-like interactions. Nevertheless, if we take the estimates for the prefactor b provided by Schäfer and Wilczek's numerical results described above and apply them at $\mu \sim 400$ MeV, they predict gaps of order 100 MeV. The consequent critical temperatures are related to the zero temperature gap Δ by the standard weak-coupling BCS result $T_c = 0.57\Delta$,^{61,65} and are therefore of order 50 MeV. We have seen that some known corrections push this estimate up while others push it down, and that the calculation whence it came is, regardless, of quantitative value only for $\mu \gg 10^8$ MeV. It is nevertheless satisfying that two very different approaches, one using zero density phenomenology to normalize models, the other using weak-coupling methods valid at asymptotically high density, yield predictions for the gaps and critical temperatures at accessible densities which are in qualitative agreement. Neither can be trusted quantitatively for quark number chemical potentials $\mu \sim 400 - 500$ MeV, as appropriate for the quark matter which may occur in compact stars. Still, both methods agree that the gaps at the Fermi surface are of order tens to 100 MeV, with critical temperatures about half as large.

$T_c \sim 50$ MeV is much larger relative to the Fermi momentum (say $\mu \sim 400 - 500$ MeV) than in low temperature superconductivity in metals. This reflects the fact that color superconductivity is induced by an attraction due to the primary, strong, interaction in the theory, rather than having to rely on much weaker secondary interactions, as in phonon mediated superconductivity in metals. Quark matter is a high- T_c superconductor by any reasonable definition. It is unfortunate that its T_c is nevertheless low enough that it is

unlikely the phenomenon can be realized in heavy ion collisions.

4.5 Challenges for the Future

While the rigorous asymptotic justification of color superconductivity is a marvelous result, there are compelling physical and mathematical motivations to go further.

For physical applications, we are interested in densities not much beyond nuclear, which (as we have seen) appears to be quite far from asymptopia. It is not at all clear, in particular, that the form of the interaction which dominates asymptotically, namely near-forward magnetic scattering, is the most important at physically achievable densities. Indeed, electric scattering — or binding through electric flux tubes! — and instantons more nearly resemble the interactions used successfully in phenomenological models of hadrons at zero density and applied to nonzero densities as described in Sections 4.2 and 4.3.

On the mathematical side, it clearly would be very desirable to have a systematic approximation framework that did not depend on selective diagram resummation, and whose results were manifestly gauge invariant. Similar problems arise in the treatment of ordinary superconductors in condensed matter physics, albeit in a simpler form since the gauge group is abelian. However, in that context the lowest-order approximation is adequate in practice since electrodynamic radiative corrections are overwhelmed, quantitatively, by many other uncertainties.

In formulating an appropriate perturbation theory, the difficulties arise due to the gauge dependence of the primary order parameter and to the complicated (in particular, non-instantaneous) nature of the microscopic interaction. The whole notion of the primary order parameter depends on fixing a gauge, and we assume that is done. On physical grounds, as we have emphasized already, one expects a weak-coupling approach to work only when it is based on perturbing around the correct, gapped ground state; but of course this begs the question of how to construct the ground state. The BCS-inspired variational procedure works well for instantaneous interactions, where one can define a simple Hamiltonian, but is very awkward for retarded interactions. As we saw in Section 4.2, in one of its many implementations (that due originally to Bogoliubov and Valatin) it takes the form of a search among “trial Hamiltonians” incorporating quadratic terms mixing particles and holes, with coefficients depending on the momentum. This suggests that one should employ trial Lagrangians with similar terms, allowing also for energy dependence, using the action variational principle popularized by Feynman in connection with the polaron problem. Such a procedure has the great advantage that one need only do perturbation theory around the ground state of the trial Lagrangian,

which can be designed to incorporate the correct physics (i.e. gaps) to begin with. In principle, the choice of gauge can simply be treated as an additional variational parameter.

Ultimately, truly quantitative results on QCD at moderately ultra-nuclear densities will probably have to await numerical work using lattice gauge theory, as has been the case for zero density. In principle, we can bypass all the difficulties involved in defining the primary condensate by working directly with the distinctive gauge-invariant parameters predicted for color-flavor locking. Specifically, one should encounter diverging susceptibilities for chiral symmetry breaking, especially in the diquark-antidiquark channel (4), and for $U(1)_B$ breaking, in the baryon number 2 channel. The corresponding vacuum expectation values, signaling chiral symmetry breaking and superfluidity, could be stabilized by adding the corresponding infinitesimal source terms. These features, and the associated appearance of Nambu-Goldstone bosons, would serve as unmistakable signatures of the color-flavor locked phase. In practice, unfortunately, all presently known numerical algorithms for QCD at finite density and zero temperature converge too slowly to be useful. The discovery of suitable algorithms for this problem stands as perhaps the greatest theoretical challenge in QCD today.

5 The Phase Diagram

In this article we focus largely on zero temperature quark matter, but it is important to understand where the 2SC and CFL phases fit on the phase diagram of QCD as a function of both temperature and density. Because QCD is asymptotically free, its high temperature and high baryon density phases are more simply and more appropriately described in terms of quarks and gluons as degrees of freedom, rather than hadrons. At high temperatures, in the resulting quark-gluon plasma (QGP) phase all of the symmetries of the QCD Lagrangian are unbroken and the excitations have the quantum numbers of quarks and gluons. At high densities, on the other hand, we have seen that quarks form Cooper pairs and new condensates develop. At high enough density, chiral symmetry is broken by color-flavor locking. At densities which are high enough that nucleons overlap and the matter is in a quark matter phase but which are not high enough for color-flavor locking, we expect to find the 2SC phase.

In this section, we describe the qualitative features of the QCD phase diagram. We choose to describe the entire phase diagram, and not just the region of low temperatures and high densities. The exploration of the higher temperature regions of the diagram is the object of extensive experimental efforts in heavy ion collision experiments at CERN and Brookhaven. Due to its topical interest, we describe the high temperature regime of the phase

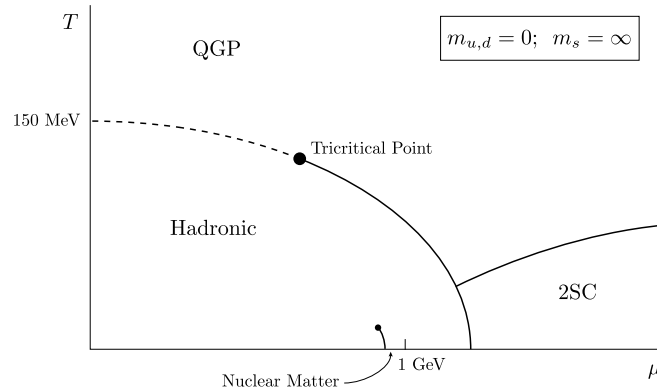


Figure 1: QCD Phase diagram for two massless quarks. Chiral symmetry is broken in the hadronic phase and is restored elsewhere in the diagram. The chiral phase transition changes from second to first order at a tricritical point. The phase at high density and low temperature is a color superconductor in which up and down quarks with two out of three colors pair and form a condensate. The transition between this 2SC phase and the QGP phase is likely first order. The transition on the horizontal axis between the hadronic and 2SC phases is likely first order. The transition between a nuclear matter “liquid” and a gas of individual nucleons is also marked. At $T = 0$, it separates the vacuum phase from the nuclear matter phase; Lorentz-boost symmetry is broken to its right but unbroken to its left. At nonzero temperature, Lorentz-boost symmetry is broken in both the nuclear gas and nuclear liquid, and this line of phase transitions may therefore end. It is thought to end at a critical point at a temperature of order 10 MeV, characteristic of the forces which bind nucleons into nuclei.

diagram in some detail, in addition to explaining how the dense quark matter phases which occupy us in the remainder of this article fit in. In Section 6 below, we refocus on cold dense quark matter, as we describe current efforts to understand how to use observed phenomena occurring in compact stars to map this region of the phase diagram.

Let us begin with a brief review of the phase changes which occur as a function of temperature at zero baryon number density.⁸⁵ That is, we begin by restricting ourselves to the vertical axis in Figures 1 through 4. This slice of the phase diagram was explored throughout the early universe during the first tens of microseconds after the big bang. It can also be studied in lattice simulations. As heavy ion collisions are performed at higher and higher energies, they create plasmas with a lower and lower baryon number to entropy ratio and therefore explore regions of the phase diagram closer and closer to the vertical axis.

In QCD with two massless quarks ($m_{u,d} = 0$; $m_s = \infty$; Figure 1) the vacuum phase, with hadrons as excitations, is characterized by a chiral condensate $\langle \bar{\psi}_L \psi_R \rangle$. Whereas the QCD Lagrangian is invariant under separate global flavor rotations of the left-handed and right-handed quarks, the presence of the chiral condensate spontaneously breaks $SU(2)_L \times SU(2)_R$ to the

subgroup $SU(2)_{L+R}$, in which only simultaneous flavor rotations of L and R quarks are allowed. Locking left- and right-handed rotations in this way breaks global symmetries and results in three massless Goldstone bosons, the pions. The chiral order parameter, a 2×2 matrix M^{ab} in flavor space, can be written in terms of four real fields σ and $\vec{\pi}$ as

$$\langle \bar{\psi}_{L\alpha}^i \psi_R^{\alpha j} \rangle = M^{ij} = \sigma \delta^{ij} + \vec{\pi} \cdot (\vec{\tau})^{ij} \quad , \quad (109)$$

where the $\vec{\tau}$ are the three Pauli matrices. $SU(2)_L$ and $SU(2)_R$ rotations act on M^{ij} from the left and right, respectively. The order parameter can also be written as a four component scalar field $\phi = (\sigma, \vec{\pi})$ and the $SU(2)_L \times SU(2)_R$ rotations are then simply $O(4)$ rotations of ϕ . In this language, the symmetry breaking pattern $SU(2)_L \times SU(2)_R \rightarrow SU(2)_{L+R}$ is described as $O(4) \rightarrow O(3)$: in the vacuum, $\langle \phi \rangle \neq 0$ and this condensate picks a direction in $O(4)$ -space. The direction in which the condensate points is conventionally taken to be the σ direction. In the presence of $\langle \sigma \rangle \neq 0$, the $\vec{\pi}$ excitations are excitations of the direction in which $\langle \phi \rangle$ is pointing, and are therefore massless goldstone modes.

At nonzero but low temperature, one finds a gas of pions, the analogue of a gas of spin waves, but $\langle \phi \rangle$ is still nonzero. Above some temperature T_c , entropy wins over order (the direction in which ϕ points is scrambled) and $\langle \phi \rangle = 0$. The phase transition at which chiral symmetry is restored is likely second order and belongs to the universality class of $O(4)$ spin models in three dimensions.⁸⁶ Below T_c , chiral symmetry is broken and there are three massless pions. At $T = T_c$, there are four massless degrees of freedom: the pions and the sigma. Above $T = T_c$, the pion and sigma correlation lengths are degenerate and finite.

In nature, the light quarks are not massless. Because of this explicit chiral symmetry breaking, the second order phase transition is replaced by an analytical crossover: physics changes dramatically but smoothly in the crossover region, and no correlation length diverges. Thus, in Figure 2, there is no sharp boundary on the vertical axis separating the low temperature hadronic world from the high temperature quark-gluon plasma. This picture is consistent with present lattice simulations,^{87,88} which suggest $T_c \sim 140 - 190$ MeV.^{89,88}

Arguments based on a variety of models^{90,91,5,6,43,92} indicate that the chiral symmetry restoration transition is first order at large μ . The 2SC quark matter phase that arises in two-flavor QCD at values of μ above this first order transition features new condensates, different from those in the hadronic phase, and these condensates do not break chiral symmetry. The fact that this is a transition in which two different condensates compete strengthens previous model-based arguments that this transition is first order.^{43,45} This suggests that the phase diagram features a critical point E at which the line of first order phase transitions present for $\mu > \mu_E$ ends, as shown in Figure 2.^c At μ_E ,

^cIf the up and down quarks were massless, E would be a tricritical point,⁹³ at which the first

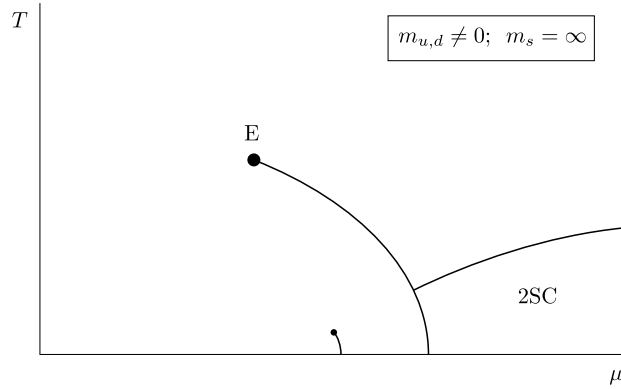


Figure 2: QCD phase diagram for two light quarks. Qualitatively as in Figure 1, except that the introduction of light quark masses turns the second order phase transition into a smooth crossover. The tricritical point becomes the critical endpoint E , which can be found in heavy ion collision experiments.

the phase transition is second order and is in the Ising universality class.^{43,92} Although the pions remain massive, the correlation length in the σ channel diverges due to universal long wavelength fluctuations of the order parameter. This results in characteristic signatures, analogues of critical opalescence in the sense that they are unique to collisions which freeze out near the critical point, which can be used to discover E .^{94,95}

Returning to the $\mu = 0$ axis, universal arguments,⁸⁶ again backed by lattice simulation,⁸⁷ tell us that if the strange quark were as light as the up and down quarks, the transition would be first order, rather than a smooth crossover. This means that if one could dial the strange quark mass m_s , one would find a critical m_s^c at which the transition as a function of temperature is second order.^{96,85} Figures 2, 3 and 4 are drawn for a sequence of decreasing strange quark masses. Somewhere between Figures 3 and 4, m_s is decreased below m_s^c and the transition on the vertical axis becomes first order. The value of m_s^c is an open question, but lattice simulations suggest that it is about half the physical strange quark mass.^{97,98} These results are not yet conclusive⁹⁹ but if they are correct then the phase diagram in nature is as shown in Figure 3, and the phase transition at low μ is a smooth crossover.

These observations fit together in a simple and elegant fashion. If we could vary m_s , we would find that as m_s is reduced from infinity to m_s^c , the critical point E in the (T, μ) plane moves toward the $\mu = 0$ axis.⁹⁴ This is shown in Figures 2-4. In nature, E is at some nonzero T_E and μ_E . When m_s is reduced to m_s^c , between Figure 3 and Figure 4, μ_E reaches zero. Of course,

order transition becomes second order. See Figure 1.

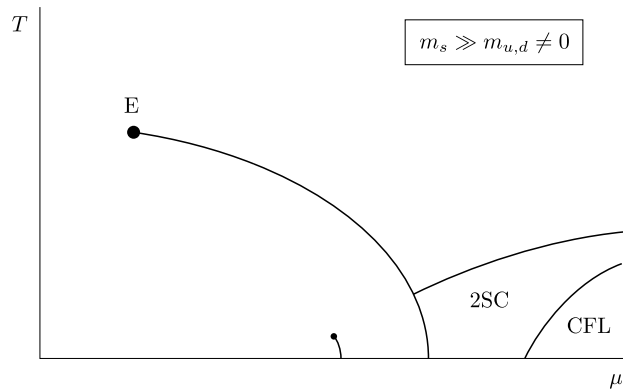


Figure 3: QCD phase diagram for two light quarks and a strange quark with a mass comparable to that in nature. The presence of the strange quark shifts E to the left, as can be seen by comparing with Figure 2. At sufficiently high density, cold quark matter is necessarily in the CFL phase in which quarks of all three colors and all three flavors form Cooper pairs. The diquark condensate in the CFL phase breaks chiral symmetry, and this phase has the same symmetries as baryonic matter which is dense enough that the nucleon and hyperon densities are comparable. The unlocking phase transition between the CFL and 2SC phases is first order.

experimentalists cannot vary m_s . They can, however, vary μ . AGS collisions with center of mass energy $\sqrt{s} = 5$ AGeV create fireballs which freeze out near $\mu \sim 500 - 600$ MeV.¹⁰⁰ SPS collisions with $\sqrt{s} = 17$ AGeV create fireballs which freeze out near $\mu \sim 200 - 300$ MeV.¹⁰⁰ In time, we will also have data from SPS collisions with $\sqrt{s} = 9$ AGeV and $\sqrt{s} = 12$ AGeV and from RHIC collisions with $\sqrt{s} = 56, 130$ and 200 AGeV and other energies.^d By dialing \sqrt{s} and thus μ , experimenters can find the critical point E .

We hope that the study of heavy ion collisions will, in the end, lead both to a quantitative study of the properties of the quark-gluon plasma phase at temperatures well above the transition and to a quantitative understanding of how to draw the phase transition region of the phase diagram. Probing the partonic matter created early in the collision relies on a suite of signatures including: the use of J/Ψ mesons, charmed mesons, and perhaps the Υ as probes; the energy loss of high momentum partons and consequent effects on the high- p_T hadron spectrum; and the detection of photons and dileptons over and above those emitted in the later hadronic stages of the collision. We will not review this program here. Instead, we focus on signatures of the critical point. The map of the QCD phase diagram which we have sketched so far is simple, coherent and consistent with all we know theoretically; the discovery of the critical point would provide an experimental foundation for the central

^dThe first data from RHIC collisions at $\sqrt{s} = 56$ AGeV and $\sqrt{s} = 130$ AGeV have already appeared.^{101,102} This bodes well for the analyses to come.

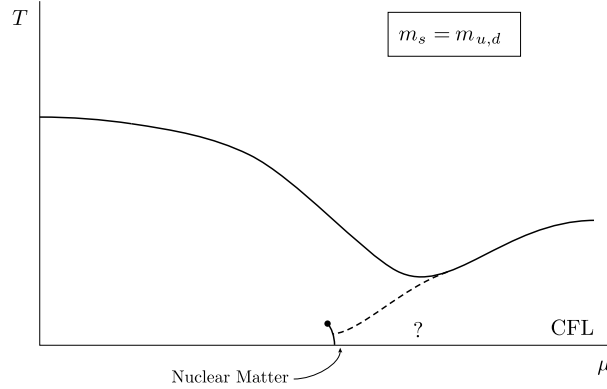


Figure 4: QCD phase diagram for three quarks which are degenerate in mass and which are either massless or light. The CFL phase and the baryonic phase have the same symmetries and may be continuously connected. The dashed line denotes the critical temperature at which baryon-baryon (or quark-quark) pairing vanishes; the region below the dashed line is superfluid. Chiral symmetry is broken everywhere below the solid line, which is a first order phase transition. The question mark serves to remind us that although no transition is required in this region, transition(s) may nevertheless arise as the magnitude of the gap increases qualitatively in going from the hypernuclear to the CFL phase. For quark masses as in nature, the high density region of the map may be as shown in Figure 3 or may be closer to that shown here, albeit with transition(s) in the vicinity of the question mark associated with the onset of nonzero hyperon density and the breaking of $U(1)_S$.¹³

qualitative feature of the landscape. This discovery would in addition confirm that in higher energy heavy ion collisions and in the big bang, the QCD phase transition is a smooth crossover. Furthermore, the discovery of collisions which create matter that freezes out near E would imply that conditions above the transition existed prior to freezeout, and would thus make it much easier to interpret the results of other experiments which study those observables which can probe the partonic matter created early in the collision.

We theorists must clearly do as much as we can to tell experimentalists *where* and *how* to find E . The “where” question, namely the question of predicting the value of μ_E and thus suggesting the \sqrt{s} to use to find E , is much harder for us to answer. First, as we have stressed in the previous Section, *ab initio* analysis of QCD in its full glory — i.e. lattice calculations — are at present impossible at nonzero μ . We must therefore rely on models. Second, an intrinsic feature of the picture we have described is that μ_E is sensitive to the mass of the strange quark, and therefore particularly hard to predict. Crude models suggest that μ_E could be $\sim 600 - 800$ MeV in the absence of the strange quark,^{43,92} this in turn suggests that in nature μ_E may have of order half this value, and may therefore be accessible at the SPS if the SPS runs with $\sqrt{s} < 17$ AGeV. However, at present theorists cannot predict the value

of μ_E even to within a factor of two. The SPS can search a significant fraction of the parameter space; if it does not find E , it will then be up to the RHIC experiments to map the $\mu < 250$ MeV region.

Although we are trying to be helpful with the “where” question, we are not very good at answering it quantitatively. This question can only be answered convincingly by an experimental discovery. What we theorists *can* do reasonably well is to answer the “how” question, thus enabling experimenters to answer “where”. This is the goal of Ref. 95. The signatures proposed there are based on the fact that E is a genuine thermodynamic singularity at which susceptibilities diverge and the order parameter fluctuates on long wavelengths. The resulting signatures are *nonmonotonic* as a function of \sqrt{s} : as this control parameter is varied, we should see the signatures strengthen and then weaken again as the critical point is approached and then passed.

The critical point E can also be sought by varying control parameters other than \sqrt{s} . Ion size, centrality selection and rapidity selection can all be varied. The advantage of using \sqrt{s} is that we already know (by comparing results from the AGS and SPS) that dialing it changes the freeze out chemical potential μ , which is the goal in a search for E .

The event-by-event fluctuations of the mean transverse momentum of the charged particles in an event, p_T , will be enhanced in collisions which freeze out near E .⁹⁵ The fluctuations measured by NA49 at $\sqrt{s} = 17$ AGeV are as perfect Gaussians as the data statistics allow,¹⁰³ as expected for freeze-out from a system in thermal equilibrium. The width of the event-by-event distribution^e of mean p_T is in good agreement with predictions based on noncritical thermodynamic fluctuations in an equilibrated resonance gas.⁹⁵ That is, NA49 data are consistent with the hypothesis that almost all the observed event-by-event fluctuation in mean p_T , an intensive quantity, is thermodynamic in origin. This bodes well for the detectability of systematic changes in thermodynamic fluctuations near E .

One analysis described in detail in Ref. 95 is based on the ratio of the width of the true event-by-event distribution of the mean p_T to the width of the distribution in a sample of mixed events. This ratio was called \sqrt{F} . NA49 has measured $\sqrt{F} = 1.002 \pm 0.002$,^{103,95} which is consistent with expectations for noncritical thermodynamic fluctuations.^f Critical fluctuations of the σ field,

^eThis width can be measured even if one observes only two pions per event;¹⁰⁴ large acceptance data as from NA49 is required in order to learn that the distribution is Gaussian, that thermodynamic predictions may be valid, and that the width is therefore the only interesting quantity to measure.

^fIn an infinite system made of classical particles which is in thermal equilibrium, $\sqrt{F} = 1$. Bose effects increase \sqrt{F} by 1 – 2%;^{105,95} an anticorrelation introduced by energy conservation in a finite system — when one mode fluctuates up it is more likely for other modes to fluctuate down — decreases \sqrt{F} by 1 – 2%;⁹⁵ two-track resolution also decreases \sqrt{F} by 1 – 2%.¹⁰³ The contributions due to correlations introduced by resonance decays and

i.e. the characteristic long wavelength fluctuations of the order parameter near E , influence pion momenta via the (large) $\sigma\pi\pi$ coupling and increase \sqrt{F} .⁹⁵ The effect is proportional to $\xi_{\text{freezeout}}^2$, where $\xi_{\text{freezeout}}$ is the σ -field correlation length of the long-wavelength fluctuations at freezeout.⁹⁵ If $\xi_{\text{freezeout}} \sim 3$ fm (a reasonable estimate, as we describe below) the ratio \sqrt{F} increases by $\sim 3-5\%$, ten to twenty times the statistical error in the present measurement.⁹⁵ This observable is valuable because data on it has been analyzed and presented by NA49, and it can therefore be used to learn that Pb+Pb collisions at 158 AGeV do *not* freeze out near E . The $3-5\%$ nonmonotonic variation in \sqrt{F} as a function of \sqrt{s} which we predict is easily detectable but is not so large as to make one confident of using this alone as a signature of E .

Once E is located, however, other observables which are more sensitive to critical effects will be more useful. For example, a $\sqrt{F_{\text{soft}}}$, defined using only the softest 10% of the pions in each event, will be much more sensitive to the critical long wavelength fluctuations. The higher p_T pions are less affected by the σ fluctuations,⁹⁵ and these relatively unaffected pions dominate the mean p_T of all the pions in the event. This is why the increase in \sqrt{F} near the critical point will be much less than that of $\sqrt{F_{\text{soft}}}$. Depending on the details of the cut used to define it, $\sqrt{F_{\text{soft}}}$ should be enhanced by many tens of percent in collisions passing near E . Ref. 95 suggests other such observables, and more can surely be found.

The multiplicity of soft pions is an example of an observable which may be used to detect the critical fluctuations without an event-by-event analysis. The post-freezeout decay of sigma mesons, which are copious and light at freezeout near E and which decay subsequently when their mass increases above twice the pion mass, should result in a population of pions with $p_T \sim m_\pi/2$ which appears only for freezeout near the critical point⁹⁵. If $\xi_{\text{freezeout}} > 1/m_\pi$, this population of unusually low momentum pions will be comparable in number to that of the “direct” pions (i.e. those which were pions at freezeout) and will result in a large signature. This signature is therefore certainly large for $\xi_{\text{freezeout}} \sim 3$ fm and would not increase much further if $\xi_{\text{freezeout}}$ were larger still.

The variety of observables which should *all* vary nonmonotonically with \sqrt{s} (and should all peak at the same \sqrt{s}) is sufficiently great that if it were to turn out that $\mu_E < 200$ MeV, making E inaccessible to the SPS, all four RHIC experiments could play a role in the study of the critical point.

The purpose of Ref. 106 is to estimate how large $\xi_{\text{freezeout}}$ can become, thus making the predictions of Ref. 95 for the magnitude of various signatures more quantitative. The nonequilibrium dynamics analyzed in Ref. 106 is guaranteed to occur in a heavy ion collision which passes near E , even if local thermal

due to fluctuations in the flow velocity are each much smaller than 1%.⁹⁵

equilibrium is achieved at a higher temperature during the earlier evolution of the plasma created in the collision. If this plasma were to cool arbitrarily slowly, ξ would diverge at T_E . However, it would take an infinite time for ξ to grow infinitely large. Indeed, near a critical point, the longer the correlation length, the longer the equilibration time, and the slower the correlation length can grow. This critical slowing down means that the correlation length cannot grow sufficiently fast for the system to stay in equilibrium. We use the theory of dynamical critical phenomena¹⁰⁷ to describe the effects of critical slowing down of the long wavelength dynamics near E on the time development of the correlation length. The correlation length does not have time to grow as large as it would in equilibrium: we find $\xi_{\text{freezeout}} \sim 2/T_E \sim 3$ fm for trajectories passing near E . Although critical slowing down hinders the growth of ξ , it also slows the decrease of ξ as the system continues to cool below the critical point. As a result, ξ does not decrease significantly between the phase transition and freezeout.

We have learned much from the beautiful gaussian event-by-event fluctuations observed by NA49. The magnitude of these fluctuations are consistent with the hypothesis that the hadronic system at freezeout is in approximate thermal equilibrium. These and other data show none of the non-gaussian features that would signal that the system had been driven far from equilibrium either by a rapid traversal of the transition region or by the bubbling that would occur near a strong first order phase transition. There is also no sign of the enhanced, but still gaussian, fluctuations which would signal freezeout near the critical point E . Combining these observations with the observation of tantalizing indications that the matter created in SPS collisions is not well described at early times by hadronic models¹⁰⁸ suggests that collisions at the SPS may be exploring the crossover region to the left of the critical point E , in which the matter is not well-described as a hadron gas but is also not well-described as a quark-gluon plasma. This speculation could be confirmed in two ways. First, if the SPS is probing the crossover region then the coming experiments at RHIC may discover direct signatures of an early partonic phase, which are well-described by theoretical calculations beginning from an equilibrated quark-gluon plasma. Second, if $\sqrt{s} = 17$ AGeV collisions are probing the crossover region not far to the left of the critical point E , then SPS data taken at lower energies would result in the discovery of E . If, instead, RHIC were to discover E with $\mu_E < 200$ MeV, that would indicate that the SPS experiments have probed the weakly first order region just to the right of E . Regardless, discovering E would take all the speculation out of mapping this part of the QCD phase diagram.

Let us now return to the high density, low temperature regions of the phase diagram. In this regime, as we have seen in previous sections, the most symmetric starting point with which to begin our analysis is the case of three

quarks with degenerate masses. In QCD with $m_s = m_{u,d}$ as in Figure 4, cold dense quark matter is in the CFL phase which has the same symmetries as the hypernuclear matter phase, characterized by a condensate of Cooper pairs of baryons.⁸ Furthermore, many non-universal features of these two phases correspond.⁸ This raises the possibility that quark matter and baryonic matter may be continuously connected,⁸ as shown in Figure 4.

Both CFL quark matter and hypernuclear matter are superfluids, characterized by a spontaneously broken global $U(1)$ symmetry associated with baryon number. Chiral symmetry is broken in these (or this!) phase. This means that as we increase the temperature from zero in Figure 4, there may be two distinct phase transitions between the CFL/hypernuclear phase and the quark-gluon plasma, as superfluidity is lost and chiral symmetry is restored. As hypernuclear matter is heated, we expect superfluidity to be lost at a lower temperature than that at which chiral symmetry is restored. At high densities, on the other hand, we expect only a single transition because both chiral symmetry breaking and superfluidity are caused by the diquark condensate which locks color to flavor. Figure 4 is drawn accordingly. The transition at which chiral symmetry is restored is first order, for the same reasons as at $\mu = 0$: there is no infrared fixed point which could describe a second order chiral symmetry restoration transition in QCD with three massless quarks.⁸⁶

Nature chooses two light quarks and one middle-weight strange quark, rather than three degenerate quarks as in Figure 4. As we have discussed in Section 3.2, a nonzero m_s weakens those condensates which involve pairing between light and strange quarks. The CFL phase requires nonzero $\langle us \rangle$ and $\langle ds \rangle$ condensates which can only exist if the associated gaps are larger than of order $m_s^2/2\mu$. If one imagines increasing m_s at fixed μ , one finds a first order unlocking transition:^{13,17} for larger m_s only u and d quarks pair and the 2SC phase is obtained. Conversely, as m_s is reduced in going from Figure 2 to 3 to 4, the region occupied by the CFL phase expands to encompass regions with smaller and smaller μ .^{13,17} For any $m_s \neq \infty$, the CFL phase is the ground state at arbitrarily high density.¹³ For larger values of m_s , there is a 2SC interlude on the horizontal axis, in which chiral symmetry is restored, before the CFL phase breaks it again at high densities. For smaller values of m_s , the possibility of quark-hadron continuity⁸ as shown in Figure 4 arises. It should be noted that when the strange and light quarks are not degenerate, the CFL phase may be continuous with a baryonic phase in which the densities of all the nucleons and hyperons are comparable; there are, however, phase transition(s) between this hypernuclear phase and ordinary nuclear matter made of neutrons and protons only.¹³

We can now describe what happens in QCD with $m_{u,d} < m_s < \infty$ as in Figure 3 to CFL quark matter as it is heated. Because the $\langle us \rangle$ and $\langle ds \rangle$ condensates are smaller than the $\langle ud \rangle$ condensate, they vanish first. At this

temperature, we find a first order unlocking phase transition at which chiral symmetry is restored.^g Above this transition, we find the 2SC phase in which only red and green u and d quarks pair.^h The Cooper pairs are $ud - du$ flavor singlets and the global flavor symmetry $SU(2)_L \times SU(2)_R$ is intact. There is also an unbroken global symmetry which plays the role of $U(1)_B$. Thus, no global symmetries are broken in this 2SC phase. There need therefore be no transition between the 2SC and quark-gluon plasma phases in Figure 3 (or in Figures 1 and 2) because neither phase breaks any global symmetries. However, this transition, which is second order in mean field theory, is likely first order in QCD due to gauge field fluctuations,⁴³ at least at high enough density.¹⁰⁹

Throughout our description of the phase diagram, we have assumed that the chemical potentials $\mu_u = \mu_d = \mu_s = \mu$ are degenerate. Different values of the strange quark m_s lead to differences between the Fermi momentum for s quarks relative to that for u and d quarks. This analysis neglects electromagnetic and weak effects. In particular, looking ahead to the study of color superconductivity in compact stars, it neglects the requirement that the quark matter be electrically neutral and in beta equilibrium. If the up, down and strange quarks were degenerate, quark matter with $\mu_u = \mu_d = \mu_s = \mu$ would be electrically neutral and in beta equilibrium. Instead, because $m_s \gg m_{u,d}$, the quark matter in a compact star must have $\mu_{d,s} - \mu_u = \mu_e > 0$, where μ_e is the electron chemical potential.³⁸ In quark matter with average quark chemical potential $\mu \sim 400 - 500$ MeV, as may occur in a compact star, reasonable estimates for μ_e are in the few tens of MeV. The presence of a small but nonzero μ_e would certainly have quantitative effects in Figures 1 to 4; we shall see in Section 6.6 that it can have qualitative effects also.

6 Color Superconductivity in Compact Stars

Our current understanding of the color superconducting state of quark matter leads us to believe that it may occur naturally in compact stars. The critical temperature T_c below which quark matter is a color superconductor is high enough that any quark matter which occurs within neutron stars that are more than a few seconds old is in a color superconducting state. In the absence of lattice simulations, present theoretical methods are not accurate enough to determine whether neutron star cores are made of hadronic matter or quark

^gThat this transition is first order can be seen both via the same argument which demonstrates that the unlocking transition between the 2SC and CFL phases at $T = 0$ is first order^{13,17} and via the fact that it is a finite temperature phase transition at which chiral symmetry is restored in a three-flavor theory.

^hAs we have seen in Section 3, in the 2SC phase at zero temperature, there may be small $J = 1$ $\langle ss \rangle$ and blue $\langle ud \rangle$ condensates; these condensates would not persist at the temperatures we are discussing here.

matter. They also cannot determine whether any quark matter which arises will be in the CFL or 2SC phase: the difference between the u , d and s Fermi momenta will be a few tens of MeV which is comparable to estimates of the gap Δ ; the CFL phase occurs when Δ is large compared to all differences between Fermi momenta. Just as the higher temperature regions of the QCD phase diagram are being mapped out in heavy ion collisions, we need to learn how to use neutron star phenomena to determine whether they feature cores made of 2SC quark matter, CFL quark matter or hadronic matter, thus teaching us about the high density region of the QCD phase diagram. It is therefore important to look for astrophysical consequences of color superconductivity.

6.1 Equation of State

Much of the work on the consequences of quark matter within a compact star has focussed on the effects of quark matter on the equation of state, and hence on the radius of the star. As a Fermi surface phenomenon, color superconductivity has little effect on the equation of state: the pressure is an integral over the whole Fermi volume. Color superconductivity modifies the equation of state at the $\sim (\Delta/\mu)^2$ level, typically by a few percent.⁵ Such small effects can be neglected in present calculations, and for this reason we will not attempt to survey the many ways in which observations of neutron stars are being used to constrain the equation of state.¹⁰

We will describe one current idea, however. As a neutron star in a low mass X-ray binary (LMXB) is spun up by accretion from its companion, it becomes more oblate and its central density decreases. If it contains a quark matter core, the volume fraction occupied by this core decreases, the star expands, and its moment of inertia increases. This raises the possibility¹¹ of a period during the spin-up history of an LMXB when the neutron star is gaining angular momentum via accretion, but is gaining sufficient moment of inertia that its angular frequency is hardly increasing. In their modelling of this effect, Glendenning and Weber¹¹ discover that LMXB's should spend a significant fraction of their history with a frequency of around 200 Hz, while their quark cores are being spun out of existence, before eventually spinning up to higher frequencies. This may explain the observation that LMXB frequencies are clustered around 250-350 Hz,¹² which is otherwise puzzling in that it is thought that LMXB's provide the link between canonical pulsars and millisecond pulsars, which have frequencies as large as 600 Hz.¹³ It will be interesting to see how robust the result of Ref. 111 is to changes in model assumptions and also how its predictions fare when compared to those of other explanations which posit upper bounds on LMXB frequencies,¹⁴ rather than a most probable frequency range with no associated upper bound.¹¹ We note here that because Glendenning and Weber's effect depends only on the equation of state and not

on other properties of quark matter, the fact that the quark matter must in fact be a color superconductor will not affect the results in any significant way. If Glendenning and Weber's explanation for the observed clustering of LMXB frequencies proves robust, it would imply that pulsars with lower rotational frequencies feature quark matter cores.

6.2 Cooling by Neutrino Emission

We turn now to neutron star phenomena which *are* affected by Fermi surface physics. For the first 10^{5-6} years of its life, the cooling of a neutron star is governed by the balance between heat capacity and the loss of heat by neutrino emission. How are these quantities affected by the presence of a quark matter core? This has been addressed recently in Refs. 115,116, following earlier work in Ref. 117. Both the specific heat C_V and the neutrino emission rate L_ν are dominated by physics within T of the Fermi surface. If, as in the CFL phase, all quarks have a gap $\Delta \gg T$ then the contribution of quark quasiparticles to C_V and L_ν is suppressed by $\sim \exp(-\Delta/T)$. There may be other contributions to L_ν ,¹¹⁵ but these are also very small. In the CFL phase, the specific heat is dominated by that of the electrons.³⁸ (There is an additional contribution from the superfluid mode in the CFL phase — i.e. the Goldstone boson associated with the spontaneous breaking of $U(1)_B$ — and there may also be small contributions from the light but not massless pseudo-Goldstone bosons associated with chiral symmetry breaking.) Although further work is required, it is already clear that both C_V and L_ν are much smaller than in the nuclear matter outside the quark matter core. This means that the total heat capacity and the total neutrino emission rate (and hence the cooling rate) of a neutron star with a CFL core will be determined completely by the nuclear matter outside the core. The quark matter core is “inert”: with its small heat capacity and emission rate it has little influence on the temperature of the star as a whole. As the rest of the star emits neutrinos and cools, the core cools by conduction, because the electrons keep it in good thermal contact with the rest of the star. These qualitative expectations are nicely borne out in the calculations presented by Page et al.¹¹⁶

The analysis of the cooling history of a neutron star with a quark matter core in the 2SC phase is more complicated. The red and green up and down quarks pair with a gap many orders of magnitude larger than the temperature, which is of order 10 keV, and are therefore inert as described above. Any strange quarks present will form an $\langle ss \rangle$ condensate with angular momentum $J = 1$ which locks to color in such a way that rotational invariance is not broken.⁴⁷ The resulting gap has been estimated to be of order hundreds of keV,⁴⁷ although applying results of Ref. 49 suggests a somewhat smaller gap, around 10 keV. The blue up and down quarks also pair, forming a $J = 1$

condensate which breaks rotational invariance.⁵ The related gap was estimated to be a few keV,⁵ but this estimate was not robust and should be revisited in light of more recent developments given its importance in the following. The critical temperature T_c above which no condensate forms is of order the zero-temperature gap Δ . ($T_c = 0.57\Delta$ for $J = 0$ condensates.⁶¹) Therefore, if there are quarks for which $\Delta \sim T$ or smaller, these quarks do not pair at temperature T . Such quark quasiparticles will radiate neutrinos rapidly (via direct URCA reactions like $d \rightarrow u + e + \bar{\nu}$, $u \rightarrow d + e^+ + \nu$, etc.) and the quark matter core will cool rapidly and determine the cooling history of the star as a whole.^{117,116} The star will cool rapidly until its interior temperature is $T < T_c \sim \Delta$, at which time the quark matter core will become inert and the further cooling history will be dominated by neutrino emission from the nuclear matter fraction of the star. If future data were to show that neutron stars first cool rapidly (direct URCA) and then cool more slowly, such data would allow an estimate of the smallest quark matter gap. We are unlikely to be so lucky. The simple observation of rapid cooling would *not* be an unambiguous discovery of quark matter with small gaps; there are other circumstances in which the direct URCA processes occur. However, if as data on neutron star temperatures improves in coming years the standard cooling scenario proves correct, indicating the absence of the direct URCA processes, this *would* rule out the presence of quark matter with gaps in the 10 keV range or smaller. The presence of a quark matter core in which *all* gaps are $\gg T$ can never be revealed by an analysis of the cooling history.

6.3 Supernova Neutrinos

We now turn from neutrino emission from a neutron star which is many years old to that from the protoneutron star during the first seconds of a supernova. Carter and Reddy¹¹⁸ have pointed out that when this protoneutron star is at its maximum temperature of order 30-50 MeV, it may have a quark matter core which is too hot for color superconductivity. As such a protoneutron star core cools over the next few seconds, this quark matter will cool through T_c , entering the color superconducting regime of the QCD phase diagram. For $T \sim T_c$, the specific heat rises and the cooling slows. Then, as T drops further and Δ increases to become greater than T , the specific heat drops rapidly. Furthermore, as the number density of quark quasiparticles becomes suppressed by $\exp(-\Delta/T)$, the neutrino transport mean free path rapidly becomes very long.¹¹⁸ This means that all the neutrinos previously trapped in the now color superconducting core are able to escape in a sudden burst. If a terrestrial neutrino detector sees thousands of neutrinos from a future supernova, Carter and Reddy's results suggest that there may be a signature of the transition to color superconductivity present in the time distribution of these neutrinos.

Neutrinos from the core of the protoneutron star will lose energy as they scatter on their way out, but because they will be the last to reach the surface of last scattering, they will be the final neutrinos received at the earth. If they are released from the quark matter core in a sudden burst, they may therefore result in a bump at late times in the temporal distribution of the detected neutrinos. More detailed study remains to be done in order to understand how Carter and Reddy’s signature, dramatic when the neutrinos escape from the core, is processed as the neutrinos traverse the rest of the protoneutron star and reach their surface of last scattering.

6.4 R-mode Instabilities

Another arena in which color superconductivity comes into play is the physics of r-mode instabilities. A neutron star whose angular rotation frequency Ω is large enough is unstable to the growth of r-mode oscillations which radiate away angular momentum via gravitational waves, reducing Ω . What does “large enough” mean? The answer depends on the damping mechanisms which act to prevent the growth of the relevant modes. Both shear viscosity and bulk viscosity act to damp the r-modes, preventing them from going unstable. The bulk viscosity and the quark contribution to the shear viscosity both become exponentially small in quark matter with $\Delta > T$ and as a result, as Madsen¹¹⁹ has shown, a compact star made *entirely* of quark matter with gaps $\Delta = 1$ MeV or greater is unstable if its spin frequency is greater than tens to 100 Hz. Many compact stars spin faster than this, and Madsen therefore argues that compact stars cannot be strange quark stars unless some quarks remain ungapped. Alas, this powerful argument becomes much less powerful in the context of a neutron star with a quark matter core. First, the r-mode oscillations have a wave form whose amplitude is largest at large radius, outside the core. Second, in an ordinary neutron star there is a new source of damping: friction at the boundary between the crust and the neutron superfluid “mantle” keeps the r-modes stable regardless of the properties of a quark matter core.^{120,119}

6.5 Magnetic Field Evolution

Next, we turn to the physics of magnetic fields within color superconducting neutron star cores.^{121,40} The interior of a conventional neutron star is a superfluid (because of neutron-neutron pairing) and is an electromagnetic superconductor (because of proton-proton pairing). Ordinary magnetic fields penetrate it only in the cores of magnetic flux tubes. A color superconductor behaves differently. At first glance, it seems that because a diquark Cooper pair has nonzero electric charge, a diquark condensate must exhibit the standard Meissner effect, expelling ordinary magnetic fields or restricting them to flux tubes

within whose cores the condensate vanishes. This is not the case.⁴⁰ In both the 2SC and CFL phase, a linear combination of the $U(1)$ gauge transformation of ordinary electromagnetism and one (the eighth) color gauge transformation remains unbroken even in the presence of the condensate. This means that the ordinary photon A_μ and the eighth gluon G_μ^8 are replaced by new linear combinations

$$\begin{aligned} A_\mu^{\tilde{Q}} &= \cos \alpha_0 A_\mu + \sin \alpha_0 G_\mu^8, \\ A_\mu^X &= -\sin \alpha_0 A_\mu + \cos \alpha_0 G_\mu^8, \end{aligned} \quad (110)$$

where $A_\mu^{\tilde{Q}}$ is massless and A_μ^X is massive. That is, $B_{\tilde{Q}}$ satisfies the ordinary Maxwell equations while B_X experiences a Meissner effect. $\sin(\alpha_0)$ is proportional to e/g and turns out to be about 1/20 in the 2SC phase and 1/40 in the CFL phase.⁴⁰ This means that the \tilde{Q} -photon which propagates in color superconducting quark matter is mostly photon with only a small gluon admixture. If a color superconducting neutron star core is subjected to an ordinary magnetic field, it will either expel the X component of the flux or restrict it to flux tubes, but it can (and does⁴⁰) admit the great majority of the flux in the form of a $B_{\tilde{Q}}$ magnetic field satisfying Maxwell's equations. The decay in time of this "free field" (i.e. not in flux tubes) is limited by the \tilde{Q} -conductivity of the quark matter. A color superconductor is not a \tilde{Q} -superconductor — that is the whole point — but it may turn out to be a very good \tilde{Q} -conductor due to the presence of electrons: if a nonzero density of electrons is required in order to maintain charge neutrality, the $B_{\tilde{Q}}$ magnetic field likely decays only on a time scale which is much longer than the age of the universe.⁴⁰ This means that a quark matter core within a neutron star can serve as an "anchor" for the magnetic field: whereas in ordinary nuclear matter the magnetic flux tubes can be dragged outward by the neutron superfluid vortices as the star spins down,¹²² the magnetic flux within the color superconducting core simply cannot decay. Even though this distinction is a qualitative one, it will be difficult to confront it with data since what is observed is the total dipole moment of the neutron star. A color superconducting core anchors those magnetic flux lines which pass through the core, while in a neutron star with no quark matter core the entire internal magnetic field can decay over time. In both cases, however, the total dipole moment can change since the magnetic flux lines which do not pass through the core can move.

6.6 Crystalline Color Superconductivity and Glitches in Quark Matter

The final consequence of color superconductivity we wish to discuss is the possibility that (some) glitches may originate within quark matter regions of

a compact star.⁴⁹ In any context in which color superconductivity arises in nature, it is likely to involve pairing between species of quarks with differing chemical potentials. If the chemical potential difference is small enough, BCS pairing occurs as we have been discussing. If the Fermi surfaces are too far apart, no pairing between the species is possible. The transition between the BCS and unpaired states as the splitting between Fermi momenta increases has been studied in electron superconductors,¹²³ nuclear superfluids²⁴ and QCD superconductors,^{13,17,125} assuming that no other state intervenes. However, there is good reason to think that another state can occur. This is the “LOFF” state, first explored by Larkin and Ovchinnikov¹²⁶ and Fulde and Ferrell²⁷ in the context of electron superconductivity in the presence of magnetic impurities. They found that near the unpairing transition, it is favorable to form a state in which the Cooper pairs have nonzero momentum. This is favored because it gives rise to a region of phase space where each of the two quarks in a pair can be close to its Fermi surface, and such pairs can be created at low cost in free energy. Condensates of this sort spontaneously break translational and rotational invariance, leading to gaps which vary periodically in a crystalline pattern. If in some shell within the quark matter core of a neutron star (or within a strange quark star) the quark number densities are such that crystalline color superconductivity arises, rotational vortices may be pinned in this shell, making it a locus for glitch phenomena.

The authors of Ref. 49, have explored the range of parameters for which crystalline color superconductivity occurs in the QCD phase diagram, upon making various simplifying assumptions. We focus primarily on a toy model in which the quarks interact via a four-fermion interaction with the quantum numbers of single gluon exchange. Also, we only consider pairing between u and d quarks, with $\mu_d = \bar{\mu} + \delta\mu$ and $\mu_u = \bar{\mu} - \delta\mu$, whereas we expect a LOFF state wherever the difference between the Fermi momenta of any two quark flavors is near an unpairing transition, including, for example, near the unlocking phase transition between the 2SC and CFL phases.

In the LOFF state, each Cooper pair carries momentum $2\mathbf{q}$ with $|\mathbf{q}| \approx 1.2\delta\mu$. The condensate and gap parameter vary in space with wavelength $\pi/|\mathbf{q}|$. In Ref. 49, we simplify the calculation by assuming that the condensate varies in space like a plane wave, leaving the determination of the crystal structure of the QCD LOFF phase to future work. We give an ansatz for the LOFF wave function, and by variation obtain a gap equation which allows us to solve for the gap parameter Δ_A , the free energy and the values of the diquark condensates which characterize the LOFF state at a given $\delta\mu$ and $|\mathbf{q}|$. We then vary $|\mathbf{q}|$, to find the preferred (lowest free energy) LOFF state at a given $\delta\mu$, and compare the free energy of the LOFF state to that of the BCS state with which it competes. The LOFF state is characterized by a gap parameter Δ_A and a diquark condensate, but not by an energy gap in the dispersion relation:

we obtain the quasiparticle dispersion relations⁴⁹ and find that they vary with the direction of the momentum, yielding gaps that vary from zero up to a maximum of Δ_A . The condensate is dominated by the regions in momentum space in which a quark pair with total momentum $2\mathbf{q}$ has both members of the pair within $\sim \Delta_A$ of their respective Fermi surfaces.

The LOFF state is favored for values of $\delta\mu$ which satisfy $\delta\mu_1 < \delta\mu < \delta\mu_2$, with $\delta\mu_1/\Delta_0 = 0.707$ and $\delta\mu_2/\Delta_0 = 0.754$ in the weak coupling limit in which $\Delta_0 \ll \mu$. (For $\delta\mu < \delta\mu_1$, we have the 2SC phase with gap Δ_0 .) At weak coupling, the LOFF gap parameter decreases from $0.23\Delta_0$ at $\delta\mu = \delta\mu_1$ (where there is a first order BCS-LOFF phase transition) to zero at $\delta\mu = \delta\mu_2$ (where there is a second order LOFF-normal transition). Except for very close to $\delta\mu_2$, the critical temperature above which the LOFF state melts will be much higher than typical neutron star temperatures. At stronger coupling the LOFF gap parameter decreases relative to Δ_0 and the window of $\delta\mu/\Delta_0$ within which the LOFF state is favored shrinks. The window grows if the interaction is changed to weight electric gluon exchange more heavily than magnetic gluon exchange.

Near the second-order critical point $\delta\mu_2$, we can describe the phase transition with a Ginzburg-Landau effective potential. The order parameter for the LOFF-to-normal phase transition is

$$\Phi(\mathbf{r}) = -\frac{1}{2} \langle \epsilon_{ab} \epsilon_{\alpha\beta\gamma} \psi^{a\alpha}(\mathbf{r}) C \gamma_5 \psi^{b\beta}(\mathbf{r}) \rangle \quad (111)$$

so that in the normal phase $\Phi(\mathbf{r}) = 0$, while in the LOFF phase $\Phi(\mathbf{r}) = \Gamma_A e^{i2\mathbf{q}\cdot\mathbf{r}}$. (The gap parameter is related to the order parameter by $\Delta_A = G\Gamma_A$.) Expressing the order parameter in terms of its Fourier modes $\tilde{\Phi}(\mathbf{k})$, we write the LOFF free energy (relative to the normal state) as

$$F(\{\tilde{\Phi}(\mathbf{k})\}) = \sum_{\mathbf{k}} \left(C_2(k^2) |\tilde{\Phi}(\mathbf{k})|^2 + C_4(k^2) |\tilde{\Phi}(\mathbf{k})|^4 + \mathcal{O}(|\tilde{\Phi}|^6) \right). \quad (112)$$

For $\delta\mu > \delta\mu_2$, all of the $C_2(k^2)$ are positive and the normal state is stable. Just below the critical point, all of the modes $\tilde{\Phi}(\mathbf{k})$ are stable except those on the sphere $|\mathbf{k}| = 2q_2$, where q_2 is the value of $|\mathbf{q}|$ at $\delta\mu_2$ (so that $q_2 \simeq 1.2\delta\mu_2 \simeq 0.9\Delta_0$ at weak coupling). In general, many modes on this sphere can become nonzero, giving a condensate with a complex crystal structure. We consider the simplest case of a plane wave condensate where only the one mode $\tilde{\Phi}(\mathbf{k} = 2\mathbf{q}_2) = \Gamma_A$ is nonvanishing. Dropping all other modes, we have

$$F(\Gamma_A) = a(\delta\mu - \delta\mu_2)(\Gamma_A)^2 + b(\Gamma_A)^4, \quad (113)$$

where a and b are positive constants. Finding the minimum-energy solution for $\delta\mu < \delta\mu_2$, we obtain simple power-law relations for the condensate and the free energy:

$$\Gamma_A(\delta\mu) = K_\Gamma(\delta\mu_2 - \delta\mu)^{1/2}, \quad F(\delta\mu) = -K_F(\delta\mu_2 - \delta\mu)^2. \quad (114)$$

These expressions agree well with the numerical results obtained by solving the gap equation.⁴⁹ The Ginzburg-Landau method does not specify the proportionality factors K_Γ and K_F , but analytical expressions for these coefficients can be obtained in the weak coupling limit by explicitly solving the gap equation,^{128,49} yielding

$$\begin{aligned} GK_\Gamma &= 2\sqrt{\delta\mu_2}\sqrt{(q_2/\delta\mu_2)^2 - 1} \simeq 1.15\sqrt{\Delta_0}, \\ K_F &= (4\bar{\mu}^2/\pi^2)((q_2/\delta\mu_2)^2 - 1) \simeq 0.178\bar{\mu}^2. \end{aligned} \quad (115)$$

Notice that because $(\delta\mu_2 - \delta\mu_1)/\delta\mu_2$ is small, the power-law relations (114) are a good model of the system throughout the entire LOFF interval $\delta\mu_1 < \delta\mu < \delta\mu_2$ where the LOFF phase is favored over the BCS phase. The Ginzburg-Landau expression (113) gives the free energy of the LOFF phase near $\delta\mu_2$, but it cannot be used to determine the location $\delta\mu_1$ of the first-order phase transition where the LOFF window terminates. (Locating the first-order point requires a comparison of LOFF and BCS free energies.)

The quark matter which may be present within a compact star will be in the crystalline color superconductor (LOFF) state if $\delta\mu/\Delta_0$ is in the requisite range. For a reasonable value of $\delta\mu$, say 25 MeV, this occurs if the gap Δ_0 which characterizes the uniform color superconductor present at smaller values of $\delta\mu$ is about 40 MeV. This is in the middle of the range of present estimates. Both $\delta\mu$ and Δ_0 vary as a function of density and hence as a function of radius in a compact star. Although it is too early to make quantitative predictions, the numbers are such that crystalline color superconducting quark matter may very well occur in a range of radii within a compact star. It is therefore worthwhile to consider the consequences.

Many pulsars have been observed to glitch. Glitches are sudden jumps in rotation frequency Ω which may be as large as $\Delta\Omega/\Omega \sim 10^{-6}$, but may also be several orders of magnitude smaller. The frequency of observed glitches is statistically consistent with the hypothesis that all radio pulsars experience glitches.¹²⁹ Glitches are thought to originate from interactions between the rigid neutron star crust, typically somewhat more than a kilometer thick, and rotational vortices in a neutron superfluid. The inner kilometer of crust consists of a crystal lattice of nuclei immersed in a neutron superfluid.¹³⁰ Because the pulsar is spinning, the neutron superfluid (both within the inner crust and deeper inside the star) is threaded with a regular array of rotational vortices. As the pulsar's spin gradually slows, these vortices must gradually move outwards since the rotation frequency of a superfluid is proportional to the density of vortices. Deep within the star, the vortices are free to move outwards. In the crust, however, the vortices are pinned by their interaction with the nuclear lattice. Models¹³¹ differ in important respects as to how the stress associated with pinned vortices is released in a glitch: for example, the vortices may break

and rearrange the crust, or a cluster of vortices may suddenly overcome the pinning force and move macroscopically outward, with the sudden decrease in the angular momentum of the superfluid within the crust resulting in a sudden increase in angular momentum of the rigid crust itself and hence a glitch. All the models agree that the fundamental requirements are the presence of rotational vortices in a superfluid and the presence of a rigid structure which impedes the motion of vortices and which encompasses enough of the volume of the pulsar to contribute significantly to the total moment of inertia.

Although it is premature to draw quantitative conclusions, it is interesting to speculate that some glitches may originate deep within a pulsar which features a quark matter core, in a region of that core which is in a LOFF crystalline color superconductor phase. A three flavor analysis is required to estimate over what range of densities LOFF phases may arise, as either $\langle ud \rangle$, $\langle us \rangle$ or $\langle ds \rangle$ condensates approach their unpairing transitions. Comparison to existing models which describe how p_F^u , p_F^d and p_F^s vary within a quark matter core in a neutron star¹³² would then permit an estimate of how much the LOFF region contributes to the moment of inertia of the pulsar. Furthermore, a three flavor analysis is required to determine whether the LOFF phase is a superfluid. If the only pairing is between u and d quarks, this 2SC phase is not a superfluid,^{5,13} whereas if all three quarks pair in some way, a superfluid *is* obtained.^{7,13} Henceforth, we suppose that the LOFF phase is a superfluid, which means that if it occurs within a pulsar it will be threaded by an array of rotational vortices. It is reasonable to expect that these vortices will be pinned in a LOFF crystal, in which the diquark condensate varies periodically in space. Indeed, one of the suggestions for how to look for a LOFF phase in terrestrial electron superconductors relies on the fact that the pinning of magnetic flux tubes (which, like the rotational vortices of interest to us, have normal cores) is expected to be much stronger in a LOFF phase than in a uniform BCS superconductor.¹³³

A real calculation of the pinning force experienced by a vortex in a crystalline color superconductor must await the determination of the crystal structure of the LOFF phase. We can, however, attempt an order of magnitude estimate along the same lines as that done by Anderson and Itoh¹³⁴ for neutron vortices in the inner crust of a neutron star. In that context, this estimate has since been made quantitative.^{135,136,131} For one specific choice of parameters,⁴⁹ the LOFF phase is favored over the normal phase by a free energy $F_{\text{LOFF}} \sim 5 \times (10 \text{ MeV})^4$ and the spacing between nodes in the LOFF crystal is $b = \pi/(2|\mathbf{q}|) \sim 9 \text{ fm}$. The thickness of a rotational vortex is given by the correlation length $\xi \sim 1/\Delta \sim 25 \text{ fm}$. The pinning energy is the difference between the energy of a section of vortex of length b which is centered on a node of the LOFF crystal vs. one which is centered on a maximum of the LOFF crystal. It is of order $E_p \sim F_{\text{LOFF}} b^3 \sim 4 \text{ MeV}$. The resulting pinning

force per unit length of vortex is of order $f_p \sim E_p/b^2 \sim (4 \text{ MeV})/(80 \text{ fm}^2)$. A complete calculation will be challenging because $b < \xi$, and is likely to yield an f_p which is somewhat less than that we have obtained by dimensional analysis. Note that our estimate of f_p is quite uncertain both because it is only based on dimensional analysis and because the values of Δ , b and F_{LOFF} are uncertain. (We have a good understanding of all the ratios Δ/Δ_0 , $\delta\mu/\Delta_0$, q/Δ_0 and consequently $b\Delta_0$ in the LOFF phase. It is of course the value of the BCS gap Δ_0 which is uncertain.) It is premature to compare our crude result to the results of serious calculations of the pinning of crustal neutron vortices as in Refs. 135,136,131. It is nevertheless remarkable that they prove to be similar: the pinning energy of neutron vortices in the inner crust is $E_p \approx 1 - 3 \text{ MeV}$ and the pinning force per unit length is $f_p \approx (1 - 3 \text{ MeV})/(200 - 400 \text{ fm}^2)$.

The reader may be concerned that a glitch deep within the quark matter core of a neutron star may not be observable: the vortices within the crystalline color superconductor region suddenly unpin and leap outward; this loss of angular momentum is compensated by a gain in angular momentum of the layer outside the LOFF region; how quickly, then, does this increase in angular momentum manifest itself at the *surface* of the star as a glitch? The important point here is that the rotation of any superfluid region within which the vortices are able to move freely is coupled to the rotation of the outer crust on very short time scales.¹³⁷ This rapid coupling, due to electron scattering off vortices and the fact that the electron fluid penetrates throughout the star, is usually invoked to explain that the core nucleon superfluid speeds up quickly after a crustal glitch: the only long relaxation time is that of the vortices within the inner crust.¹³⁷ Here, we invoke it to explain that the outer crust speeds up rapidly after a LOFF glitch has accelerated the quark matter at the base of the nucleon superfluid. After a glitch in the LOFF region, the only long relaxation times are those of the vortices in the LOFF region and in the inner crust.

A quantitative theory of glitches originating within quark matter in a LOFF phase must await further calculations, in particular a three flavor analysis and the determination of the crystal structure of the QCD LOFF phase. However, our rough estimate of the pinning force on rotational vortices in a LOFF region suggests that this force may be comparable to that on vortices in the inner crust of a conventional neutron star. Perhaps, therefore, glitches occurring in a region of crystalline color superconducting quark matter may yield similar phenomenology to those occurring in the inner crust. This is surely strong motivation for further investigation.

Perhaps the most interesting consequence of these speculations arises in the context of compact stars made entirely of strange quark matter. The work of Witten¹³⁸ and Farhi and Jaffe¹³⁹ raised the possibility that strange quark matter may be stable relative to nuclear matter even at zero pressure.

If this is the case it raises the question whether observed compact stars—pulsars, for example—are strange quark stars^{140,141} rather than neutron stars. A conventional neutron star may feature a core made of strange quark matter, as we have been discussing above.ⁱ Strange quark stars, on the other hand, are made (almost) entirely of quark matter with either no hadronic matter content at all or with a thin crust, of order one hundred meters thick, which contains no neutron superfluid.^{141,142} The nuclei in this thin crust are supported above the quark matter by electrostatic forces; these forces cannot support a neutron fluid. Because of the absence of superfluid neutrons, and because of the thinness of the crust, no successful models of glitches in the crust of a strange quark star have been proposed. Since pulsars are observed to glitch, the apparent lack of a glitch mechanism for strange quark stars has been the strongest argument that pulsars cannot be strange quark stars.^{143,144,145} This conclusion must now be revisited.

Madsen's conclusion¹¹⁹ that a strange quark star is prone to r-mode instability due to the absence of damping must also be revisited, since the relevant oscillations may be damped within or at the boundary of a crystalline color superconductor region.

The quark matter in a strange quark star, should one exist, would be a color superconductor. Depending on the mass of the star, the quark number densities increase by a factor of about two to ten in going from the surface to the center.¹⁴¹ This means that the chemical potential differences among the three quarks will vary also, and there could be a range of radii within which the quark matter is in a crystalline color superconductor phase. This raises the possibility of glitches in strange quark stars. Because the variation in density with radius is gradual, if a shell of LOFF quark matter exists it need not be particularly thin. And, we have seen, the pinning forces may be comparable in magnitude to those in the inner crust of a conventional neutron star. It has recently been suggested (for reasons unrelated to our considerations) that certain accreting compact stars may be strange quark stars,¹⁴⁶ although the evidence is far from unambiguous.¹⁴⁷ In contrast, it has been thought that, because they glitch, conventional radio pulsars cannot be strange quark stars. Our work questions this assertion by raising the possibility that glitches may originate within a layer of quark matter which is in a crystalline color superconducting state.

There has been much recent progress in our understanding of how the presence of color superconducting quark matter in a compact star would affect five different phenomena: cooling by neutrino emission, the pattern of the arrival times of supernova neutrinos, the evolution of neutron star magnetic

ⁱNote that a convincing discovery of a quark matter core within an otherwise hadronic neutron star would demonstrate conclusively that strange quark matter is *not* stable at zero pressure, thus ruling out the existence of strange quark stars. It is not possible for neutron stars with quark matter cores and strange quark stars to both be stable.

fields, r-mode instabilities and glitches. Nevertheless, much theoretical work remains to be done before we can make sharp proposals for which astrophysical observations can teach us whether compact stars contain quark matter, and if so whether it is in the 2SC or CFL phase.

Acknowledgments

We are grateful to M. Alford, B. Berdnikov, J. Berges, J. Bowers, J. Kundu, T. Schäfer, E. Shuryak, E. Shuster and M. Stephanov for enjoyable and fruitful collaboration. This work is supported in part by the Department of Energy under cooperative research agreement #DF-FC02-94ER40818. The work of KR was supported in part by a DOE OJI Award and by the A. P. Sloan Foundation. Preprint MIT-CTP-3049.

References

1. D. J. Gross and F. Wilczek, Phys. Rev. Lett. **30**, 1343 (1973); H. D. Politzer, Phys. Rev. Lett. **30**, 1346 (1973).
2. J. C. Collins and M. J. Perry, Phys. Rev. Lett. **34**, 1353 (1975).
3. B. Barrois, Nucl. Phys. **B129**, 390 (1977); S. Frautschi, Proceedings of workshop on hadronic matter at extreme density, Erice 1978; B. Barrois, “Nonperturbative effects in dense quark matter”, Cal Tech PhD thesis, UMI 79-04847-mc (1979).
4. D. Bailin and A. Love, Phys. Rept. **107**, 325 (1984), and references therein.
5. M. Alford, K. Rajagopal and F. Wilczek, Phys. Lett. **B422**, 247 (1998) [hep-ph/9711395].
6. R. Rapp, T. Schäfer, E. V. Shuryak and M. Velkovsky, Phys. Rev. Lett. **81**, 53 (1998) [hep-ph/9711396].
7. M. Alford, K. Rajagopal and F. Wilczek, Nucl. Phys. **B537**, 443 (1999) [hep-ph/9804403].
8. T. Schäfer and F. Wilczek, Phys. Rev. Lett. **82**, 3956 (1999) [hep-ph/9811473].
9. R. Rapp, T. Schäfer, E. V. Shuryak and M. Velkovsky, Annals Phys. **280**, 35 (2000) [hep-ph/9904353].
10. T. Schäfer, Nucl. Phys. **B575**, 269 (2000) [hep-ph/9909574].
11. I. A. Shovkovy and L. C. Wijewardhana, Phys. Lett. **B470**, 189 (1999) [hep-ph/9910225].
12. N. Evans, J. Hormuzdiar, S. D. Hsu and M. Schwetz, Nucl. Phys. **B581**, 391 (2000) [hep-ph/9910313].
13. M. Alford, J. Berges and K. Rajagopal, Nucl. Phys. **B558**, 219 (1999) [hep-ph/9903502].

14. S. Elitzur, Phys. Rev. **D12**, 3978 (1975).
15. E. Fradkin and S. Shenker, Phys. Rev. **D19**, 3682 (1979); T. Banks and E. Rabinovici, Nucl. Phys. **B160**, 349 (1979).
16. M. Srednicki and L. Susskind, Nucl. Phys. **B187**, 93 (1981).
17. T. Schäfer and F. Wilczek, Phys. Rev. **D60**, 074014 (1999) [hep-ph/9903503].
18. D. K. Hong, M. Rho and I. Zahed, Phys. Lett. **B468**, 261 (1999) [hep-ph/9906551].
19. R. Casalbuoni and R. Gatto, Phys. Lett. **B464**, 111 (1999) [hep-ph/9908227].
20. M. Alford, J. Berges and K. Rajagopal, Phys. Rev. Lett. **84**, 598 (2000) [hep-ph/9908235].
21. D. T. Son and M. A. Stephanov, Phys. Rev. **D61**, 074012 (2000) [hep-ph/9910491]; erratum, *ibid.* **D62**, 059902 (2000) [hep-ph/0004095].
22. M. Rho, A. Wirzba and I. Zahed, Phys. Lett. **B473**, 126 (2000) [hep-ph/9910550].
23. D. K. Hong, T. Lee and D. Min, Phys. Lett. **B477**, 137 (2000) [hep-ph/9912531].
24. C. Manuel and M. H. Tytgat, Phys. Lett. **B479**, 190 (2000) [hep-ph/0001095].
25. M. Rho, E. Shuryak, A. Wirzba and I. Zahed, Nucl. Phys. **A676**, 273 (2000) [hep-ph/0001104].
26. K. Zarembo, Phys. Rev. **D62**, 054003 (2000) [hep-ph/0002123].
27. S. R. Beane, P. F. Bedaque and M. J. Savage, Phys. Lett. **B483**, 131 (2000) [hep-ph/0002209].
28. D. H. Rischke, Phys. Rev. **D62**, 054017 (2000) [nucl-th/0003063].
29. D. K. Hong, Phys. Rev. **D62**, 091501 (2000) [hep-ph/0006105].
30. T. Schäfer, nucl-th/0007021.
31. M. A. Nowak, M. Rho, A. Wirzba and I. Zahed, hep-ph/0007034.
32. V. A. Miransky, I. A. Shovkovy and L. C. Wijewardhana, hep-ph/0009173.
33. C. Manuel and M. Tytgat, hep-ph/0010274.
34. R. Casalbuoni, R. Gatto and G. Nardulli, hep-ph/0010321.
35. D. K. Hong, S.-T. Hong and Y.-J. Park, hep-ph/0011027.
36. D. H. Rischke, Phys. Rev. **D62**, 034007 (2000) [nucl-th/0001040].
37. G. Carter and D. Diakonov, Nucl. Phys. **B582**, 571 (2000) [hep-ph/0001318].
38. Very recent work, not yet published, calls this assertion into question. K. Rajagopal and F. Wilczek, in preparation.
39. D. B. Kaplan and A. E. Nelson, Phys. Lett. **B175**, 57 (1986).
40. M. Alford, J. Berges and K. Rajagopal, Nucl. Phys. **B571**, 269 (2000) [hep-ph/9910254].

41. R. L. Jaffe, Phys. Rev. Lett. **38**, 195, 617(E) (1977).
42. V. A. Miransky, I. A. Shovkovy and L. C. Wijewardhana, Phys. Rev. **D62**, 085025 (2000) [hep-ph/0009129].
43. J. Berges and K. Rajagopal, Nucl. Phys. **B538**, 215 (1999) [hep-ph/9804233].
44. R. D. Pisarski and D. H. Rischke, Phys. Rev. Lett. **83**, 37 (1999) [nucl-th/9811104].
45. G. W. Carter and D. Diakonov, Phys. Rev. **D60**, 016004 (1999) [hep-ph/9812445].
46. F. Sannino, Phys. Lett. **B480**, 280 (2000) [hep-ph/0002277]; R. Casalbuoni, Z. Duan and F. Sannino, hep-ph/0004207; S. D. Hsu, F. Sannino and M. Schwetz, hep-ph/0006059.
47. T. Schäfer, Phys. Rev. **D62**, 094007 (2000) [hep-ph/0006034].
48. J. Hosek, hep-ph/9812516 and hep-ph/0011034.
49. M. Alford, J. Bowers and K. Rajagopal, hep-ph/0008208.
50. UKQCD Collaboration, Phys. Rev. **D59** (1999) 116002; S. Hands, J. B. Kogut, M. Lombardo and S. E. Morrison, Nucl. Phys. **B558**, 327 (1999) [hep-lat/9902034]; S. Hands, I. Montvay, S. Morrison, M. Oevers, L. Scorzato and J. Skullerud, hep-lat/0006018.
51. J. B. Kogut, M. A. Stephanov and D. Toublan, Phys. Lett. **B464**, 183 (1999) [hep-ph/9906346]; J. B. Kogut, M. A. Stephanov, D. Toublan, J. J. Verbaarschot and A. Zhitnitsky, Nucl. Phys. **B582**, 477 (2000) [hep-ph/0001171].
52. D. V. Deryagin, D. Yu. Grigoriev and V. A. Rubakov, Int. J. Mod. Phys. **A7**, 659 (1992).
53. E. Shuster and D. T. Son, Nucl. Phys. **B573**, 434 (2000) [hep-ph/9905448].
54. B. Park, M. Rho, A. Wirzba and I. Zahed, Phys. Rev. **D62**, 034015 (2000) [hep-ph/9910347].
55. R. Rapp, E. Shuryak and I. Zahed, hep-ph/0008207.
56. D. T. Son and M. A. Stephanov, hep-ph/0005225.
57. N. Evans, S. D. H. Hsu and M. Schwetz, Nucl. Phys. **B551**, 275 (1999) [hep-ph/9808444]; Phys. Lett. **B449**, 281 (1999) [hep-ph/9810514].
58. T. Schäfer and F. Wilczek, Phys. Lett. **B450**, 325 (1999) [hep-ph/9810509].
59. D. T. Son, Phys. Rev. **D59**, 094019 (1999) [hep-ph/9812287].
60. N. O. Agasian, B. O. Kerbikov and V. I. Shevchenko, Phys. Rept. **320**, 131 (1999) [hep-ph/9902335].
61. R. D. Pisarski and D. H. Rischke, Phys. Rev. **D60**, 094013 (1999) [nucl-th/9903023]; Phys. Rev. **D61**, 051501 (2000) [nucl-th/9907041]; Phys. Rev. **D61**, 074017 (2000) [nucl-th/9910056];
62. D. K. Hong, Phys. Lett. **B473**, 118 (2000) [hep-ph/9812510]; Nucl. Phys.

- B582**, 451 (2000) [hep-ph/9905523].
63. D. K. Hong, V. A. Miransky, I. A. Shovkovy and L. C. Wijewardhana, Phys. Rev. **D61**, 056001 (2000), erratum *ibid.* **D62**, 059903 (2000) [hep-ph/9906478].
 64. T. Schäfer and F. Wilczek, Phys. Rev. **D60**, 114033 (1999) [hep-ph/9906512].
 65. W. E. Brown, J. T. Liu and H. Ren, Phys. Rev. **D61**, 114012 (2000) [hep-ph/9908248]; Phys. Rev. **D62**, 054016 (2000) [hep-ph/9912409]; Phys. Rev. **D62**, 054013 (2000) [hep-ph/0003199].
 66. S. D. Hsu and M. Schwetz, Nucl. Phys. **B572**, 211 (2000) [hep-ph/9908310].
 67. B. Vanderheyden and A. D. Jackson, Phys. Rev. **D62**, 094010 (2000) [hep-ph/0003150].
 68. S. R. Beane, P. F. Bedaque and M. J. Savage, nucl-th/0004013; S. R. Beane and P. F. Bedaque, Phys. Rev. **D62**, 117502 (2000) [nucl-th/0005052].
 69. K. Rajagopal and E. Shuster, Phys. Rev. **D62**, 085007 (2000) [hep-ph/0004074].
 70. C. Manuel, Phys. Rev. **D62**, 114008 (2000) [hep-ph/0006106].
 71. For a recent review and references, see O. Philipsen, hep-lat/0011019.
 72. S. Chandrasekharan and U. Wiese, Phys. Rev. Lett. **83**, 3116 (1999) [cond-mat/9902128].
 73. R. Shankar, Rev. Mod. Phys. **66**, 129 (1993) and references therein.
 74. J. Polchinski, hep-th/9210046.
 75. M. A. Shifman, A. I. Vainshtein and V. I. Zakharov, Nucl. Phys. **B163**, 46 (1980).
 76. T. Schäfer and E. V. Shuryak, Rev. Mod. Phys. **70**, 323 (1998).
 77. J. Bardeen, L. N. Cooper and J. R. Schrieffer, Phys. Rev. **106**, 162 (1957); **108**, 1175 (1957).
 78. Y. Nambu and G. Jona-Lasinio, Phys. Rev. **122**, 345 (1961); **124**, 246 (1961).
 79. D. Bailin and A. Love, Supersymmetric Gauge Field Theory and String Theory, (IOP, London, 1994).
 80. N. N. Bogoliubov, Nuovo Cimento **7**, 694 (1958); J. Valatin, Nuovo Cimento **7**, 843 (1958).
 81. M. LeBellac, Thermal Field Theory, Cambridge University Press, (Cambridge, 1996).
 82. G. M. Eliashberg, Zh. Eksp. Teor. Fiz. **34**, 735 (1960); translation Sov. Phys. JETP **11**, 696 (1960).
 83. C. Manuel, Phys. Rev. **D62**, (6009) [hep-ph/0005040].
 84. D. Boyanovsky and H. J. de Vega, hep-ph/0009172.
 85. For a longer review, see K. Rajagopal, in Quark-Gluon Plasma 2, (World

- Scientific, 1995) 484, ed. R. Hwa [hep-ph/9504310].
86. R. Pisarski and F. Wilczek, Phys. Rev. **D29**, 338 (1984); F. Wilczek, Int. J. Mod. Phys. **A7**, 3911 (1992); K. Rajagopal and F. Wilczek, Nucl. Phys. **B399**, 395 (1993).
 87. For reviews, see F. Karsch, hep-lat/9909006; E. Laermann Nucl. Phys. Proc. Suppl. **63**, 114 (1998); and A. Ukawa, Nucl. Phys. Proc. Suppl. **53**, 106 (1997).
 88. A. Ali Khan *et al.*, [CP-PACS Collaboration], hep-lat/0008011.
 89. For example, S. Gottlieb *et al.*, Phys. Rev. **D55**, 6852 (1997); F. Karsch, hep-lat/9909006.
 90. A. Barducci, R. Casalbuoni, S. DeCurtis, R. Gatto, G. Pettini, Phys. Lett. **B231**, 463 (1989); Phys. Rev. **D41**, 1610 (1990); S.P. Klevansky, Rev. Mod. Phys. **64**, 649 (1992); A. Barducci, R. Casalbuoni, G. Pettini and R. Gatto, Phys. Rev. **D49**, 426 (1994).
 91. M. A. Stephanov, Phys. Rev. Lett. **76**, 4472 (1996) [hep-lat/9604003]; Nucl. Phys. Proc. Suppl. **53**, 469 (1997) [hep-lat/9607060].
 92. M. A. Halasz, A. D. Jackson, R. E. Shrock, M. A. Stephanov and J. J. Verbaarschot, Phys. Rev. **D58**, 096007 (1998) [hep-ph/9804290].
 93. For a review, see I. Lawrie and S. Sarbach in Phase Transitions and Critical Phenomena **9**, 1 (Academic Press, 1984), ed. C. Domb and J. Lebowitz.
 94. M. Stephanov, K. Rajagopal and E. Shuryak, Phys. Rev. Lett. **81**, 4816 (1998) [hep-ph/9806219].
 95. M. Stephanov, K. Rajagopal and E. Shuryak, Phys. Rev. **D60**, 114028 (1999) [hep-ph/9903292].
 96. F. Wilczek, Int. J. Mod. Phys. **A7**, 3911 (1992); K. Rajagopal and F. Wilczek, Nucl. Phys. **B399**, 395 (1993).
 97. F. Brown *et al.*, Phys. Rev. Lett. **65**, 2491 (1990).
 98. JLQCD Collaboration, Nucl. Phys. Proc. Suppl. **73**, 459 (1999).
 99. Y. Iwasaki *et al.*, Phys. Rev. **D54**, 7010 (1996).
 100. See, e.g., P. Braun-Munzinger, J. Stachel, J. P. Wessels and N. Xu, Phys. Lett. **B344**, 43 (1994); *ibid.* **B365**, 1 (1996); P. Braun-Munzinger and J. Stachel, Nucl. Phys. **A638**, 3 (1998).
 101. B. B. Back *et al.*, [PHOBOS Collaboration], to appear in Phys. Rev. Lett., hep-ex/0007036.
 102. K. H. Ackerman *et al.*, [STAR Collaboration], nucl-ex/0009011.
 103. H. Appelshauser *et al.* [NA49 Collaboration], Phys. Lett. **B459**, 679 (1999).
 104. A. Bialas and V. Koch, Phys. Lett. **B456**, 1 (1999) [nucl-th/9902063].
 105. St. Mrowczynski, Phys. Lett. **B430**, 9 (1998) [nucl-th/9712030].
 106. B. Berdnikov and K. Rajagopal, Phys. Rev. **D61**, 105017 (2000) [hep-ph/9912274].

107. P. C. Hohenberg and B. I. Halperin, *Rev. Mod. Phys.* **49**, 435 (1977).
108. Reviewed in U. Heinz and M. Jacob, *nucl-th/0002042*.
109. R. D. Pisarski, *Phys. Rev.* **C62**, 035202 (2000) [*nucl-th/9912070*].
110. For a review, see H. Heiselberg and M. Hjorth-Jensen, *Phys. Rept.* **328**, 237 (2000).
111. N. K. Glendenning and F. Weber, *astro-ph/0003426*. See also D. Blaschke, H. Grigorian and G. Poghosyan, *astro-ph/0008005*.
112. M. van der Klis, to appear in *Ann. Rev. Astronomy and Astrophysics*, (2000) [*astro-ph/0001167*].
113. R. Wijnands and M. van der Klis, *Nature* **394**, 344 (1998); D. Chakrabarty and E. Morgan, *Nature* **394**, 346 (1998).
114. L. Bildsten, *Astrophys. J.* **501** L89 [*astro-ph/9804325*]; N. Andersson, D. I. Jones, K. D. Kokkotas and N. Stergioulas, *Astrophys. J.* **534**, L75 (2000) [*astro-ph/0002114*].
115. D. Blaschke, T. Klahn and D. N. Voskresensky, *Astrophys. J.* **533**, 406 (2000) [*astro-ph/9908334*]; D. Blaschke, H. Grigorian and D. N. Voskresensky, *astro-ph/0009120*.
116. D. Page, M. Prakash, J. M. Lattimer and A. Steiner, *Phys. Rev. Lett.* **85**, 2048 (2000) [*hep-ph/0005094*].
117. C. Schaab *et al.*, *Astrophys. J. Lett* **480** (1997) L111 and references therein.
118. G. W. Carter and S. Reddy, *Phys. Rev.* **D62**, 103002 (2000) [*hep-ph/0005228*].
119. J. Madsen, *Phys. Rev. Lett.* **85**, 10 (2000) [*astro-ph/9912418*].
120. L. Bildsten and G. Ushomirsky, *Astrophys. J.* **529**, L75 (2000) [*astro-ph/9911155*]; N. Andersson *et al.* in Ref. 114; L. Lindblom, B. J. Owen and G. Ushomirsky, *astro-ph/0006242*.
121. D. Blaschke, D. M. Sedrakian and K. M. Shahabasian, *Astron. and Astrophys.* **350**, L47 (1999) [*astro-ph/9904395*].
122. For reviews, see J. Sauls, in *Timing Neutron Stars*, J. Öggleman and E. P. J. van den Heuvel, eds., (Kluwer, Dordrecht: 1989) 457; and D. Bhattacharya and G. Srinivasan, in *X-Ray Binaries*, W. H. G. Lewin, J. van Paradijs, and E. P. J. van den Heuvel eds., (Cambridge University Press, 1995) 495.
123. A. M. Clogston, *Phys. Rev. Lett.* **9**, 266 (1962); B. S. Chandrasekhar, *App. Phys. Lett.* **1**, 7 (1962).
124. A. Sedrakian and U. Lombardo, *Phys. Rev. Lett.* **84**, 602 (2000). Isospin asymmetric nuclear matter may also admit LOFF pairing, as discussed recently in A. Sedrakian, *nucl-th/0008052*.
125. P. F. Bedaque, *hep-ph/9910247*.
126. A. I. Larkin and Yu. N. Ovchinnikov, **47**, 1136 (1964); translation: *Sov. Phys. JETP* **20**, 762 (1965).

127. P. Fulde and R. A. Ferrell, Phys. Rev. **135**, A550 (1964).
128. S. Takada and T. Izuyama, Prog. Theor. Phys. **41**, 635 (1969).
129. M. A. Alpar and C. Ho, Mon. Not. R. Astron. Soc. **204**, 655 (1983).
For a recent review, see A.G. Lyne in *Pulsars: Problems and Progress*, S. Johnston, M. A. Walker and M. Bailes, eds., 73 (ASP, 1996).
130. J. Negele and D. Vautherin, Nucl. Phys. **A207**, 298 (1973).
131. For reviews, see D. Pines and A. Alpar, Nature **316**, 27 (1985); D. Pines, in *Neutron Stars: Theory and Observation*, J. Ventura and D. Pines, eds., 57 (Kluwer, 1991); M. A. Alpar, in *The Lives of Neutron Stars*, M. A. Alpar et al., eds., 185 (Kluwer, 1995). For more recent developments and further references, see M. Ruderman, Astrophys. J. **382**, 587 (1991); R. I. Epstein and G. Baym, Astrophys. J. **387**, 276 (1992); M. A. Alpar, H. F. Chau, K. S. Cheng and D. Pines, Astrophys. J. **409**, 345 (1993); B. Link and R. I. Epstein, Astrophys. J. **457**, 844 (1996); M. Ruderman, T. Zhu, and K. Chen, Astrophys. J. **492**, 267 (1998); A. Sedrakian and J. M. Cordes, Mon. Not. R. Astron. Soc. **307**, 365 (1999).
132. N. K. Glendenning, Phys. Rev. **D46**, 1274 (1992); N. K. Glendenning, *Compact Stars* (Springer-Verlag, 1997); F. Weber, J. Phys. G. Nucl. Part. Phys. **25**, R195 (1999).
133. R. Modler *et al.*, Phys. Rev. Lett. **76**, 1292 (1996).
134. P. W. Anderson and N. Itoh, Nature **256**, 25 (1975).
135. M. A. Alpar, Astrophys. J. **213**, 527 (1977).
136. M. A. Alpar, P. W. Anderson, D. Pines and J. Shaham, Astrophys. J. **278**, 791 (1984).
137. M. A. Alpar, S. A. Langer and J. A. Sauls, Astrophys. J. **282**, 533 (1984).
138. E. Witten, Phys. Rev. **D30**, 272 (1984).
139. E. Farhi and R. L. Jaffe, Phys. Rev. **D30**, 2379 (1984).
140. P. Haensel, J. L. Zdunik and R. Schaeffer, Astron. Astrophys. **160**, 121 (1986).
141. C. Alcock, E. Farhi and A. Olinto, Phys. Rev. Lett. **57**, 2088 (1986); Astrophys. J. **310**, 261 (1986).
142. N. K. Glendenning and F. Weber, Astrophys. J. **400**, 647 (1992).
143. A. Alpar, Phys. Rev. Lett. **58**, 2152 (1987).
144. J. Madsen, Phys. Rev. Lett. **61**, 2909 (1988).
145. R. R. Caldwell and J. L. Friedman, Phys. Lett. **B264**, 143 (1991).
146. X.-D. Li, I. Bombaci, M. Dey, J. Dey, E. P. J. van den Heuvel, Phys. Rev. Lett. **83**, 3776 (1999); X.-D. Li, S. Ray, J. Dey, M. Dey, I. Bombaci, Astrophys. J. **527**, L51 (1999); B. Datta, A. V. Thampan, I. Bombaci, astro-ph/9912173; I. Bombaci, astro-ph/0002524.
147. D. Psaltis and D. Chakrabarty, Astrophys. J. **521**, 332 (1999); D. Chakrabarty, Phys. World **13**, No. 2, 26 (2000).